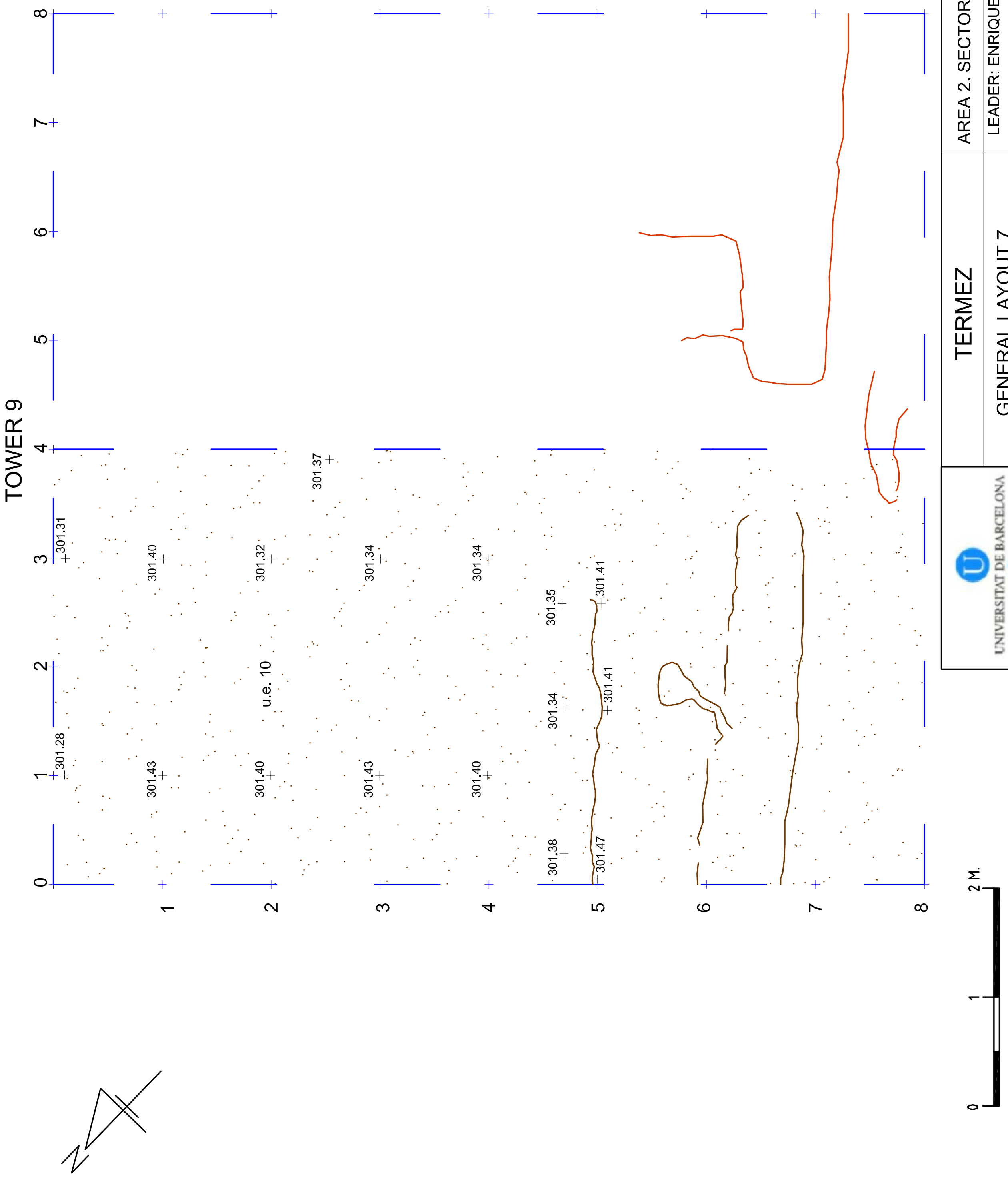

No.

07

AREA 2. SECTOR 4. RB 2 SAMPLE TRENCH

LEADER: ENRIQUE ARIÑO GIL
DRAWING AND DIGITAL IMAGING: JÚLIA MIQUEL

OCTOBER 2010

TERMEZ

GENERAL LAYOUT 7

SCALE 1:50

UNIVERSITAT DE BARCELONA

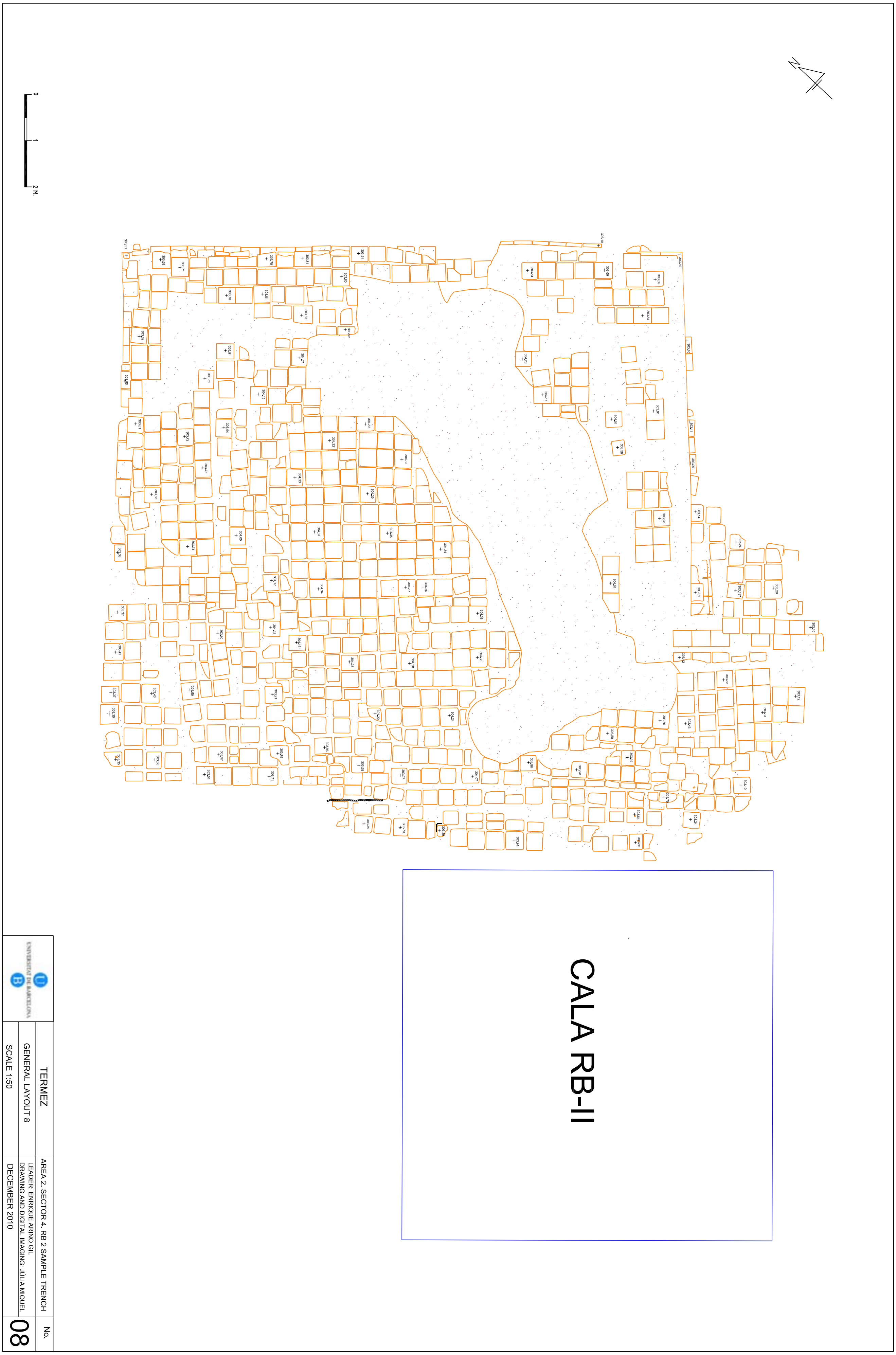
0
1
2 M.
CALA RB-II
UNIVERSITAT DE BARCELONA
TERMEZ
GENERAL LAYOUT 8
SCALE 1:50
AREA 2. SECTOR 4. RB 2 SAMPLE TRENCH
LEADER: ENRIQUE ARIÑO GIL
DRAWING AND DIGITAL IMAGING: JÚLIA MIQUEL
DECEMBER 2010
No.
08

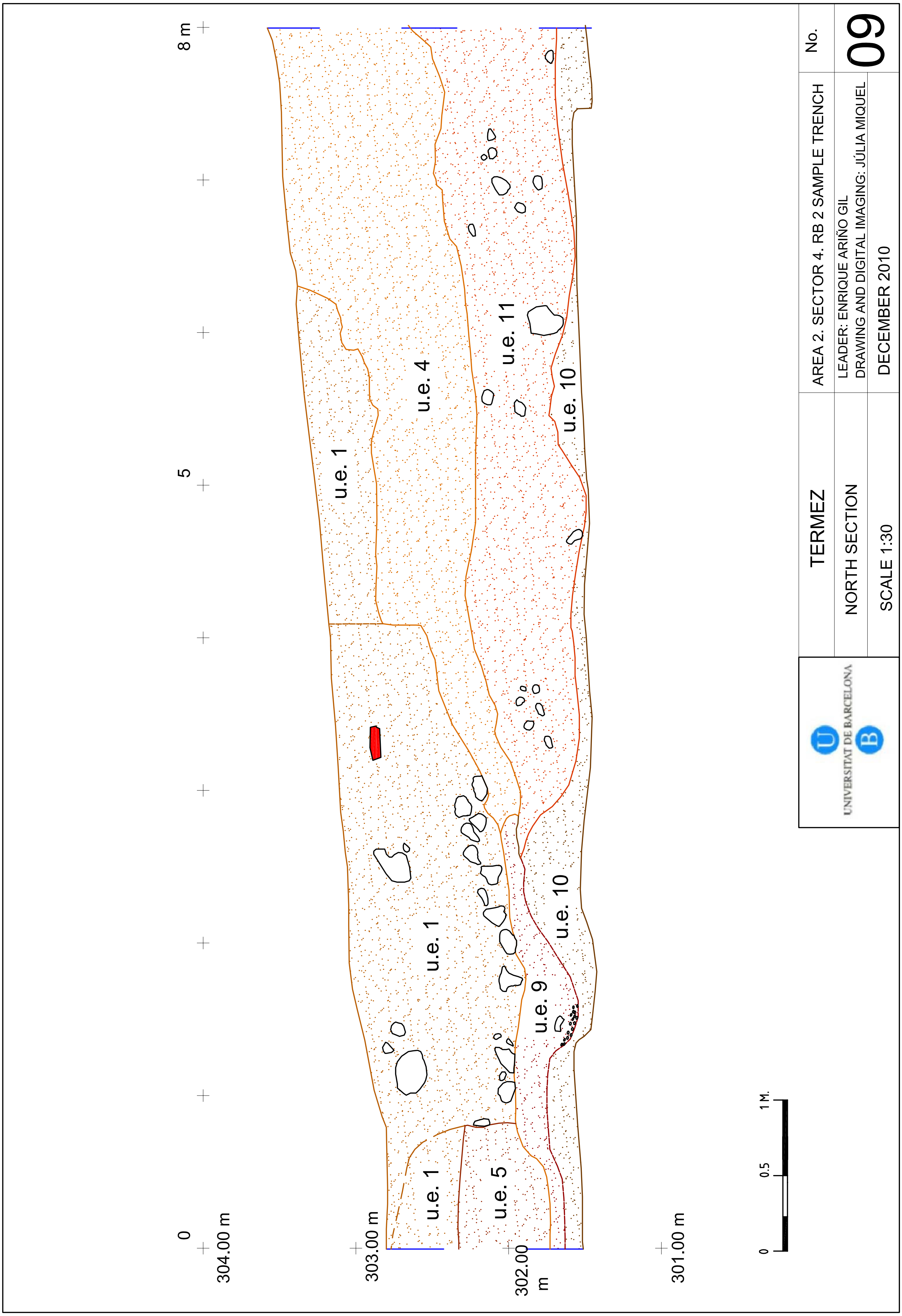

TERMEZ

NORTH SECTION

SCALE 1:30

AREA 2. SECTOR 4. RB 2 SAMPLE TRENCH

LEADER: ENRIQUE ARIÑO GIL

DRAWING AND DIGITAL IMAGING: JÚLIA MIQUEL

DECEMBER 2010

No.

09

UNIVERSITAT DE BARCELONA

North section of RB2 sample trench

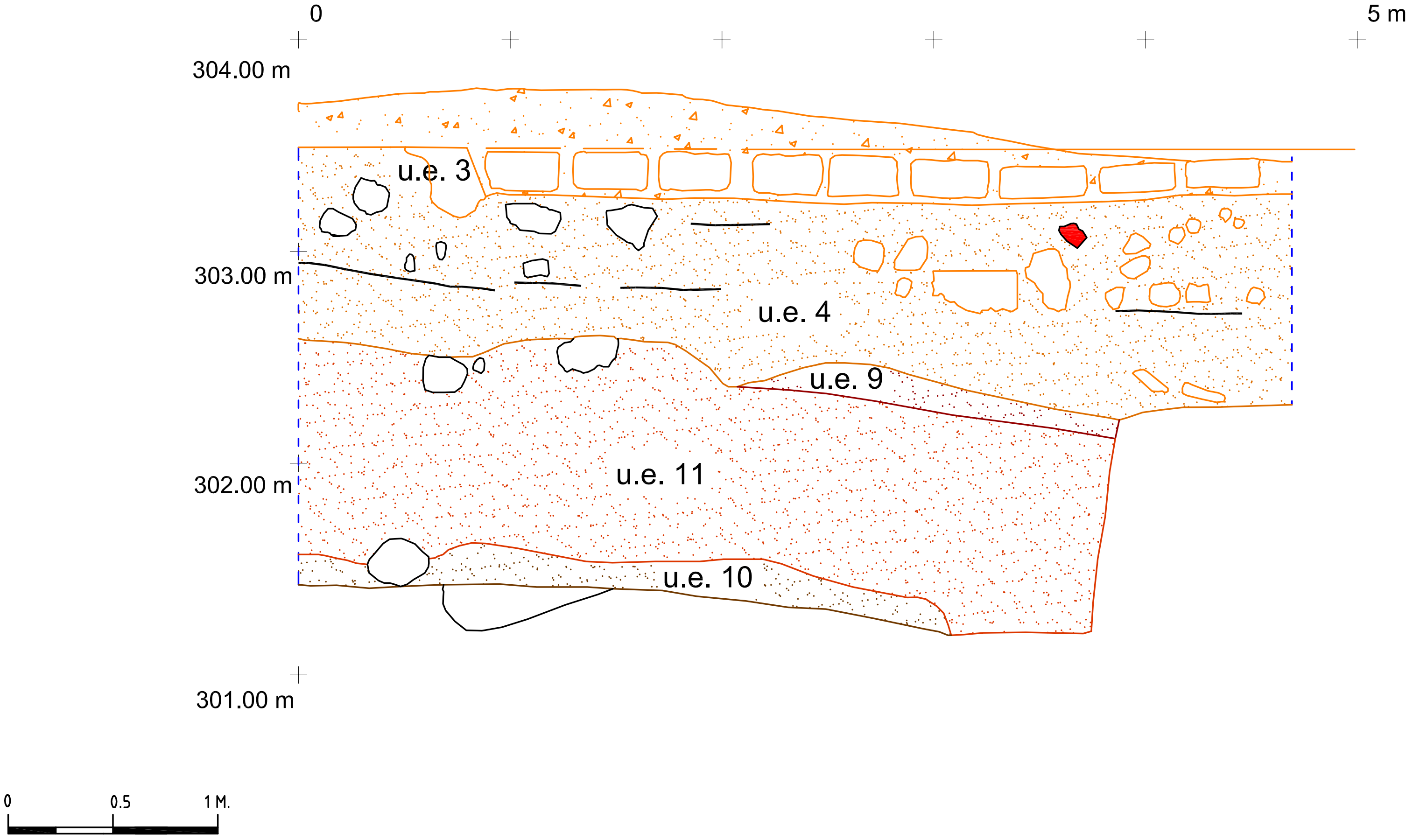

UNIVERSITAT DE BARCELONA	TERMEZ	AREA 2. SECTOR 4. RB 2 SAMPLE TRENCH	No.
	EAST SECTION	LEADER: ENRIQUE ARIÑO GIL DRAWING AND DIGITAL IMAGING: JÚLIA MIQUEL	10
	SCALE 1:30	DECEMBER 2010	

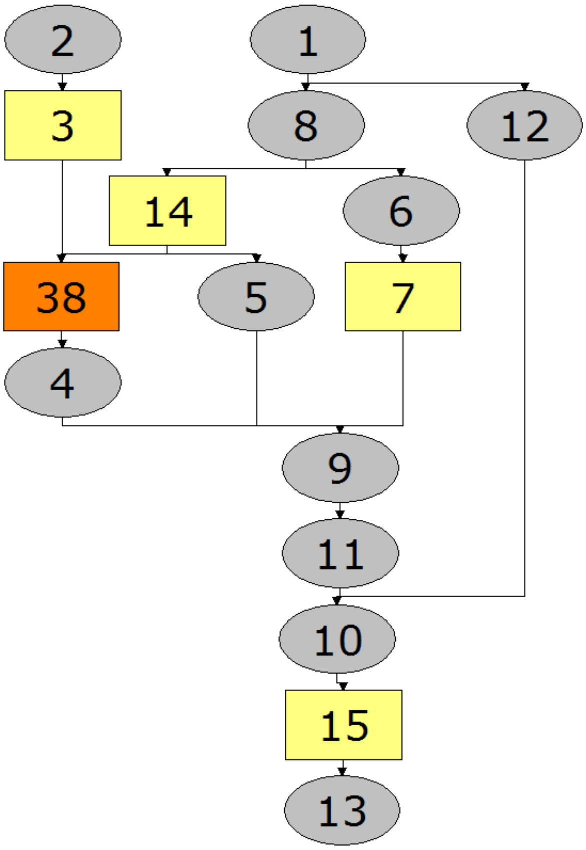
2
1
3
8
12
14
6
38
5
7
4
9
11
10
15
13

RB2 - SU 1

Definition: Surface level

Interpretation: A hillside deposit formed by slope dragging, which would justify its heterogeneous composition and its low level of compaction.

Observations: Surface level. Very loose, dragged down slope. Sand matrix, brown in colour, embedded with adobe fragments, large sandstone nodules and siltstone nodules. SU 1 yielded several fragments of white limestone (39 fragments in total) as well as fragments of mud brick (18 in total). Contains pottery.

Material:

Slipware:	85 shaped frags., 176 shapeless frags.
Common ware:	155 shaped frags., 677 shapeless frags.
Cooking ware:	4 shaped frags., 3 shapeless frags.
Cerámica Yuezhi:	1 shaped frag.
Large containers:	6 shaped frags., 55 shapeless frags.
Channels:	(earthen pipe: 14 frags.)
Stone building elements:	(Limestone: 8 frags con forma, 31 sin forma.)
Mud bricks	18 frags.
Other:	Hand mill (1 frag.) Alabaster spindle whorl Clay sphere

Archaeologist: E. Ariño

Composition	Sand, fragments of rock and adobe
Formation	Hillside deposit
Thickness	20-90 cm
Covering (Stratum)	8-5-12-4-11
Covering (Negative)	14

RB2- SU 1

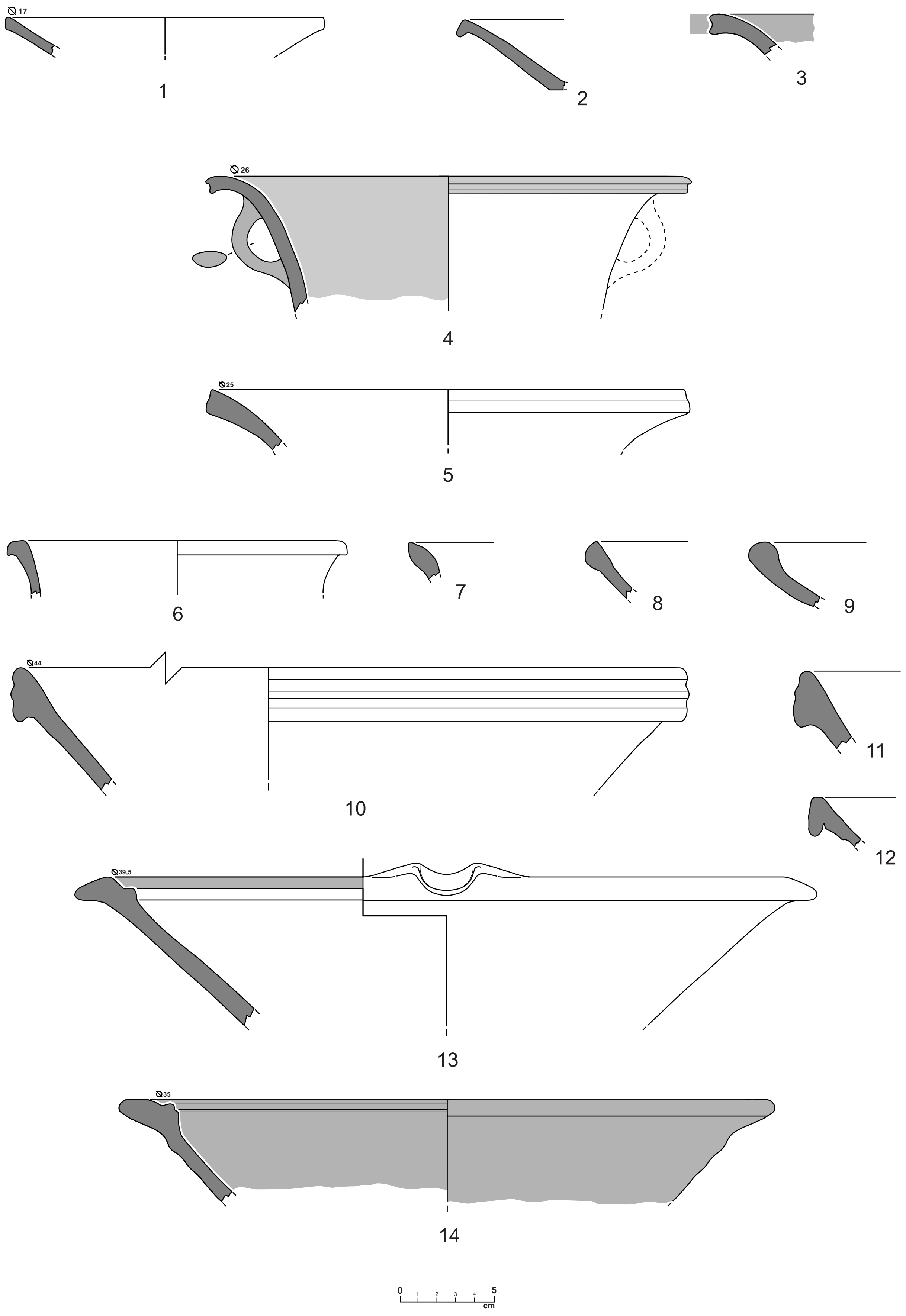

RB2-SU 1

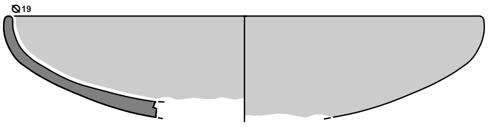

15

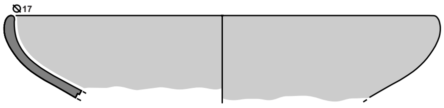

16

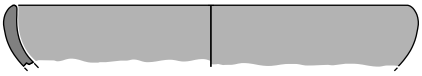

17

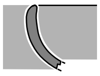

18

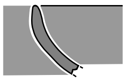

19

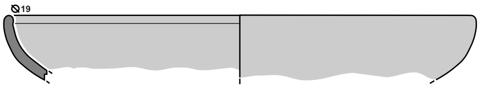

20

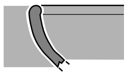

21

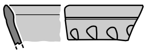

22

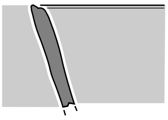

23

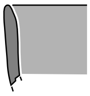

24

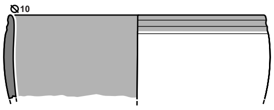

25

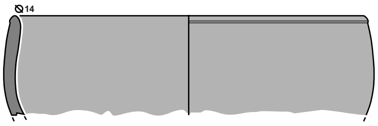

26

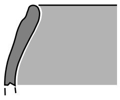

27

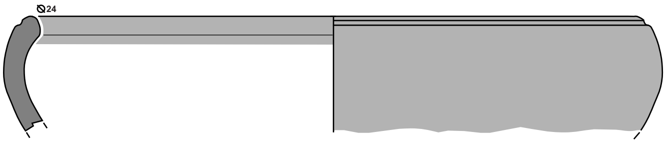

28

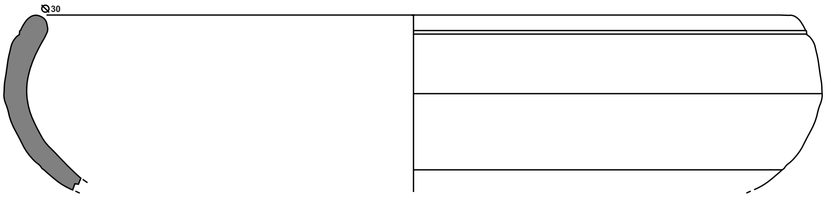

29

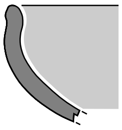

30

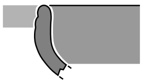

31

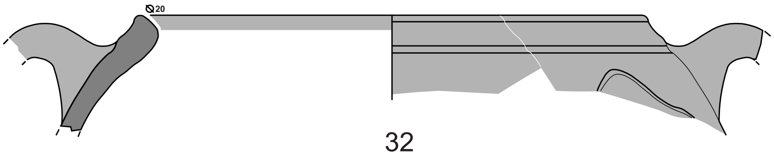

32

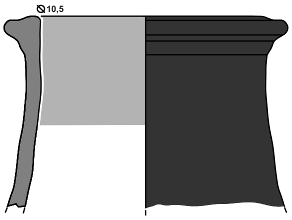

33

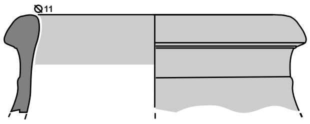

34

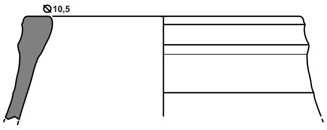

35

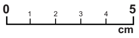

RB2- SU 1

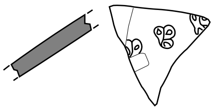
36

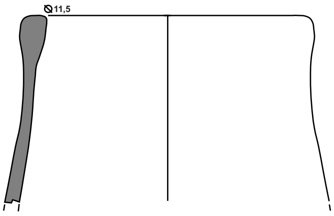

37

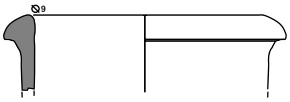

38

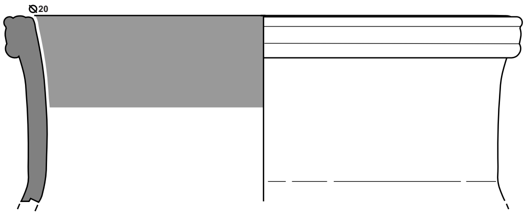

39

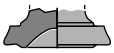
40

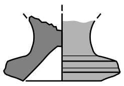
41

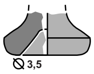

42

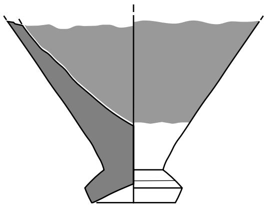
43

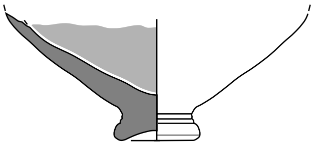
44

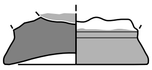
45

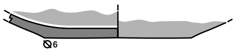

46

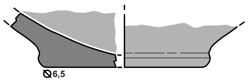

47

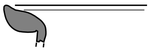
48

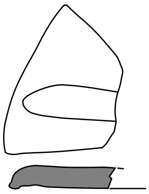
49

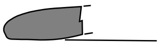
50


51

Cooking ware (48-51)

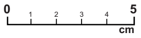

RB2 - SU 2

Definition: Grey sand

Interpretation: A deposit that fills in SU 3. SU 2 is of indeterminate chronology and formation.

Observations: Grey sand. Small deposit that fills in SU 3. SU 2 yielded only 2 potsherds and 4 bone fragments.

Material: Slipware: 1 shaped frag., 1 shapeless frag.

Archaeologist: E. Ariño

Composition	Sand
Formation	Indeterminate
Thickness	c. 20 cm
Rellena a (Negativa)	3

RB2 - SU 3

Definition: Small hole in adobe fortification wall

Interpretation: Hole of indeterminate chronology, but of human origin, because a carefully placed mud brick is preserved on one of its sides. It may have served as a post hole.

Observations: Small hole in the surface of tower 9. No contact with SU 1.

Archaeologist: E. Ariño

Filled in by (Stratum)	2
Intersecting (Structure)	38

RB2 - SU 4

Definition: Level of fallen adobe bricks

Interpretation: This stratum has the morphology of a level formed by the collapse of a structure. However, its location and its stratigraphic relationships indicate that it served at some time as a foundation for an fortification wall of Tchingiz Tepe. The stratum may have been formed from the collapse of the earlier fortification and was later used as a foundation for a new curtain wall, which would correspond to a phase of alteration or repair.

Observations: Fragments of adobe bricks in a fallen position. Clay matrix, although much sand is observed at the base of the stratum. SU 4 has some embedded, large nodules of sandstone. It contains pottery.

Material:

Slipware:	22 shaped frags., 29 shapeless frags.
Common ware:	19 shaped frags., 131 shapeless frags.
Cooking ware:	4 shaped frags., 3 shapeless frags.
Large containers:	1 shaped frags., 7 shapeless frags.
Channels:	(earthen pipe: 3 frags.)
Bone:	7 frags. (35 grs.)
Otros:	A fragment of vitrified pottery

BENEATH THE FORTIFICATION

Slipware:	3 shaped frags., 14 shapeless frags.
Common ware:	7 shaped frags., 31 shapeless frags.
Cooking ware:	1 shaped frags.
Cerámica gris con engobe:	2 frags. shapeless frags
Large containers:	2 shapeless frags.
Channels:	(earthen pipe: 1 frag.)
Bone:	1 frags. (4 grs.)

Archaeologist: E. Ariño

Composition	Fragments of adobe brick in a clay matrix
Formation	Natural agents?
Thickness	40-115 cm
Covered by (Stratum)	1
Rested on by (Structure)	38
Intersected by (Negative)	14
Covering (Stratum)	9-11

RB2 SU 4

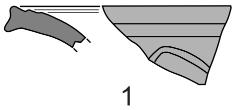

1

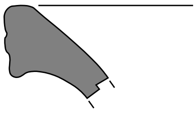

2

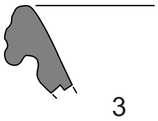

3

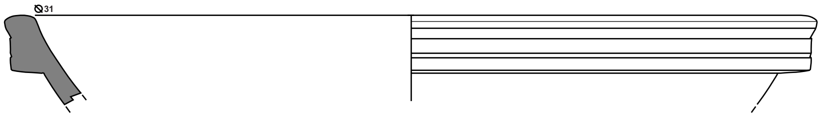

4

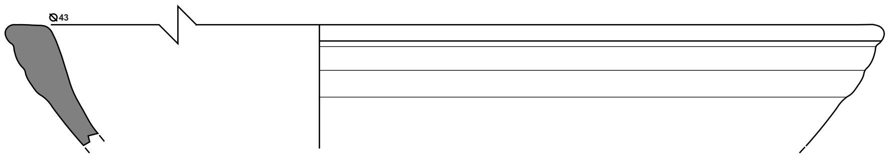

5

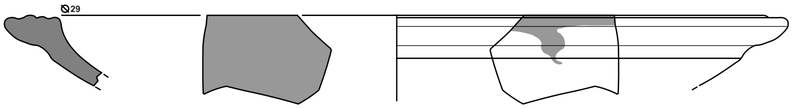

6

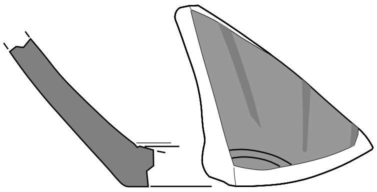

7

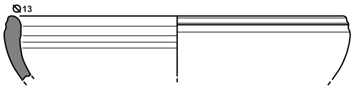

8

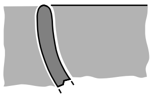

9

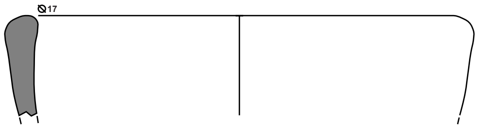

10

11

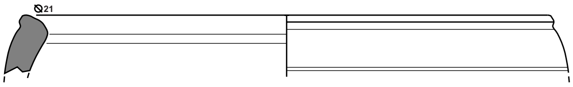

12

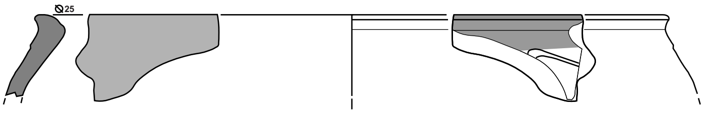

13

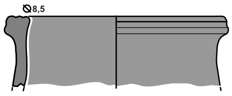

14

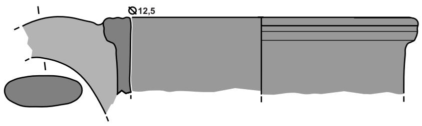

15

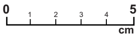

RB2 SU 4

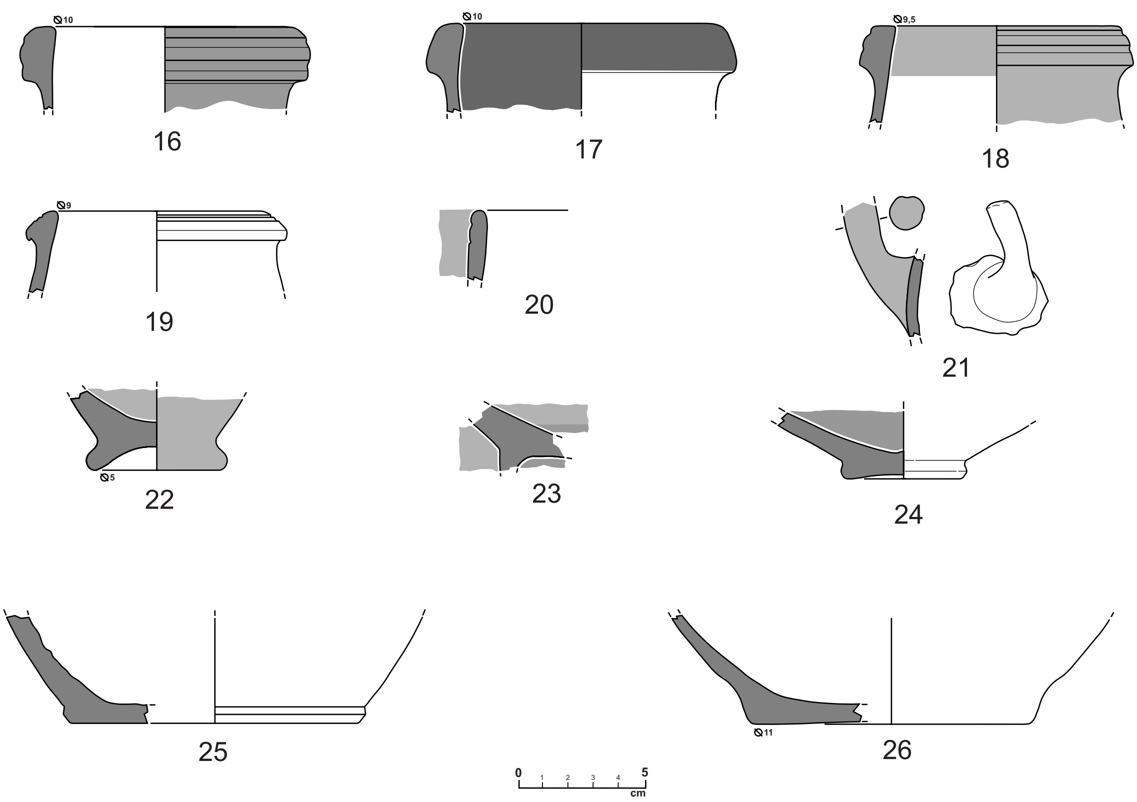

RB2 - SU 5

Definition: Compact clay

Interpretation: Level of compact clay. SU 5 may be a level of foundation for the fortification wall of Tchingiz Tepe (or for one of the alterations affecting it) and be equivalent to SU 4.

Observations: Level of compact clay. The base presents a higher presence of sand and rock nodules. It contains pottery.

Material:

Slipware:	9 shaped frags., 15 shapeless frags.
Common ware:	10 shaped frags., 55 shapeless frags.
Cooking ware:	1 shapeless frags.
Large containers:	1 shaped frags., 7 shapeless frags.
Channels:	(earthen pipe: 12 frags.)
Bone:	3 frags. (54 grs.)

Archaeologist: E. Ariño

Composition	Clay
Formation	Human origins?
Thickness	45-60 cm
Covered by (Stratum)	1
Intersected by (Negative)	14
Covering (Stratum)	9

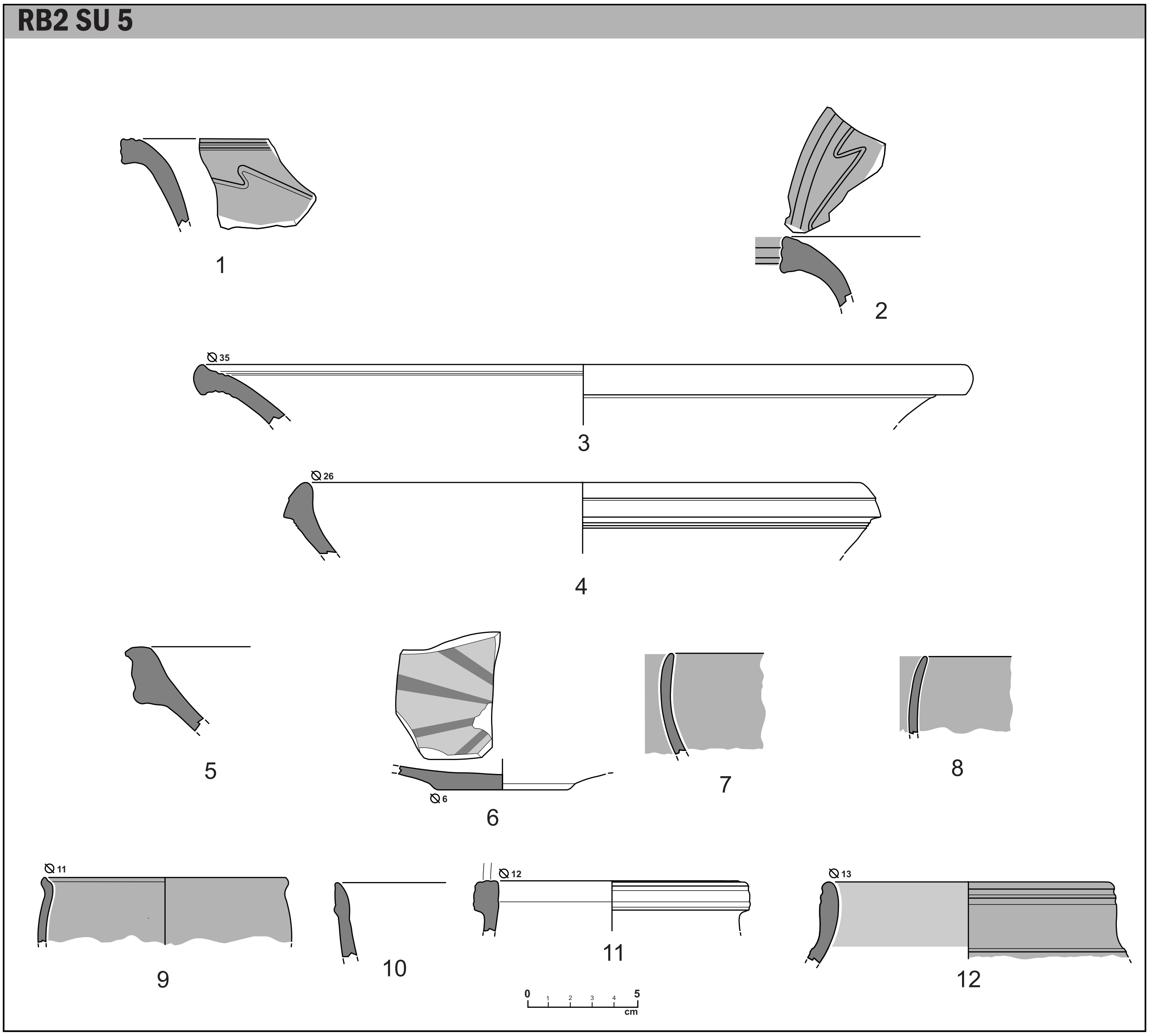
RB2 SU 5
1
2
Ø 35
3
Ø 26
4
5
Ø 6
6
7
8
Ø 11
9
10
Ø 12
11
Ø 13
12
0 1 2 3 4 5
cm

RB2 - SU 6

Definition: Level of ash

Interpretation: Ash from a fire. It may have been formed from a single use.

Observations: Level of ash and charcoal of little thickness or expanse. It contains pottery.

Material:

Slipware:	2 shaped frags., 2 shapeless frags.
Common ware:	6 shapeless frags.
Large containers:	2 shapeless frags.

Bone: 3 frags. (18 grs.)

Archaeologist: E. Ariño

Composition	Ash and charcoal
Formation	Human origins?
Thickness	1-20 cm
Covered by (Stratum)	8
Filling (Negative)	7

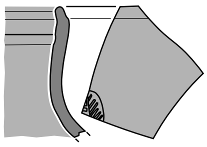

1

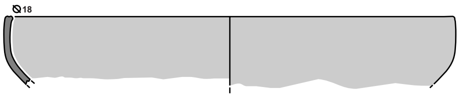

2

RB2 - SU 7

Definition: Fire

Interpretation: Fire. Probably used only once.

Observations: Negative of little depth and expanse, excavated in SU 9. It has three fragments of adobe brick in its central area.

Archaeologist: E. Ariño

Covered by (Stratum)	8
Filled in by (Stratum)	6
___________________	
Intersecting (Stratum)	9
______________________________	

RB2 - SU 8

Definition: Fragments of rock and fallen adobe bricks

Interpretation: Considered a hillside deposit, formed by slope dragging, which would justify the presence of fallen adobe bricks from the fortification wall, together with large fragments of rock from the altered roof of the substrate.

Observations: Level formed by large nodules of sandstone, siltstone and fallen adobe bricks, embedded in a clay matrix, although the matrix is very scanty. It contains pottery.

Material:

Slipware:	8 shaped frags., 13 shapeless frags.
Common ware:	21 shaped frags., 86 shapeless frags.
Cooking ware:	1 frag. shaped
Grey engobe pottery::	1 frag. shaped
Channels:	(earthen pipe: 7 frags.)
Large containers:	1 shapeless frag.
Bone:	96 frags. (400 grs.)
Other:	A ceramic tile with engobe A fragment of a clay pony

Archaeologist: E. Ariño

Composition	Fragments of adobe and rock in a clay matrix
Formation	Hillside deposit?
Thickness	20-60 cm
Covered by (Stratum)	1
Covering (Stratum)	6
Covering (Negative)	14-7

RB2 SU 8

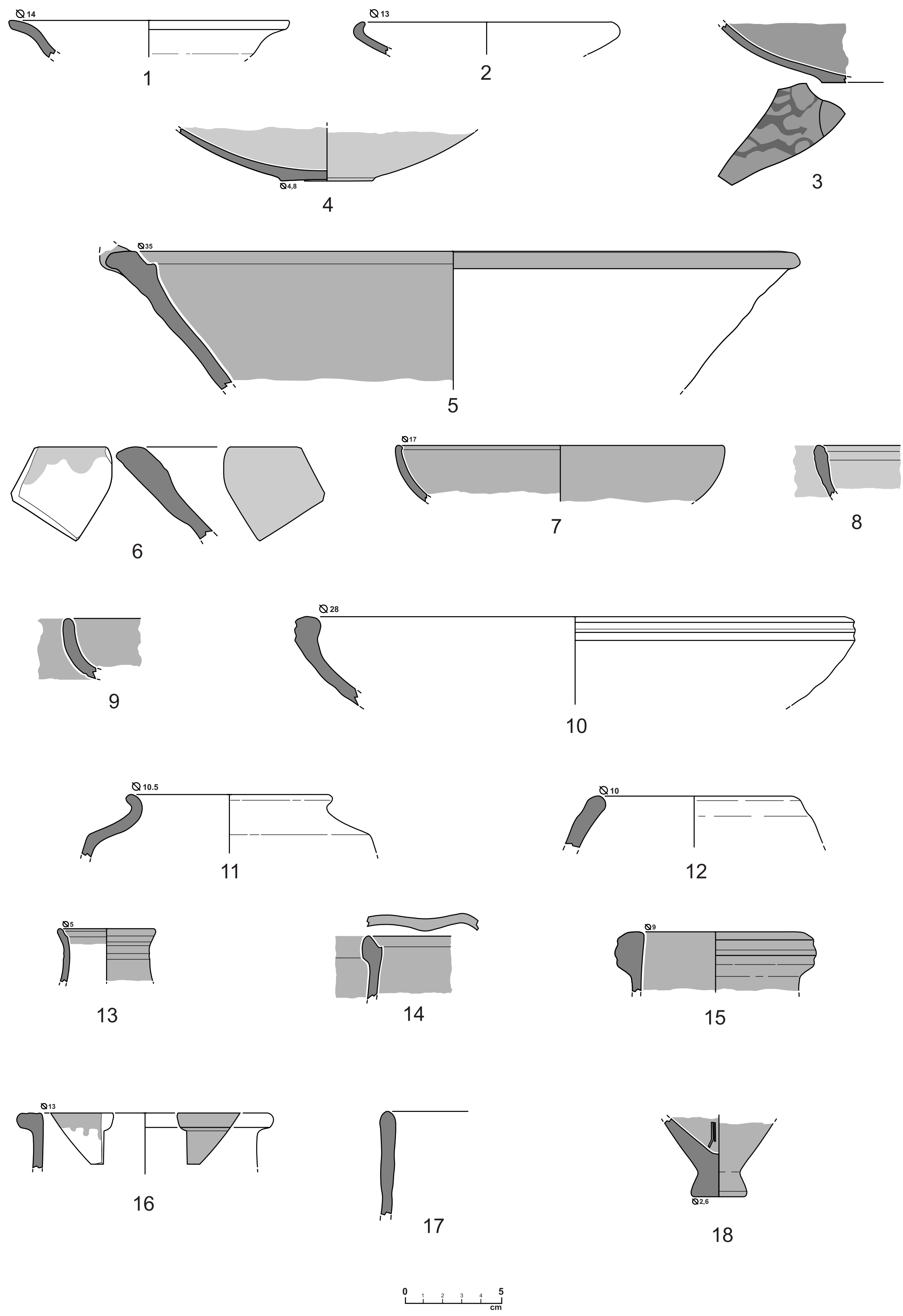
⌀ 14
1
⌀ 13
2
3
⌀4,8
4
⌀35
5
6
⌀17
7
8
9
⌀ 28
10
⌀ 10.5
11
⌀ 10
12
⌀5
13
14
⌀9
15
⌀13
16
17
⌀2,6
18
0
1
2
3
4
5
cm

RB2 - SU 9

Definition: Level yellowish-grey sand

Interpretation: Level of sand. SU 9 forms part of the levels of foundation of the fortification wall of Tchingiz Tepe or one of the alterations affecting the fortification.

Observations: Level of yellowish-grey sand with scarce fragments of adobe. It contains pottery. This stratum incorporates part of the materials of the underlying stratum (SU 10) because no interfaces of separation were uncovered in the process of excavating the northwestern corner of the trench.

Material:

Slipware:	16 shaped frags., 14 shapeless frags.
Common ware:	5 shaped frags., 56 shapeless frags.
Cooking ware:	1 shapeless frag.
Channels:	(earthen pipe: 3 frags.)
Stone building elements:	(Limestone: 1 frag.)
Bone:	5 frags. (8 grs.)
Other:	A mollusc shell

Composition	Sand
Formation	Human origins?
Thickness	c. 20 cm
Covered by (Stratum)	5-4
Intersected by (Negative)	7
Covering (Stratum)	10-11

RB2 EU 9

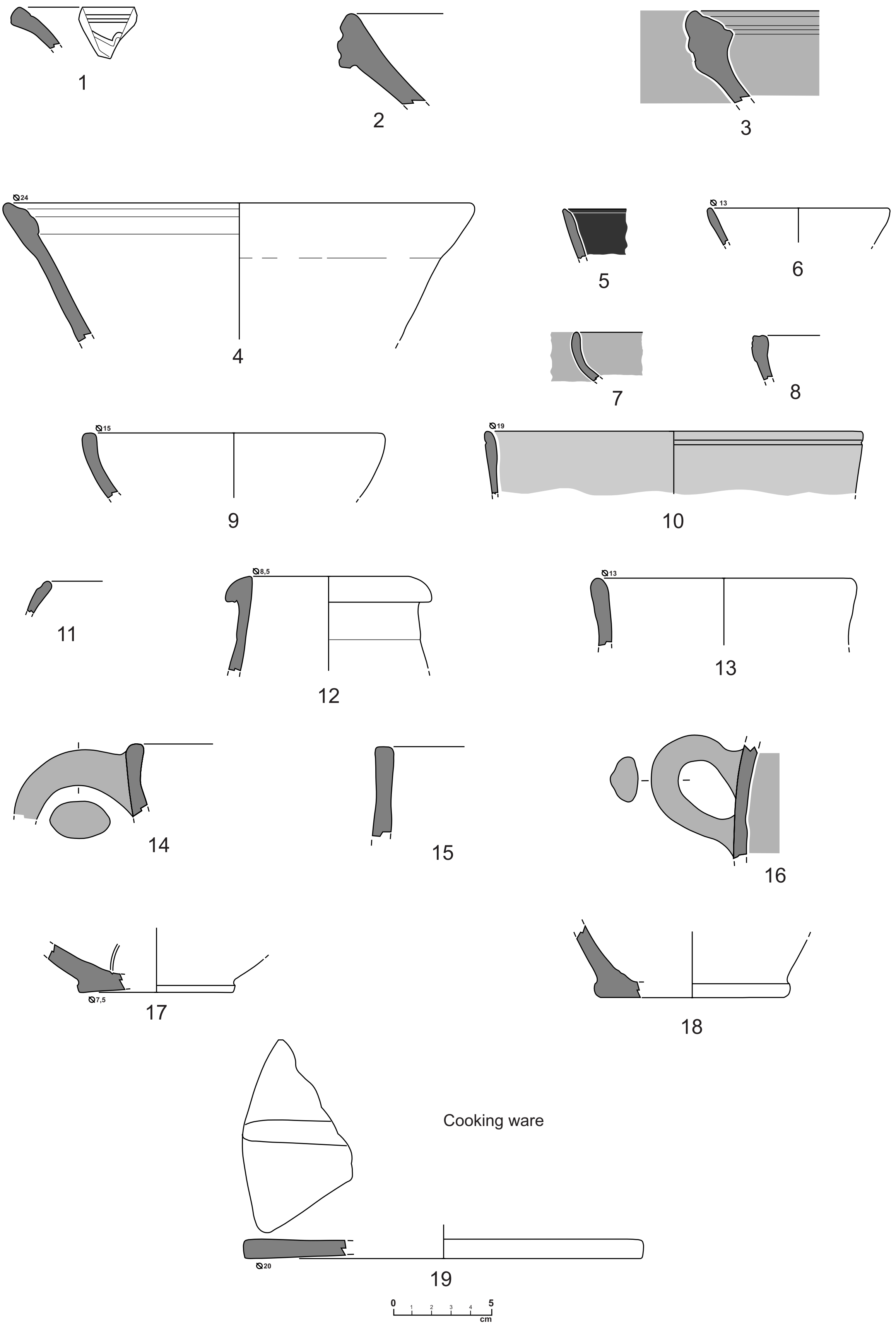
1
2
3
Ø24
4
5
Ø 13
6
7
8
Ø15
9
Ø19
10
11
Ø8,5
12
Ø13
13
14
15
16
Ø7,5
17
18
Cooking ware
Ø20
19
0 1 2 3 4 5
cm

RB2 - SU 10

Definition: Compact red clay

Interpretation: Forms part of the levels of foundation of the fortification wall of Tchingiz Tepe (or of one of the alterations affecting it), leading to the speculation that it could be a stratum of human formation. However, the stratum may be a hillside deposit.

Observations: A portion of the materials from this stratum were incorporated erroneously in SU 9 because the interfaces of separation were not uncovered in the northwestern corner of the trench during excavation.

Material:

Slipware:	11 shaped frags., 22 shapeless frags.
Common ware:	14 shaped frags., 40 shapeless frags.
Cooking ware:	3 shapeless frags.
Large containers:	1 shaped frag.
Grey engobe pottery:	2 shapeless frags.
Channels:	(earthen pipe: 3 frags.)
Bone:	7 frag. (15 grs.)

Archaeologist: E. Ariño

Composition	
Formation	
Thickness	
Covered by (Stratum)	11-12-9
Covering (Stratum)	13
Covering (Negative)	15

RB2 SU 10

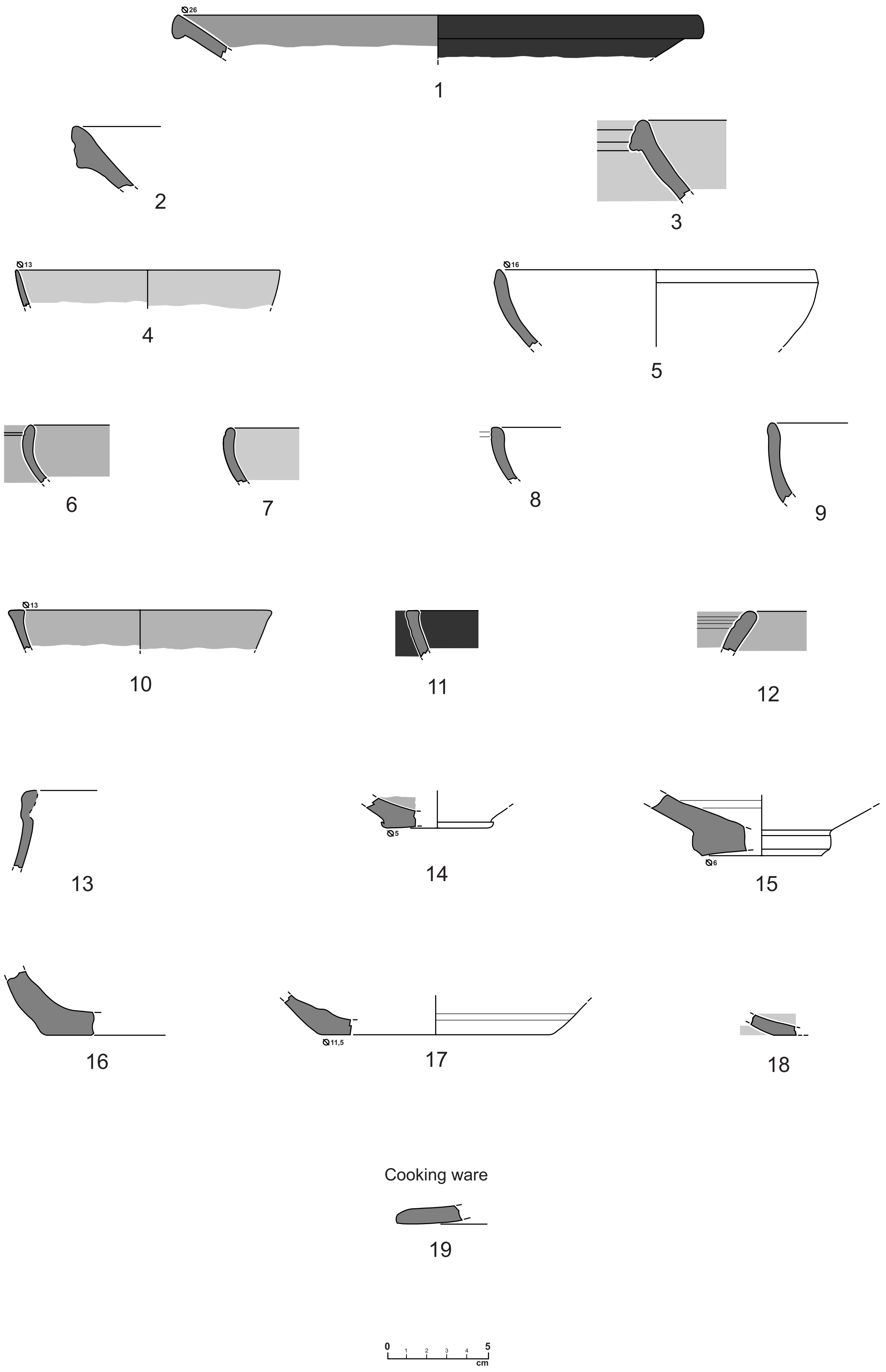
⌀26
1
2
3
⌀13
4
⌀16
5
6
7
8
9
⌀13
10
11
12
13
⌀5
14
⌀6
15
16
⌀11,5
17
18
Cooking ware
19
0
1
2
3
4
5
cm

RB2 - SU 11

Definition: Sand and small fragments of sandstone

Interpretation: Forms part of the levels of foundation of the fortification wall of Tchingiz Tepe (or of one of the alterations affecting it), leading to the speculation that it could be a stratum of human formation. However, the stratum may be a hillside deposit.

Observations: Small fragments of rock (sandstone and siltstone) in a grey sand matrix. It contains no pottery.

Archaeologist: E. Ariño

Composition	Sand and small sandstone fragments
Formation	Human origins? Hillside deposit?
Thickness	
Rested on by (Structure)	38
Covered by (Stratum)	4-1-9
Covering (Stratum)	10

RB2 - SU 12

Definition: Sand and small fragments of sandstone

Interpretation: Forms part of the levels of foundation of the fortification wall of Tchingiz Tepe (or of one of the alterations affecting it), leading to the speculation that it could be a stratum of human formation. However, the stratum may be a hillside deposit.

Observations: Small fragments of rock (sandstone and siltstone) in a sand matrix. It contains pottery, albeit in small quantities. It is equivalent to SU 11, but a step exists between the two strata to justify their individual treatment.

Material:

Slipware:	2 shaped frags., 4 shapeless frags.
Common ware:	2 shaped frags., 17 shapeless frags.
Large containers:	2 shaped frags.
Channels:	(earthen pipe: 5 frags.)

Archaeologist: E. Ariño

Composition	Sand and small fragments of sandstone
Formation	Human origins?
Thickness	
Covered by (Stratum)	1
Covering (Stratum)	10

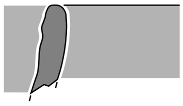

1

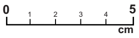

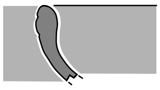

2

RB2 - SU 13

Definition: Bedrock

Interpretation: Substrate.

Observations: Substrate. Grey sandstone.

Archaeologist: E. Ariño

Intersected by (Negative)	15
Covered by (Stratum)	10

SU 13, 15

RB2 - SU 14

Definition: Interfaces. Level of demolition

Interpretation: Interfaces. Level of demolition affecting the fortification wall of Tchingiz Tepe and its foundations.

Observations: Interfaces. Surface of the demolition of the fortification wall of Tchingiz Tepe and its foundations.

Archaeologist: E. Ariño

Covered by (Stratum)	1-8
Intersecting (Structure)	38
Intersecting (Stratum)	4-5

RB2 - SU 15

Definition: Cut in the substrate

Interpretation: Intentional cutting in the substrate. Possible preparation for the foundation of the first fortification of Tchingiz Tepe.

Observations: A small step, with a maximum height of approximately 25 cm, carved in the sandstone substrate.

Archaeologist: E. Ariño

Covered by (Stratum)	10
Intersecting (Stratum)	13

RB2 - SU 38

Definition: Fortification wall of adobe bricks

Interpretation: Level formed part of the adobe fortification of Tchingiz Tepe. It is highly unlikely that the portion of the fortification affected by the excavation corresponds to the original curtain wall. In the western part of the tower, immediately above the excavated levels and between the adobe bricks of tower 9, at least two white lines can be seen, indicating an eliminated wall cladding, which would be a sign that tower 9 presents several phases of occupation and renovation. In addition, immediately beneath two visible courses of adobe bricks in the western stratigraphic cross-section, it is possible see a thin reddish line, possibly evidence of the floor of a hearth. The excavation yielded no remains of the floor of this possible dwelling, which would appear to have been completely demolished, because it would reach a level higher than the roof of SU 1.

Observations: At least two courses of adobe bricks are conserved from the adobe fortification in the western curtain wall at tower 9, although they are quite eroded.

Archaeologist: E. Ariño

Composition	Wall of adobe bricks
Formation	Human origins
Thickness	
Intersected by (Negative)	1
Resting on (Stratum)	4-11

Report on the analysis of charred wood remains from Tchingiz Tepe (Termez)

Raquel Piqué
Archaeological Analysis Service
Universitat Autònoma de Barcelona

The analysis of charcoal from archaeological sites makes it possible to identify the plant raw materials used by human groups at different times in history. Throughout history, plant raw materials have been largest resource used in the production of energy through combustion. Before the widespread use of fossil fuels (coal, gas and oil) in the nineteenth century, wood and charcoal were commonly adopted for domestic use and in crafts. The analysis of residue from combustion can show how a society has satisfied its energy demands and, at the same time, how the management of forest resources has changed with increases in energy demands or as a result of environmental changes.

Wood is gathered by a society from the forested areas surrounding its settlements. Clearly, the offering of resources in its surrounding affects a society's use of raw materials: the availability of resources is a condition for use. Nonetheless, not all raw materials in the environment are used simply because they are available. Social factors also have an effect on the design of strategies for managing resources. On the one hand, the demand or amount of energy needed to ensure production and reproduction determines the amount of raw material to gather. On the other hand, the technological capabilities and social relations affecting production are also determinant factors. The design of strategies for managing resources is also influenced by factors such as transport capability, the possibility of reproducing resources and the specialisation of sectors of society in the production of plant-based fuel (e.g., woodcutters and coal miners).

Based on the analysis of charcoal, we can reconstruct strategies for the supply and use of plant-based fuel. First, by identifying the trees and bushes in the landscape that were used by groups of humans, we can evaluate how fuel is gathered (e.g., catchment areas and random or selective patterns of collection) and obtain crucial information on the transformations undergone by the landscape and how the increasing pressure of humans influenced this environment. Second, we can evaluate how fuel was used, examining the activities to which it was linked and specifying differences between the domestic and crafts areas.

The objective of examining charcoal from the excavations at Termez is to analyse how wood resources were used. By characterising the strategies for the supply and use of fuel, we can gain an understanding of the settlement's ongoing influence on its environment, any transformations occurring in the strategies of fuel provision and use, and the causes behind these changes.

Methodology

In order to identify the charred wood remains, we compare their microanatomy with current reference samples. Microanatomic study requires the observation of three anatomic sections of wood: transverse, radial longitudinal and transverse longitudinal. Charcoal is fractured manually and the surfaces obtained are studied with the aid of an optical microscope with reflected light, equipped with dark field-bright field and objective lenses that allow magnification of 50 to 400 times. For reference material, we have used the collection of current charred wood in the Archaeological Analysis Services of the Universitat Autònoma de Barcelona and specialist bibliography (Schweingruber 1990).

Analysed material and results

The analysed samples come from three SUs: SU 6, SU 23 and SU 36. The samples were abundant and in a good state of conservation. Given the abundance of the remains, a sampling was carried out with diversity in mind: 75 fragments were studied in the case of SU 23 and SU 36, while 50 fragments of charcoal were analysed for SU 6, which reflected greater diversity. In total, the analysis examined 200 fragments of charcoal, making the sample very representative for the purposes of documenting the most frequently used species. The analysis was able to establish the consumption of a minimum number of 12 species: Mediterranean hackberry (*Celtis australis*), oleaster (*Eleagnus angustifolia*), an indeterminate type of juniper (*Juníperus sp*), monocotyledons, plane tree (*Platanus sp*), an indeterminate fruit tree (*Rosaceae/Maloideae*), a second indeterminate fruit tree (*Prunus sp*), an indeterminate willow or poplar (*Salicaceae*), tamarisk (*Tamarix sp*), elm (*Ulmus sp*) and common grape vine (*Vitis vinifera*).

Sector	RB-Z	RA	RA	
SU	SU 6	SU23	SU36	Total
Number of sample	25	10	14	
Celtis australis	1			1
Eleagnus angustifolia	16	8	2	26
Indeterminada		1	2	3
Juniperus sp		1	3	4
Monocotiledònia		11	1	12
No determinable		4	3	7
Platanus orientalis	31	2	22	55
Rosaceae/Maloideae			1	1
Prunus sp		1		1
Salicaceae		37	32	69
Tamarix sp		5	8	13
Ulmus sp	2		1	3
Vitis vinifera		5		5
Total	50	75	75	200

Table 1.- Results of the anthracological analysis

Below, a detailed description is provided of the anatomical characteristics, ecological requirements and known uses of the species listed above.

Celtis australis (Mediterranean hackberry))

Anatomy

- Transverse section (figure 1): Porous wood. Latewood pores are associated with tangential and oblique bands of parenchyma.
- Tangential section (figure 2): Rays are 4 to 8 cells in width.
- Radial section: Heterogeneous rays. Helicoidal thickenings in small vessels.

Ecology

- The hackberry lives in sandy, well-drained soil, even if the soil is poor. It cannot live in shady places.

Properties of the wood

- The wood is very hard, of medium density and very flexible. It is used in woodworking (e.g. with lathes) and to make charcoal.

Charcoal characteristics

- The charcoal is primarily in shapeless fragments. The growth rings have a strong to moderate curvature.

Figure 1.- Transverse section of *Celtis australis*

Figure 2.- Tangential longitudinal section of *Celtis australis*

Eleagnus angustifolia **(oleaster)**

Anatomy

- Transverse section (figures 3 and 4): Porous to semiporous wood. Isolated vessels.
- Radial and tangential longitudinal section (figure 5): homogeneous 2- to 5-seriate rays. Presence of spiral thickenings.

Ecology

- A species native to western and central Asia, the oleaster principally grows on the woodland riverbanks and in other wet environments. It forms mixed woods with tamarisk. It can tolerate soil salinity.

Properties of the wood

- Oleaster is considered a good fuel.

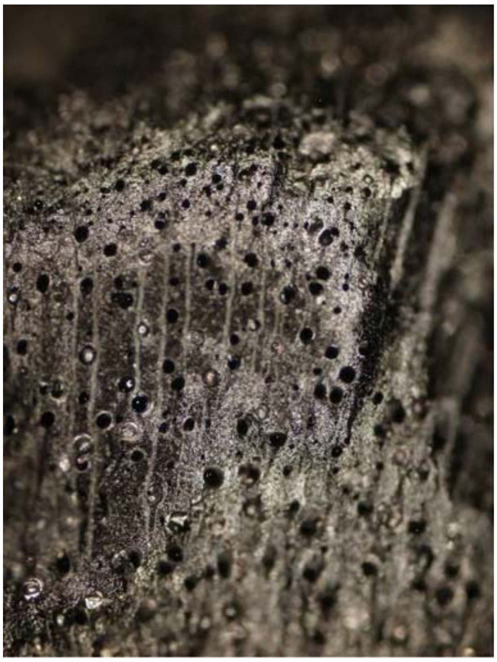

Figure 3.- Transverse section of *Eleagnus angustifòlia*

Figure 4.- Transverse section of Eleagnus angustifòlia

Figure 5.- Tangential longitudinal section of Eleagnus angustifolia

Charcoal characteristics

- In general, the fragments are shapeless. Growth rings principally show weak or moderate curvature, but in some cases strong as well, indicating primarily the use of wood of a certain calibre.

Indeterminate

Two fragments have not been determined because their anatomy does not coincide with the anatomy described in the consulted bibliography or the modern reference materials.

Anatomy

- Transverse section (figure 6): diffuse wood. Vessels are large, isolated or in groups of two.
- Tangential section (Figure 7): biseriate and triseriate rays. Small intravascular pitting. Simple perforation plates.

Figure 6.- Transverse section of an indeterminate species

Figure 7.- Tangential section of an indeterminate species

***Juniperus* sp.** (juniper)

Anatomy

- Transverse section (figure 8): homoxylous wood. Resin ducts absent.
- Radial tangential section (figure 9): very short rays, between 2 and 5 cells in width. Cross-hatching with cuppressoid pitting.

Ecology

- Several species of juniper are native to Central Asia, including *Juniperus excelsa*, J. *polycarpos* and J. *semiglobosa*. They occupy a wide range of habitats.

Properties of the wood

- It is used to make charcoal and in carpentry and joinery.

Charcoal characteristics

- Shapeless fragments, growth rings with weak curvature. They come from a large trunk or branch.

Figure 8.- Transverse section of *Juniperus sp*

Figure 9.- Tangential longitudinal section of *Juniperus sp*

Monocotyledons

This group includes remains showing the presence of primary xylem and phloem (figures 10, 11 and 12). The remains are fragments of variable calibre, between 1-3 cm in diameter. Based on the dimensions of the remains, we believe that they could be from a kind of reed. However, we do not discard the possibility that different species may be represented in the remains.

Figure 10.- Transverse section of monocotiledònia1

Figure 11.- Transverse section of monocotiledònia 2

Figure 12.- Transverse section of monocotiledònia 3

Platanus orientalis (Plane tree)

Anatomy

- Transverse section (figure 13): diffuse to semiporous wood. Highly numerous, clustered vessels.
- Very distinct growth rings with rays that flare at this height. Diffuse apotracheal parenchyma.
- Radial and tangential longitudinal section (figure 14 and 15): Simple and scalariform perforation plates with a variable number of bars. Homogeneous rays, between 4 and 10 cells in width and up to 2 mm in length.

Ecology

Deciduous tree that lives near rivers and streams.

Properties of the wood

- Hardwood, hard to split and not very durable. It is used in carpentry.

Charcoal characteristics

- The sample primarily contains shapeless fragments, with growth rings that have a weak to moderate curvature, indicating that they come from branches or trunks of some size.

Figure 13.- Transverse section of Platanus orientalis

Figure 14.- Tangential longitudinal section of *Platanus orientalis*

Figure 15.- Radial longitudinal section of *Platanus orientalis*

Prunus sp (cherry, peach, etc)

Anatomy

- Transverse section (figure 16): Semiporous wood, vessels in radial rows and in groups
- Radial tangential section (figure 17): rays of four to six cells in width, uniseriate. Heterogeneous rays, vessels with spiral thickenings.

Ecology

- Fruit tree from which different species and varieties are cultivated. It is not possible to determine whether this is from a cultivated or wild species.

Charcoal characteristics

Shapeless fragments. Weak to moderate curvature.

Figure 16.- Transverse section of *Prunus sp*

Figure 17.- Pla tangencial *Prunus sp*

Rosaceae/Maloideae (pear, apple, etc)

A large number of genera and species with highly similar anatomy belong to this group, including *Pirus* (pear), *Malus* (apple), *Crataegus* (hawthorn), *Sorbus* (rowan).

Anatomy

- Transverse section (figure 18): diffuse porosity, isolated vessels of small size.
- Radial and tangential section (figure 19): biseriate rays, homogeneous, simple perforation plates

Ecology

- Some specimens are cultivated to obtain edible food. It is not possible to establish from the anatomy whether the sample is from a domestic species.

Charcoal characteristics

Shapeless fragments. Weak to moderate curvature.

Figure 18.- Transverse section of *Rosaceae/Maloideae*

Figure 19.- Tangential longitudinal section of *Rosaceae/Maloideae*

Salicaceae (willow, black poplar, white poplar)

Salix sp and *Populus sp* share most of their anatomical traits. Distinguishing between them is only possible by means of the heterogeneity and homogeneity of their rays, although this is not always possible to observe clearly. We have chosen to consider the remains within the broader group of Salicaceae.

Anatomy

- Transverse section (figure 20): Diffuse or semiporous wood. The pores can appear isolated or in short rows of rays.
- Radial and tangential section (figure 21): The rays are uniseriate, homogeneous and heterogeneous.

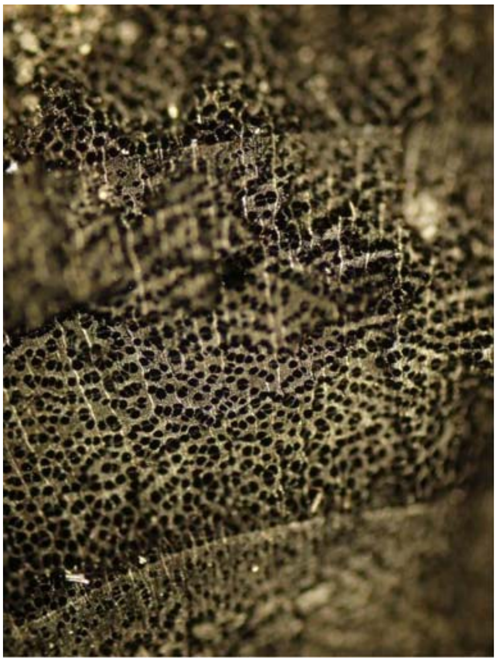

Figure 20.- Transverse section of *Salicaceae*

Figure 21.- Pla longitudinal *Salicaceae*

Ecology

- The species is basically found on the banks of rivers and streams.

Properties of the wood

- Wood of moderate hardness and very low density. It is used in carpentry.

Charcoal characteristics

- The charcoal fragments are very large and have a very weak curvature of the growth rings, which together with the size of the remains suggests that the fragments come from large trunks and branches.

Tamarix sp. (tamarisk bush)

Anatomy

- Transverse section (figure 22): Porous wood. The vessels are solitary or in small groups.
- Radial tangential section (figure 23): multiseriate rays of up to 20 cells in width, heterogeneous.

Ecology

- Tamarisk bushes live on the banks of rivers and streams in arid and saline terrains.

Charcoal characteristics

- Shapeless fragments.

Figure 22.- Transverse section of de Tamarix sp

Figure 23.- Tangential longitudinal section of de *Tamarix sp*

Ulmus sp (elm)

Anatomy

- Transverse section (figure 24): Porous wood; the vessels of earlywood appear solitary or in groups of up to three, while the latewood appears in tangential/oblique groups with parenchyma.
- Radial and tangential longitudinal section: the rays have between 4 and 5 cells in width. Cells of rays are homogeneous, vessels with spiral thickenings.

Figure 24.- Transverse section of *Ulmus sp*

Ecology

- This species typically inhabits riverbank woodlands.

Properties of the wood

- Hardwood of medium to low density. It is used in joinery, carpentry and woodturning.

Vitis vinifera **(common grape vine)**

Based on anatomy, it is not possible to distinguish the wild variety from the cultivated variety.

Anatomy

- Transverse section (figure 25): Porous wood tending to semiporous. Very large vessels, solitary or clustered in radial rows in latewood.

Figure 25.- Transverse section of Vitis vinifera

Figure 26.- Tangential longitudinal section of *Vitis vinifera*

- Radial and tangential longitudinal section (figure 26): Multiseriate rays. Vessels with scalariform perforation plates with a large number of bars.

Ecology

- In a wild state, the common grape vine lives on riverbanks. Many varieties of this species are cultivated.

Charcoal characteristics

- The remains correspond to branches of variable thickness, up to approximately 20 mm in diameter. In one case, it was possible to count up to 7 growth rings. The time of cutting cannot be established.

Discussion of the results

The set of charcoal fragments collected in the 2010 season at Tchinguiz Tepe have a highly diverse composition. The taxa determined by the analysis reflect a large degree of taxa living in wet environments near waterways: *Eleagnus angustifolia*, *Platanus orientalis*, *Salicaceae*, *Tamarix*, *Ulmus*. These taxa represent 86% of the remains, indicating that this type of plant community was systematically used to obtain plant fuel. These taxa also include species that are highly tolerant of soil salinity (*Tamarix*, *Eleagnus*), which are species that frequently form mixed woodlands in Central Asia (CAREC 2006). Riverine species are also well-represented in the anthracological collection from the previous season (Piqué 2009), although we have been able to establish a greater diversity of this type of vegetation this year. In addition, *Celtis australis* is a species typical of dry environments and also common in Central Asia.

Another noteworthy subset of the sample is made up of species that can be used for food. Three of the established taxa correspond to fruit trees: *Pomoidea*, *Prunus sp*, *Vitis vinifera*. They represent 3.6% of the remains. Based on the anatomy, it is not possible to determine whether the wood remains correspond to domestic species, but we cannot discard some relationship with arboriculture. The use of pruning as a source of fuel is a common practice in societies where arboriculture is practiced. Among the remains of grape vine, we found branches of small diameter, strengthening the idea that they resulted from pruning. In one case, we were able to count the age of the branch at the time it was cut; it was seven years old. The analysis from the previous season (Piqué 2009) also yielded remains of other fruit trees, especially the common fig (*Ficus carica*) and the common grape vine (*Vitis vinifera*).

Monocotyledons made up 6.2% of the identified remains and constituted a group that was difficult to interpret, because it was not possible to determine the specific species to which the remains corresponded. The remains were stems with large diameters, reaching 1 to 3 cm, suggesting that they may correspond to some large grasses. Several species of monocotyledons grow in Central Asia.

Lastly, we also found *Juniperus sp*, but the species could not be established and, therefore, its specific origin could not be established either. It is represented in only four remains, indicating isolated use.

In conclusion, the sample points to a use of local species for wood, which constitutes the bulk of fuel. Clippings from pruning were probably used as well. The great taxonomic diversity of the remains indicates an unspecialised use of fuel. The charcoal remains corresponded principally to shapeless remains, except in the case of Vitis vinifera and the monocotyledons, in which the original morphology could not be observed.

These results contrast with the results obtained from the previous season (table 2), because a larger number of taxa have been determined. However, in both cases, riverine species are the best represented, indicating that the same catchment areas were visited to obtain wood as a raw material. The specific processes of formation of the SUs would explain the observed differences.

sector SU	2010 RB-Z SU8	2010 RA SU 23	2010 RA SU 36	2008 SU 26	2008 KPT-C14-4
Celtis australis	2	0	0	0	0
Eleagnus angustifolia	32	11,26761	4,255319	0	0
Ficus carica	0	0	0	0	19,60784
Fraxinus sp	0	0	0	0	23,52941
Graminea	0	0	0	100	0
indeterminada	0	1,408451	4,255319	0	0
Juniperus sp	0	1,408451	6,382979	0	0
Monocotiledònia	0	15,49296	2,12766	0	0
no determinable	0	5,633803	6,382979	0	0
Platanus orientalis	62	2,816901	46,80851	0	38,23529
Pomoideae	0	0	2,12766	0	0
Prunus sp	0	1,408451	0	0	0
Salicaceae	0	52,11268	68,08511	0	7,843137
Tamarix sp	0	7,042254	17,02128	0	0
Ulmus sp	4	0	2,12766	0	0
Vitis vinifera	0	7,042254	0	0	10,78431
Total taxa	4	9	9	1	5

Table 2.- Comparison of the results from 2010 and 2008 seasons, expressed in %

Bibliografia

CENTRAL ASIA REGIONAL ECONOMIC COOPERATION (CAREC) 2006 Non Wood Forest Products in Central Asia and Caucasus. Roma: FAO

PIQUÉ, R. (2009). Informe de l'anàlisi antracològica de Termez. Servei d'Anàlisis Arqueològiques

SCHWEINGRUBER, F. (1990) Anatomy of European Woods. Bern/Stuttgart: Paul Haupt

Analysis of fecal phytoliths and spherulites in samples of sediment from the archaeological site at Tchingiz Tepe, Termez

Marta Portillo , Carolina Sánchez i Rosa Maria Albert
Grup d'Estudis Paleoecològics i Geoarqueològics, GEPEG,
Universitat de Barcelona

Introduction

Our analysis addressed fecal phytoliths and spherulites in two samples from Tchingiz Tepe (Termez, Uzbekistan). The analysed samples come from sediments retrieved during the archaeological interventions of 2009 in sector RC (SU 2). This stratigraphic unit is defined as a level of demolition related to the collapse of the wall of the fortification, made up of adobe bricks and abundant building material (Ariño, 2009). The chief objective of analysing the phytoliths and spherulites was to identify the plant and fecal microremains in these sediments.

Methodology

A description of the methodology used in the extraction, identification and quantification of phytoliths appears below (Albert et al., 1999). A sediment sample of approximately 1 g is treated with 10 ml of a solution of hydrochloric acid (3N HCl) and nitric acid (3N HNO_3). When the sample has been clarified to remove the acid, a quantity of approximately 10 ml of hydrogen peroxide (H_2O_2) at 30% is added. The purpose of these processes is to remove the carbonates and phosphates, as well as the organic material, because they can hamper the correct identification and quantification of phytoliths. After application of these processes, what remains are only the components that are most insoluble and resistant to acid. Included in these components are phytoliths. The insoluble fraction left from the attack by the acids is called the acid-insoluble fraction (AIF). The mineral components of the AIF are then separated by density in order to concentrate the phytoliths in the same fractions. To perform the separation of the fractions, we concluded the preparation procedure by adding 5 ml of sodium polytungstate [Na_6 (H_2 W_{12} O40) H_2O] at a density of 2.4 g/ml.

To examine the samples under a microscope, we prepared slides with approximately 1 mg of material and added 3 or 4 drops of Merck's New Entellan. The samples were mixed with the Entellan so that it was randomly distributed and then they were covered. The total area of the sample on the slide was estimated by counting the total number of fields containing sediment. The phytoliths were counted in a known number of fields selected at random under 400 magnifications. It was always possible to count at least 200 phytoliths. Counting this number of phytoliths was shown to give a margin of error of around 20% in the interpretation of the results (Albert and Weiner, 2001). The morphological assignment of phytoliths is based on the specialist literature (Twiss et al., 1969; Brown, 1984; Rosen, 1992; Mulholland and Rapp, 1992; Piperno, 2006) and on the International Code for Phytolith Nomenclature (Madella *et al*., 2005). The descriptions are based on the identification of the cells in which phytoliths are formed. When this was not possible, strictly geometric criteria were adopted.

In the analysis of spherulites (fecal microremains), we followed the methods proposed by Canti (1999). We prepared slides with approximately 1 mg of material and mixed them with New Entellan (Merck) so that the sample was homogeneously dispersed. The total area of the sample was quantified by counting the total number of fields containing sediment, in the same manner described above for the phytoliths. The slides were examined under an Olympus BX41 optical microscope and digital images were taken with an Olympus Colour View Ilu camera.

Results

Table 1 relates the description and location of the analysed samples, together with the principal results obtained from the quantitative analysis of phytoliths and spherulites. These results are expressed as the percentage of the acid-insoluble fraction (AIF), the total number of phytoliths estimated per gram of AIF, the number of phytoliths identified morphologically, the percentage of phytoliths altered by the effects of dissolution and the number of spherulites per gram of sediment.

The results obtained from analysing the acid-insoluble fraction (AIF) show a similar mineralogical composition in the two analysed samples. The percentage of AIF (fraction composed principally of clay, quartz and phytoliths) varies between 70% and 73%, approximately (Table 1). This is a relatively high proportion, indicating that the sediments are principally made up of silica materials.

With respect to the quantitative analysis of the phytoliths, the results vary significantly. The total number of phytoliths estimated per gram of AIF ranges from 846,000 and 3.2 million (samples 1 and 2, RC-2-1 and 2, respectively) (Table 1). Another important aspect to bear in mind when interpreting the results is the state of preservation of the phytoliths in the examined sediments. In general, signs of chemicals alteration could be seen on their surfaces, although in most cases this dissolution did not affect the morphological characterisation of the phytoliths. The percentage of phytoliths affected by the chemical dissolution stood at around 6% in both samples (Table 1), which can be considered relatively low.

Number of sample	Unit	% AIF	No. of phytoliths per 1 g of AIF	No. of phytoliths identified	% altered phytoliths	No. of spherulites per 1 g of sediment	Description
1	UE 2	73.4	846.000	446	5,6	515.000	Sediment RC-2-1
2	UE 2	70.2	3.266.000	779	5,8	1.065.000	Sediment RC-2-2

Table 1. Tchingiz Tepe, Termez (Uzbekistan). Description and location of the analysed samples and principle results obtained from the analysis of phytoliths and spherulites.

The results from the morphological analysis of the phytoliths appear in Figure 1. The results are clustered according to type of plant and plant part in which the phytoliths were formed. A similar plant component can be seen, with a clear predominance of monocotyledons, mostly characterised by the family of graminoids (more than 80% of the total of quantified phytoliths, Fig.1). The phytoliths of graminoids have been studied morphologically according to which come from stems and leaves and which come from the inflorescences, the part of these plants were the seeds can be found (Fig. 2). In the latter case, the results were definitely homogeneous. The phytoliths derived from the inflorescences are represented by percentages that range approximately from 45% to 49% (Fig. 2). The abundance of short cells (Fig. 3a) indicates that these graminoids are largely from type C3 (Twiss, 1992), which fall under the subfamily Pooideae. To a lesser extent, the analysis also identified another type of short cell that is diagnostic of the subfamilies Cloridoideae and Panicoideae (Fig. 3b). The parts of the inflorescences are well characterised by the elevated presence of long cells with spiny, dendritic edges (fig. 3c). There are also graminoids with silicified multicellular structures (silica skeletons or multicellular phytoliths). Some of these structures are formed of long dendritic cells and specific epidermal appendages, such as papillae (Fig. 3d). With respect to the characteristic morphologies of the leaves of the same group of plants, the results identified the presence of bulliform and trichome cells (Fig. 3e).

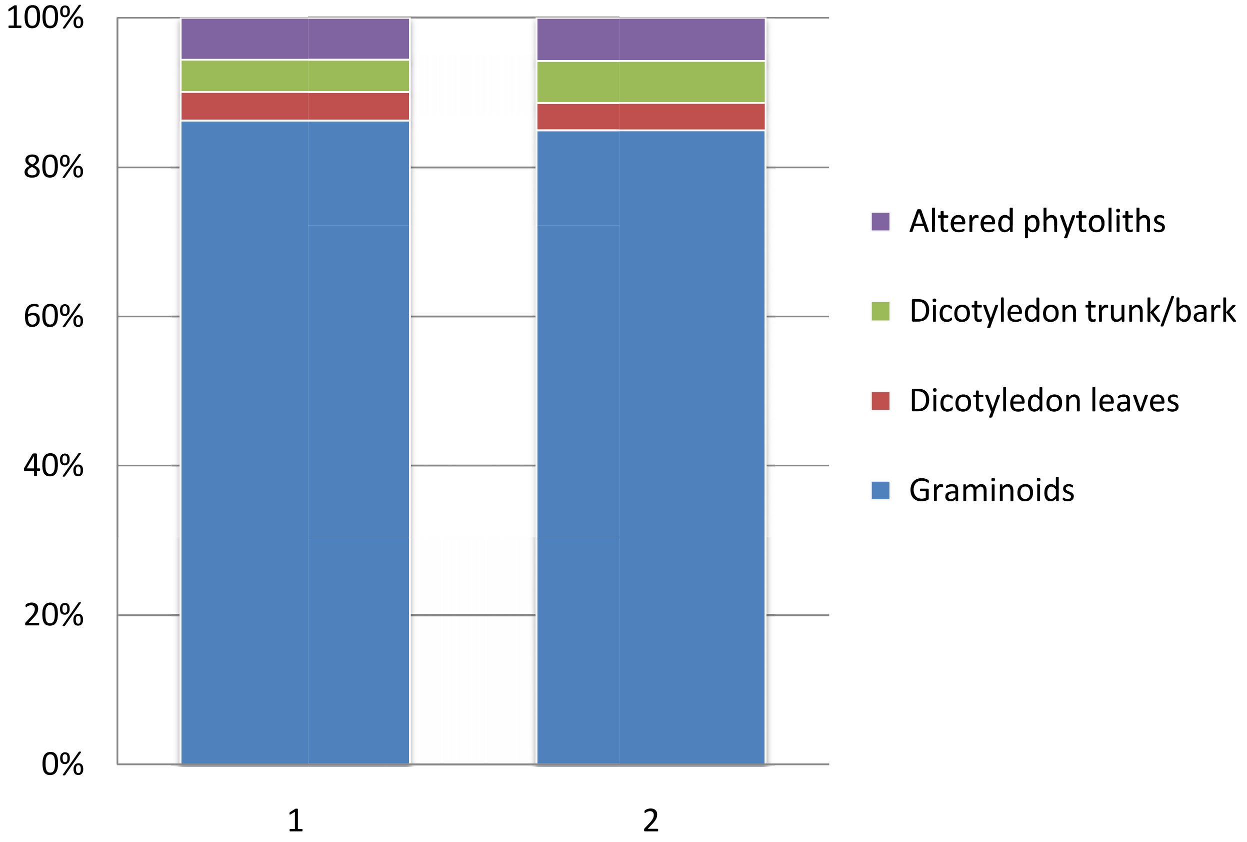

Fig. 1: Results of the morphological analysis of the phytoliths identified in the samples.

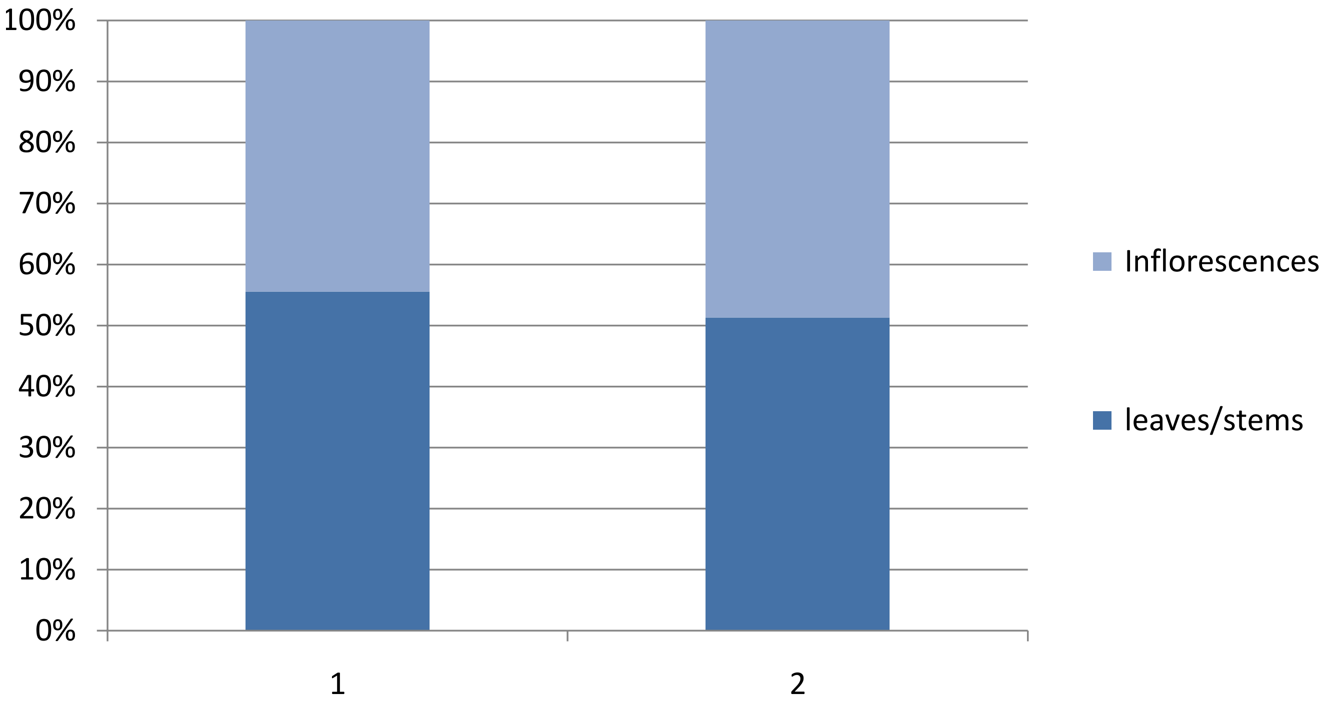

Fig. 2: Results of the morphological analysis of the phytoliths of graminoids. Comparison of the percentage of leaves/stems and inflorescences.

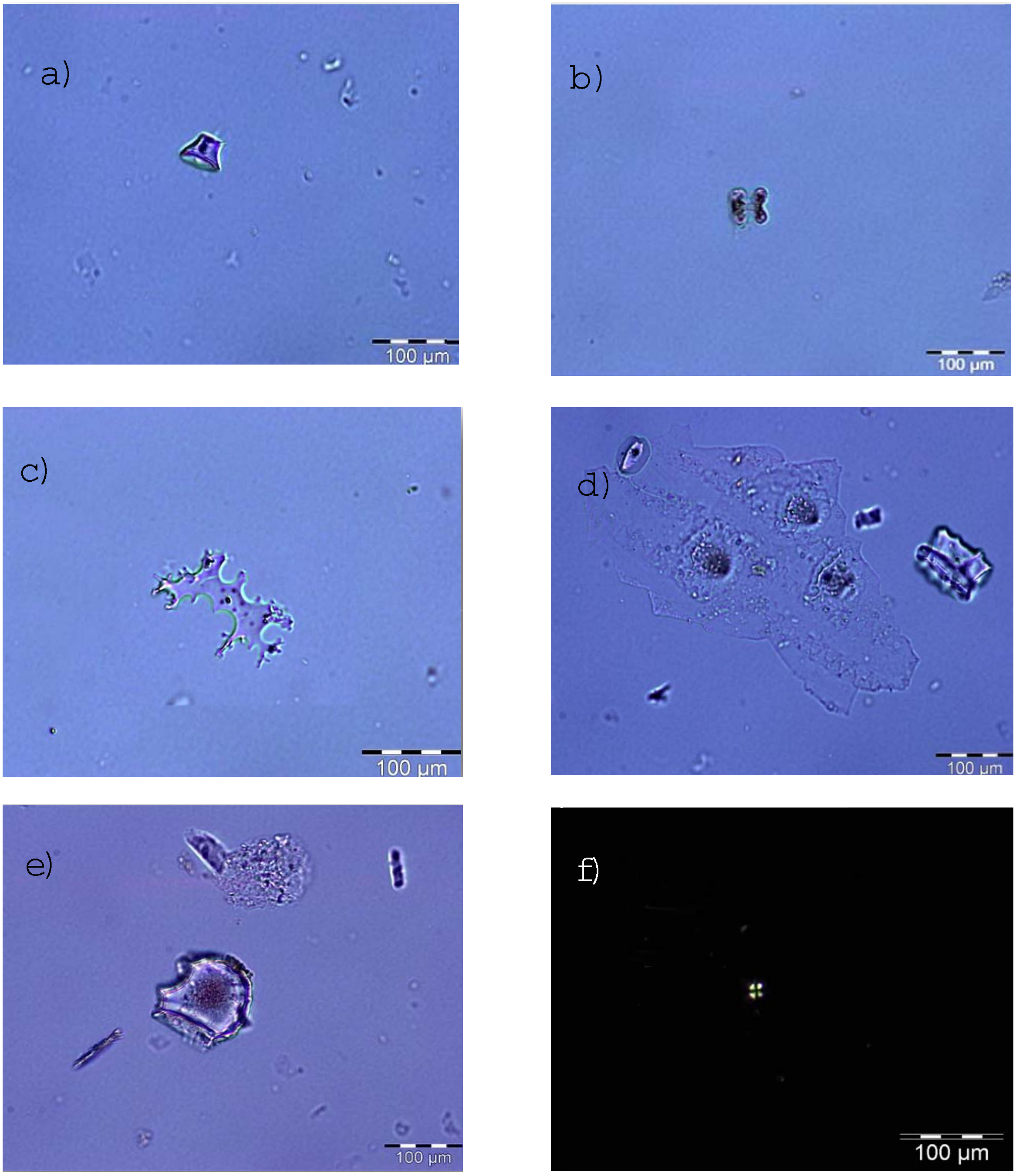

Fig. 3: Microphotographs of phytoliths and other microremains identified in the samples. The photographs were taken at 400x: a) short cell, b) bilobed short cell, c) dendritic long cell, d) multicellular structure with long cells and papillae, e) bulliform cell, f) fecal spherulite.

Lastly, the analysis identified the presence of fecal spherulites (Table 1, Fig. 3f). Spherulites are crystals of calcium carbonate produced in the digestive tract of certain animals, largely herbivores, which are found in excrement and can be deposited in sediments together with other remains (Brochier et al., 1992; Canti, 1997, 1998, 1999). Spherulites are direct indicators of fecal remains.

Interpretation

The analysis uncovered homogeneity among the examined sediments at the level of mineral composition and plant composition, which were similar. The only significant differences observed in the sample concern the amounts of phytoliths and spherulites obtained, which were more abundant in sample 2 (sediment RC-2-2). You can also see a clear correlation between the abundance of fecal and plant microremains in both samples. These results indicate that the analysed sediments are at least partly made up of fecal remains.

The observed plant component basically corresponds to graminoids of the Poaceae subfamily, which are characteristic of temperate and wet climates. This group includes such important cereals as wheat, barley and oats. However, the morphologies of the phytoliths identified in this analysis are not diagnostic of any species in particular. We observed silicified multicellular structures, also called silica skeletons. Multicellular structures are produced in abundance when a significant silicification of the plant exists and its analysis permits taxonomic characterisation at the level of genus and species (Rosen, 1992 and 1999), especially when the structures come from the inflorescent parts of cereals. Unfortunately, the morphologies of multicellular phytoliths observed in these sediments, most of which correspond to the parts of leaves and stems of graminoids, do not allow for accurate taxonomic assignment. Lastly, the identified morphologies of phytoliths indicate that this type of plant is represented by all of its parts, inflorescences, stems and leaves, supporting the idea that they were introduced into the site complete.

As noted earlier, the presence of relatively high concentrations of fecal spherulites suggests that these plants were possibly introduced as a component of the diet of domestic animals and were deposited in the sediments as excrement and products derived from it. The observed remains could correspond to a diet rich in graminoids, which would have been ingested as forage at the archaeological site itself or consumed in the vicinity of the site and later deposited in excrement. The presence of the inflorescent parts of these plants indicates a period of spring-summer, which is when the plants flower, or possibly plants from the last harvest given to the animals as a supplement to their diet. In any case, the concentrations of phytoliths and spherulites in the archaeological context under analysis, interpreted as a level of demolition corresponding to the collapse of a wall, could relate to a building material made up partly of the stems and leaves of cereals, presumably domestic, with additional fecal material rich in graminoids. This type of practice can be readily observed to the present day in areas such as North Africa and the Middle East, where these materials are commonly used in the manufacture of abode bricks, roofs, cladding for walls and pavements, floors, etc. The ethnoarchaeological references are highly numerous (Miller, 1984; Anderson and Ertug-Yaras, 1998; Zapata *et al*., 2003, among others).

Livestock manure is an omnipresent material in pastoral and agro-pastoral settlements, from the first domestication of livestock, and it provides a valuable source of palaeoeconomic and palaeoenvironmental information (Shahack-Gross, 2011). Fecal remains provide information on the diversity of socioeconomic activities and specifically on the herding and diet of domestic livestock, as well as data on the ecological and environmental conditions. Numerous ethnographic references address the use of this raw material as fertilizer, fuel, degreasing agent or building materials, which are some of the most common applications (Miller, 1984; Reddy, 1998; Anderson and Ertug-Yaras, 1998; Sillar, 2000). The integrated analysis of phytoliths and spherulites is a highly effective tool in the identification of this type of material in the archaeological record. These studies have been able to identify domestic spaces allocated to the stabling of livestock in several Neolithic sites in the Levant (Albert and Henry 2005; Matthews, 2005; Portillo *et al*., 2009; Portillo and Albert, accepted for publication), including urban contexts (Shahack-Gross *et al*., 2005, Albert *et al*., 2008; Matthews, 2011), as well as the use of excrement as fuel (Portillo et al. 2010; Portillo and Albert, under review) and fecal remains associated with building material in urban contexts of the Levant and North Africa (Albert *et al*., 2008; Portillo and Albert, under review). Given the positive results obtained in this pilot study at Termez, the application of integrated studies of phytoliths and spherulites will make it possible to obtain new data on the ancient inhabitants of the site.

Final considerations

The results obtained through quantitative and morphological analysis of phytoliths reveal the presence of plant remains in the analysed sediments, fundamentally represented by the Poaceae subfamily of graminoids. The correlation between the amount of phytoliths and spherulites indicates a component of fecal origin, presumably remains of the excrement of domesticated animals. This plant and fecal component is associated with the collapse of a wall of the fortification in which building elements such as adobe bricks can be observed macroscopically.

In summary, the results obtained in this pilot study are definitely promising with respect to the potential of integrated studies examining plant and fecal microremains in future interventions at the site.

Bibliography

Albert, R.M., Henry, D. 2005. Herding and agricultural activities in Ain Abu Nukhayla (Wadi Rum, Jordan). The results of phytoliths and spherulite analyses, Páleorient, 30 (2), 81-92.

Albert, R.M., Weiner, S. 2001. Study of phytoliths in prehistoric ash layers using a quantitative approach, en Meunier, J.D., Colin, F. (eds.) Phytoliths, Applications in Earth Sciences and Human History. A.A. Balkema Publishers. Lisse, 251-266.

Albert, R.M., Tsatskin, A., Ronen, A., Lavi, O., Estroff, L., Lev-Yadun, S., Weiner, S. 1999. Mode of occupation of Tabun Cave, Mt. Carmel Israel, during the Mousterian period: A study of the sediments and the phytoliths, Journal of Archaeological Science, 26 (10), 1249-1260.

Albert, R.M., Shahack-Gross, Cabanes, D., Gilboa, A., Lev-Yadun, S., Portillo, M., Sharon, I., Boaretto, E., Weiner, S., 2008. Phytolith-rich layers from the Late Bronze and Iron Ages at Tel Dor (Israel): mode of formation and archaeological significance, Journal of Archaeological Science 35, 57-75.

Anderson, S.; Ertug-Yaras F. 1998. Fuel fodder and faeces: an ethnographic and botanical study of dung fuel use in central Anatolia. Environmental Archaeology 1, 99-110.

Ariño, E., 2009. Archaeological record: sector RC (Tchinguiz Tepe). In: Gurt, J.M.; Pidaev, S.; Rauret, A.M.; Stride, S. (dirs). Preliminary Report of the work of the International Pluridisciplinary Archaeological Expedition to Bactria (2009), IPAEB series, Barcelona – Tashkent.

Brochier, J.E., Villa, P., Giacomarra, M., Tagliacozzo, A., 1992. Shepherds and sediments: geo-ethnoarchaeology of pastoral sites. Journal of Anthropological Archaeology 11, 47-102.

Brown, D.A., 1984. Prospects and limits of a phytolith key for grasses in the central United States. Journal of Archaeological Science 11, 345-368.

Canti, M.G., 1997. An investigation of microscopic calcareous spherulites from herbivore dungs. Journal of Archaeological Science 24, 219-231.

Canti, M.G., 1998. The micromorphological identification of faecal spherulites from archaeological and modern materials. Journal of Archaeological Science 25, 435-444.

Canti, M.G., 1999. The production and preservation of faecal spherulites: Animals, environment and taphonomy. Journal of Archaeological Science 26, 251-258.

Madella, M., Alexandre, A., Ball, T.B., 2005. International Code for phytolith Nomenclature 1.0, Annals of Botany 96, 253-260.

Matthews, W., 2005. Micromorphological and microstratigraphic traces of uses of space. In: Hodder

Figure 4: Cross-section W.

Figure 5: RC-2. Cross-section W

I. (Ed.), Inhabiting Çatalhöyük: Reports from the 1995-99 Seasons. MacDonald Institute for Archaeological Research and British Institute of Arcaheology at Ankara, Cambridge, pp. 355-398.

Matthews, W., 2010. Geoarchaeology and taphonomy of plant remains and microarchaeological residues in early urban environments in the Ancient Near East. Quaternary International 214, 98–113.

Miller, N.F., 1984. The use of dung as a fuel: an ethnographic example and an archaeological application. Paléorient 10 (2), 71-79.

Mulholland, S.C., Rapp Jr. G., 1992. A morphological clasification of grass silica-bodies. In: Rapp Jr. G., Mulholland, S.C. (Eds.), Phytolith Systematics, Emerging Issues, Advances in Archaeological and Museum Science. Plenum Press, New York, pp. 65-89.

Piperno, D.R., 2006. Phytoliths: A comprehensive guide for archaeologists and paleoecologists. AltaMira Press, Lanham.

Reddy, S.N., 1999. Fueling the hearths in India: the role of dung in paleorthnobotanical interpretation. Paleorient 24, 61e70.

Portillo, M., Albert R.M., acceptat, Early crop cultivation and caprine herding: The phytolith and phaecal spherulite evidence. Henry, D.O (Ed.) The Sands of Time: The Desert Neolithic Settlement at Ayn Abu Nukhayla.

Portillo, M., Albert R.M., en revisió, Husbandry practices and livestock dung at the Numidian site of Althiburos (el Médéina, Kef Governorate, northern Tunisia): the phytolith and spherulite evidence, Journal of Archaeological Science.

Portillo, M., Albert R.M., D.O. Henry, 2009, Domestic activities and spatial distribution in Ain Abu Nukhayla (Wadi Rum, Southern Jordan): The use of phytoliths and spherulites studies, Quaternary International, 193, 174-183.

Portillo, M., Albert, R.M., Kadowaki, S., Nishiaki, Y., 2010, Domestic activities at Early Neolithic Tell Seker al-Aheimar (Upper Khabur,Northeastern Syria) through phytoliths and spherulites studies. In: Delhon, C., Théry-Parisot, I., Thiébault, S. (Eds.), Des hommes et des plantes : exploitation du milieu et gestion des ressources végétales de la Préhistoire à nos jours. Éditions ADPCA, Antibes,19–30.

Reddy, S.N., 1998. Fueling the hearths in India: the role of dung in paleoethnobotanical interpretation. Paléorient 24 (2), 61–70.

Rosen, A.M. 1992, Preliminary identification of silica skeletons from Near Eastern archaeological sites: an anatomical approach, in Rapp, Jr.G.; Mullholland, S.C. (eds.)

Phytolith Systematics. Plenum Press. New York, 129-148.

Rosen, A.M. 1993, Phytolith evidence for early cereal exploitation in the Levant, en Pearsall, D.M., Piperno, D.R. (eds.). Current research in phytolith analysis: applications in archaeology and palaeocology. Masca Research Papers in Science and Archaeology, 10. The University Museum of Archaeology and Anthropology. University of Pennsylvania. Philadelphia, 160-171.

Rosen, A.M., Weiner, S. 1994, Identifying ancient irrigation: a new method using opaline phytoliths form Emmer wheat, Journal of Archaeological Science, 21, 125-132.

Shahack-Gross, R., Albert, R.M., Gilboa, A, Nagar-Hilman, O., Sharon I., Weiner, S. 2005, A Geoarchaeological Study of Sedimentary Deposits Associated with Early Iron Age Phoenician Monumental Construction at Tel Dor (Israel) Reveals Diverse Modes of Occupation, Journal of Archaeological Science, 32, 1417-1431.

Shahack-Gross, R., 2011. Herbivorous livestock dung: formation, taphonomy, methods for identification, and archaeological significance. Journal of Archaeological Science 38, 205-218.

Sillar, B., 2000. Dung by preference: the choice of fuel as an example of how Andean pottery production is embedded within wider technical, social and economic practices. Archaeometry 42 (1), 43-60.

Simpson, I.A., Vésteinsson, O., Adderley, W.P., McGovern, Th.H., 2003. Fuel resource utilisation in landscapes of settlement. Journal of Archaeological Science 30, 1401-1420.

Twiss, P.C., 1992. Predicted world distribution of C3 and C4 grass phytoliths. In: G,.Rapp, Jr., S.C. Mulholland (Eds.), Phytolith Systematics: Emerging Issues, Advances in Archaeological and Museum Science. Plenum Press, New York: 113-128.

Twiss, P.C., Suess, E., Smith, R.M., 1969. Morphological classification of grass phytoliths. Soil Science Society of America Proceedings 33, 109-115.

Zapata, L., Ibáñez, J. J., González Urquijo, J. E. and Peña-Chocarro, L. 200. Las casas de cubierta vegetal del Rif occidental: aspectos arquitectónicos, simbólicos y sociales. El Pajar. Cuaderno de Etnografía Canaria 14, 137- 143.

Report on Radiocarbon Dating

Joan S. Mestres i Torres, Anna Maria Rauret

With the objective of determining their age, the University of Barcelona's Radiocarbon Dating Laboratory has received from Dr Anna Maria Rauret Dalmau and Dr Josep Maria Gurt Esparraguera of the Department of Prehistory, Ancient History and Archaeology of the University of Barcelona, three samples of charcoal and two samples of bones from *Termez* (Surxondaryo province, Southern Uzbekistan). The identification of the samples and their types are listed here:

Sector AC2/1	**Charcoal**
Sector AC2/2	**Bones**
Sector AC2/2	**Bones**
Sector RC2/1	**Charcoal**
Sector RC2/2	**Charcoal**

1. DESCRIPTION AND TREATMENT OF THE MATERIAL RECEIVED

The first sample comprised fragments of charcoal covered in earth in a matrix of disaggregated and hardened sand with the presence of shell fragments. The largest charcoal fragment measured 23 mm, but the others were not larger than 13 mm.

The second sample comprised the following fragments of fauna's bones:

One molar, 45 mm long
Nine fragments of diaphysis ranging between 30 and 63 mm in length
A fragment of vertebra measuring 19 mm
Three fragments of epiphysis joined to a part of their respective diaphyses, 42, 57 and 88 mm long

The third sample also comprised fauna's bone fragments, with the following composition:

One molar, 40 mm long
Three fragments of diaphysis with incomplete periphery, 23, 67 and 130 mm long
Two fragments of epiphysis joined to a part of their respective diaphysis, 59 and 92 mm long

All the bone fragments had earth adhering to their surface.

The fourth and fifth samples comprised fragments of charcoal covered in earth in a matrix of sand. These two fragments were 21 and 28 mm in length.

The quantity of material received for each of samples is indicated in the second column in Table I.

1.1. Treatment of the charcoal

The first charcoal sample was passed through a 1 mm sieve. In the largest grain size fraction, the fragments of charcoal and lumps of earth were extracted using pincers; the lumps of earth were taken apart with care and were shown not to contain charcoal in their interior. The smallest grain size fraction was passed through a 500 μm sieve, and from the two resulting fractions the charcoal fragments were extracted with the aid of pincers.

The other two charcoal samples were passed through a 500 μm sieve. From the larger fractions the charcoal fragments were extracted, while the smaller fractions were rejected because they did not contain charcoal.

Where possible, the surfaces of the largest carbon fragments were cleaned with a brush to eliminate the earth adhering to their surface. Then, in order to be able to observe and to eliminate any possible intrusions of foreign materials, they were fragmented along their natural fracture lines. Finally, the clean charcoal fragments were ground to a dust. The amount of clean material from each of the samples is recorded in Table I, column 3.

The ground material was treated with 2M hydrochloric acid at 95°C for 18 hours to eliminate the carbonates originating from the percolating water and/or the soil and the acid soluble fraction. In order to eliminate any humic acid originating from the soil plant matter, the insoluble residue resulting from the treatment with acid was suspended in water and was treated with successive 1M ammonia additions at room temperature until the pH of the suspension was high enough to ensure the complete elimination of acidic substances. Finally, the residue resulting from this treatment was boiled with 0.4M hydrochloric acid in order to eliminate the carbonates originating from the atmosphere. In this way, we obtained a purified charcoal residue free of carbonates and humic acids, and hence suitable for dating. The quantities and percentage yields of purified carbon are recorded in Table I, columns 4 and 5.

1.2. Treatment of the bone material

The earth covering the bone fragments in each sample was cleaned with a metal brush. The fragments of diaphysis which still preserved all their periphery were fractured longitudinally to facilitate their observation and the elimination of the earth and other foreign bodies that might be found inside the medullary canal: The interior surfaces were also cleaned using a brush. Finally, the clean material, whose weight is shown in the third column of Table I, was ground to a size below 250 μm.

The ground bone material was treated with 2M hydrochloric acid so as to eliminate the mineral fraction and the possible carbonates from the percolating waters. The insoluble residue, comprising mainly collagen, the rest of the organic matter and the small amount of earth which had remained in the corners of the surface or in the trabecula, were treated with a 0.006M solution of hydrochloric acid at 95°C for 18 hours in order to produce the hydrolysis of collagen to gelatin and thus achieve its dissolution. Finally, evaporating the solutions resulting from the hydrolysis we obtained a material comprising gelatin, which was suitable for dating. The quantity of gelatin recovered and its yield are shown in the fourth and fifth columns in Table I. The gelatin obtained from each of the fractions underwent C and N elemental analysis in order to evaluate the C/N ratio, which is indicated in the sixth column of the table

Reference for identification	Original material (g)	Ground clean material (g)	Purified charcoal --- Gelatin extracted (g)	Yield (%)	C/N Ratio
Sector AC2/1 Charcoal	11.0	3.2	1.0	31.2	– –
Sector AC2/2 Bones	103.3	89.7	2.1	2.3	3.13
Sector AC2/3	77.3	63.1	2.1	1.3	3.01
Sector RC2/1	11.5	5.5	3.5	63.6	– –
Sector RC2/2	15.2	4.9	3.2	65.3	– –

Table I: Material received and treatment applied

2. PREPARATION OF THE ACTIVITY COUNT: BENZENE SYNTHESIS

As the radiocarbon content cannot be measured directly from the purified charcoal or the gelatin from bone samples, these materials have to be transformed into a suitable chemical compound that allows the ^{14}C activity to be measured by liquid scintillation. We now describe the chemical procedure that leads to the preparation of benzene, the compound we require.

The quantity of purified charcoal recovered from the first sample and the amount of gelatine recovered from the bones was too small to be able to perform the radiometric measurement of the ^{14}C content with an acceptable level of precision. For this reason it was sent to the National Accelerator Centre in Seville for measurement using accelerator mass spectroscopy (AMS).

The purified charcoal from the fourth and fifth samples of charcoal was burnt in a combustion pump under oxygen pressure. The carbon dioxide resulting from combustion, once purified and dried, was left for three weeks in order to allow the levels of ^{222}Rn radioactivity associated with it to decay. Once this time had elapsed, we determined the ^{13}C isotopic abundance of the material by mass spectrometry in a small sample of carbon dioxide. Then the remaining carbon dioxide was reduced with lithium metal to lithium carbide; this was then hydrolysed to produce acetylene with water with a low tritium content and, finally, the acetylene was converted catalytically to benzene (MESTRES *et al.,* 1991).

3. RADIOMETRIC MEASURES

To measure the radioactivity of the benzene resulting from the synthesis described above, and which contained the carbon present in the material to be dated, the benzene was diluted gravimetrically with inactive analytical reagent grade benzene to 5.2 ml. With this mixture, we prepared the solutions for measuring the activity, weighing out accurately 5,000 ml of benzene with a 0.005 ml tolerance into low-potassium glass vials together with appropriate amounts of the scintillators Bu-PBD and Bis-MSB in solid form, and having previously been weighed

Oxalic acid II, supplied by the National Institute of Standards and Technology (USA), served as the reference substance for the measurement of initial activity. This was oxidised to carbon dioxide with a potassium permanganate solution and then transformed into benzene as described above for the other samples (*loc. cit.*). The preparation of the solution for the initial measurement of activity was also conducted in the same manner as for the other samples.

The background value for each vial was determined by measuring two reference blanks prepared in the same way as for the samples, but using inactive benzene for the measuring solution.

The samples, two standards of initial activity and two reference blanks for the background measurement were counted in a period of time 62.5 hours (fourth sample) and 55 hours (fifth sample) each, divided into fifty-minute intervals, in a liquid scintillation counter (LKB Wallace 1217 Rackbeta). The efficiency of the measurement for each interval was determined using a calibration curve of the efficiency as a function of quenching. The calibration curve had been previously established from activity standards prepared in our laboratory (*loc. cit.*).

4. RESULTS AND DISCUSSION

The results of the ^{13}C isotope ($\delta^{13}C$) abundance measures and the results of the count and measure of the radioactivity, together with their uncertainty expressed as one times the standard deviation (*loc. cit*), are shown in Table II. For comparative purposes we also include the values of isotopic abundance determined by AMS. It can be seen that the value of ^{13}C isotope abundance measured was normal for all the samples, except for the first charcoal sample which was abnormally high: for the charcoal and the bone collagen fraction the values range between -23 and -27‰ and between -18 and -22‰ respectively (Stuiver and Polach, 1977).

Sample	**$\delta^{13}C$ (‰)**	**Amount of benzene measured (g)**	**Count estimate (cpm)**	**Back-ground (cpm)**	**Net count rate (cpm)**	**Count efficiency (%)**	**Normalized count estimate of benzene sample, A_{SN} (cpm/g)**	**Normalized count estimate of standard benzene, A_{0N} (cpm/g)**
AC2/1 **Charcoal**	–12.01							
AC2/2 **Bones**	–21.07							
AC2/3 **Bones**	–20.83							
RC2/1 **Charcoal 1**	–26.516	2,1986	16,392±0.066	2,924±0.043	13,468±0,079	72,855±0.026	8,434±0.049	10,628±0.027
RC2/2 **Charcoal 2**	–26.942	1,7562	13,666±0,064	2,967±0,043	10,699±0,077	72,869±0.025	8,393±0.061	10,628±0,027

Table II: Results of the radio metric measurements

Calculation of the radiocarbon age is based on the experimental results shown in Table II, using the following equation:

$$R = \frac{T_{1/2}}{\ln 2} \times \ln \frac{A_{0N}}{A_{SN}} \qquad (T_{½} = 5568 \text{ years})$$

where A_{0N} represents the initial activity and A_{SN} represents the residual activity in the dated material corrected by isotopic fractionation of ^{14}C.

Applying the above equation to the measurements obtained enables us to calculate the radiocarbon date. The dating results $^{(1)}$, either using mass spectrometry (AMS) or radiometry, and the radiocarbon date code assigned by the Laboratories are shown here:

– Termez/Sector AC2 –

1	**UBAR-1125/CNA 1121**	**1955 ± 35 BP**	Charcoal
2	**UBAR-1126/CNA 1122**	**1925 ± 40 BP**	Bones
3	**UBAR-1127/CNA 1123**	**2155 ± 40 BP**	Bones

– Termez/Sector RC2 –

1	**UBAR-1090**	**1860 ± 50 BP**	Charcoal
2	**UBAR-1091**	**1890 ± 60 BP**	Charcoal

These results can only be reliably applied to the samples received.

Even though the collagen from the bones is not susceptible to carbon exchange with the outside, carbon may be acquired through the chemical combination of collagen with the humic acids of the soil to form humic-protein complexes. Humic acids combined with collagen cannot be separated from this using standard chemical means and they become integrated in the collagen extracted from the bone in the form of gelatin. Since the humic acids in the soil were formed after the bone, they may affect the accuracy of the radiocarbon dating. The probability of the incorporation of humic acids from the soil increases with the degree of deterioration of the bone, which is reflected by a low collagen content. Since in the bones studied the collagen content was not particularly high (see Table I, sixth column), to assess the possibility of incorporation of humic acids in the collagen analysed, we determined the C/N ratio through elemental analysis of the gelatin resulting from the extraction of the collagen. For the collagen from well-preserved fossil bones the C/N ratio must be below 3.6 (De Niro, 1985). As shown in the table, the C/N ratios reported in the two fractions of the bone sample dated were not above the critical value; this means that no humic-protein complexes were present in the collagen used for the dating and thus supports the accuracy of the radiocarbon dates obtained.

The pairs of experimental radiocarbon dates

UBAR-1125/CNA1121 – **UBAR-1126/CNA 1122**
UBAR-1090 – **UBAR-1091**

come from materials from the same archaeological level, and inside each pair the values are statistically indistinguishable. For this reason, each of the radiocarbon dates of the pair may be a different experimental expression of the same physical date (Mestres, 2008) attributable to the formation of the archaeological level. This consideration does not rule out the possibility that the two materials are synchronous, as already indicated by their presence in the same archaeological level, and so the mean weighted by the variance of the two experimental radiocarbon dates is a closer approximation to the real radiocarbon date (the physical date) attributable to the archaeological level. Under these considerations the results of the datings are shown below:

– Termez/Sector AC2 –

1+2	**UBAR-1125/CNA 1121** **UBAR-1126/CNA 1122**	**1940 ± 25 BP**
3	**UBAR-1127/CNA 1123**	**2155 ± 40 BP**

– Termez/Sector RC2 –

1+2	**UBAR-1090/1091**	**1875 ± 40 BP**

5. CALIBRATION OF RADIOCARBON DATES

Radiocarbon dating is based on the assumption that the specific ^{14}C content present in the materials has remained unchanged over time. However, this hypothesis is not strictly accurate, since there will have been fluctuations in the ^{14}C content over time. As such, the dates calculated on the basis of this hypothesis are conventional in nature, since they present deviations with respect to the dates expressed on the solar time scale and define what has come to be known as the radiocarbon time scale. The transformation of a radiocarbon date into a date expressed on the solar time scale is known as calibration. Measuring the radiocarbon age of tree rings whose age has been previously ascertained using dendrochronological techniques, a curve has been drawn spanning the last 12,400 years (Reimer *et al.,* 2004), relating the conventional radiocarbon age to the age to the age expressed on the solar time scale. This curve, known as the calibration curve, is not a monotonic function and does not establish a one-to-one relationship between the radiocarbon time scale and the solar time scale, but rather more than one solar date may correspond to each radiocarbon date.

Owing to the non-linear character and the complexity of the calibration curve, the probability distribution of the true calibrated date around the experimental calibrated date is not normal, as it is in the case of the probability distribution of the true radiocarbon date around the experimental radiocarbon date. The probability distribution of the true calibrated date is asymmetrical and complex and it presents distinct modes around which one or more probability intervals can be defined. The sum of the intervals is equal to a probability of 68.3% or 95.4% (STUIVER AND REIMER, 1993). The two values are chosen by analogy to the probability distribution of the radiocarbon date and they correspond to the probability that the true radiocarbon date falls within an interval of time which, centring on the experimental radiocarbon date, has a half-width equivalent to once or twice the standard deviation, respectively.

Table III shows the results of calibrating the radiocarbon dates. The details contained in each column are as listed below:

Columns A and B:	Dating material reference and radiocarbon date code assigned by this Laboratory, respectively.
Column C:	Radiocarbon date with uncertainty expressed in terms of standard deviation.
Column D:	Experimental calibrated dates(2) corresponding to the intersection of the radiocarbon date with the calibration curve. They correspond to the maximum modes of the probability distribution of the calibrated data.
Columns E and F:	Calibrated date intervals centred on the modes of probability distribution for the true calibrated date corresponding to a total probability of 68.3%

and the probability associated with each interval, respectively. In this set of intervals there is a probability of 68.3% that the true calibrated date will be found.

Columns G and H: Calibrated date intervals centred on the modes of distribution of probability of the true calibrated date corresponding to a total probability of 95.,4% and the probability associated with each interval, respectively. In this set of intervals there is a probability of 95.4% that the true calibrated date will be found.

A	B	C	D	E	F	G	H
AC2/1+2	UBAR-1125 CNA 1121 UBAR-1126 CNA 1122	1940±25 BP	cal AD 65	cal AD 24—83	68,3%	cal AD 3—125	95,4%
AC2/3	UBAR-1127 CNA 1123	2155±40 BP	cal BC 198	cal BC 352—295 cal BC 229—220 cal BC 211—156 cal BC 136—114	27,4% 3,1% 30,0% 7,8%	cal BC 360—273 cal BC 262— 88 cal BC 76— 57	32,6% 60,0% 2,8%
RC2/1+2	UBAR-1090 UBAR-1091	1875± 40 BP	cal AD 128	cal AD 78— 143 cal AD 147— 171 cal AD 193— 210	45,4% 12,9% 10,0%	cal AD 57— 237	95,4%

Table III: Calibration of radiocarbon dates

The appendix contains additional information on the calibration. Figure 1 shows the portion of the calibration curve involved in the calibration of the radiocarbon dates and it enables us to appreciate any incidents or possible distortions in the radiocarbon time scale in specific chronological regions. Figures 2 show the probability distribution of the true calibrated date and enable us to appreciate the intervals with the highest probability indicated in columns E and G in Table III. Finally, Figures 3 show the cumulative probability curve that enables us to calculate the probability that the true calibrated date lies in a time interval equivalent to the difference between the ordinates corresponding to the interval extremes; by way of example, Figure 3A shows the calculation of the probability that the true calibrated date is found in the first century AD, which turns out to be 83.3%.

6. GENERAL DISCUSSION

Figure 1 shows that, in spite of the accuracy of the radiocarbon date for UBAR-1127/CNA1123, the time interval that contains the true date, calibrated with a specific precision is very wide (see Table III, columns E and G and Figure 2B). The discrepancy is due to the fact that the intersection of the experimental radiocarbon date with the calibration curve appears at a point preceded by an area affected by an inversion of the slope, which produces a deep fall and the flattening of the curve. The calibration of the radiocarbon date in this chronological region means that various time zones may contain the true calibrated date with a privileged probability, either due to the approximation to the drop in the calibration curve to the experimental radiocarbon date or due to the intersection of the curve with the experimental radiocarbon date. As a result, the true calibrated date may be in a wide temporal region corresponding to the flattening of the curve, and manifests itself as a wide probability distribution with a markedly multimodal character (see Figure 2B). The notable width of probability distribution also explains the fact that none of the time intervals of the archaeological date based on archaeological or historical data present a particularly high probability (see Figure 3B), since the said interval may represent only a small fraction inside the wide time interval that covers the entire distribution probability.

Given the nature of the procedure, radiocarbon dating establishes the date of the formation of the materials and not that of the archaeological events of which these materials form a part. The experimental date measured is an approximation to a physical date (Mestres, 2000, 2003, 2008), which in the case of carbon dating refers to the moment of the formation of the plant tissues that make up the plant material and which later give rise to the charcoal, and, in the case of the bones, refers to a moment in the formation of bone collagen slightly before the individual's death, assuming he/she was an adult (Geyh, 2001). In no case, however, does the physical date refer to the archaeological date that we wish to know, if by this we understand ascertaining when the plant materials were transformed into charcoal or when charcoal or bones were deposited in the archaeological structures or levels that we wish to date. For the physical date to correspond to the archaeological date, we must fulfil the conditions of association and synchrony (*loc. cit.*).

NOTES AND BIBLIOGRAPHY

(1) BP (before present): used to represent a date expressed on the radiocarbon time scale where present is defined as AD 1950. The date is always accompanied by the degree of uncertainty, expressed as the standard deviation corresponding to the set of radiometric measurements.

(2) cal BC (Before Christ): used to represent a calibrated date, expressed in years before Christ, based on radiocarbon dating

(3) cal AD (*anno domini*): used to represent a calibrated date, expressed in years after Christ, based on radiocarbon dating.

De Niro, M.J., 1985: "Post-mortem preservation and alteration of in vivo bone collagen isotope ratios in relation to palaeodietary reconstruction". *Nature* **317**, pp. 806-809.

Geyh, M.A., 2000: "Experience with Bomb-^{14}C Dating of Human Bones and Fur". Presented at the *17th International Radiocarbon Conference*. Israel, June 2000.

Mestres, J.S. (2000): "La datació per Radiocarboni. Una visió actual" in *Tribuna d'Arqueologia 1997-1998,* pp. 195-239. Generalitat de Catalunya, Departament de Cultura. Barcelona.

Mestres, J.S., 2003: "La química i la cronologia: La datació per radiocarboni". *Revista de la Societat Catalana de Química* 4, pp. 10-25

Mestres, J.S., 2008: "El temps a la prehistòria i el seu establiment a través de la datació per radiocarboni". *Cypsela* **17**, p. 11-21

Mestres, J.S.; J.F. García and G. Rauret, 1991: "The Radiocarbon Laboratory at the University of Barcelona". *Radiocarbon* **31**(1), p. 23-34.

Reimer, P.J, G.L. Baillie, E. Bard, A. Bayliss, J.W. Beck, C.J.H. Bertrand, P.G. Blackwell, C.E. Buck, G.S. Burr, K.B. Cutler, P.E. Damon, R.L. Edwards, R.G. Fairbanks, M. Friederich, T.P. Guilderson, A.G. Hogg, K.A. Hughen, B. Kromer, G. McCormac, S. Manning, C.B. Ramsey, R.W. Reimer, S. Remmele, J.R. Southon, M. Stuiver, S. Talamo, F.W. Taylor, J. van der Plicht and C.E. Weyhenmeyer. 2004: "IntCal04 Terrestrial Radiocarbon Age Calibration 0–26 cal kyr BP". *Radiocarbon* **46**(3), pp. 1029-1058.

Stuiver, M. and H. Polach, 1977: "Discussion: Reporting of ^{14}C Data". *Radiocarbon* **19**(3), p. 358

APPENDIX

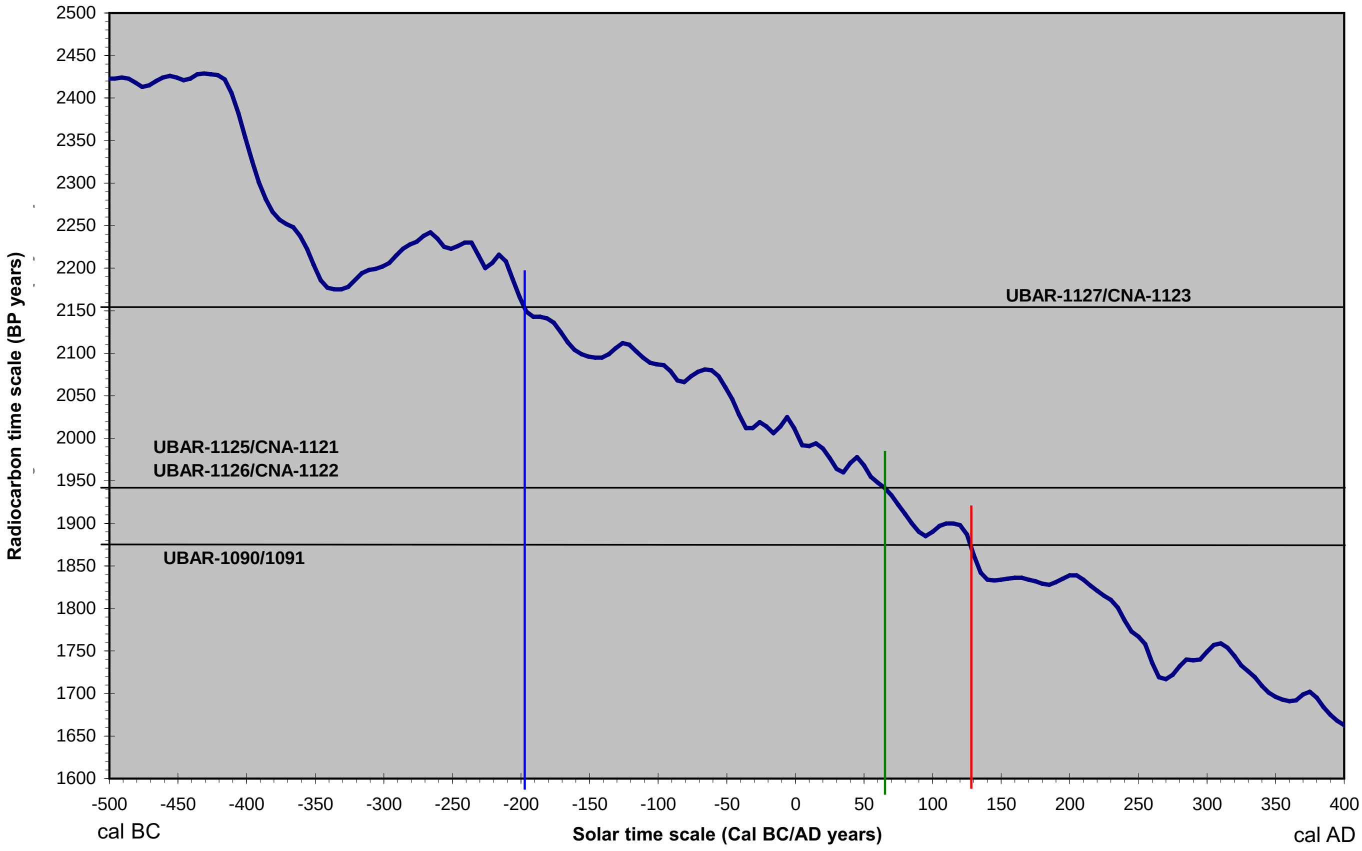

Figura 1

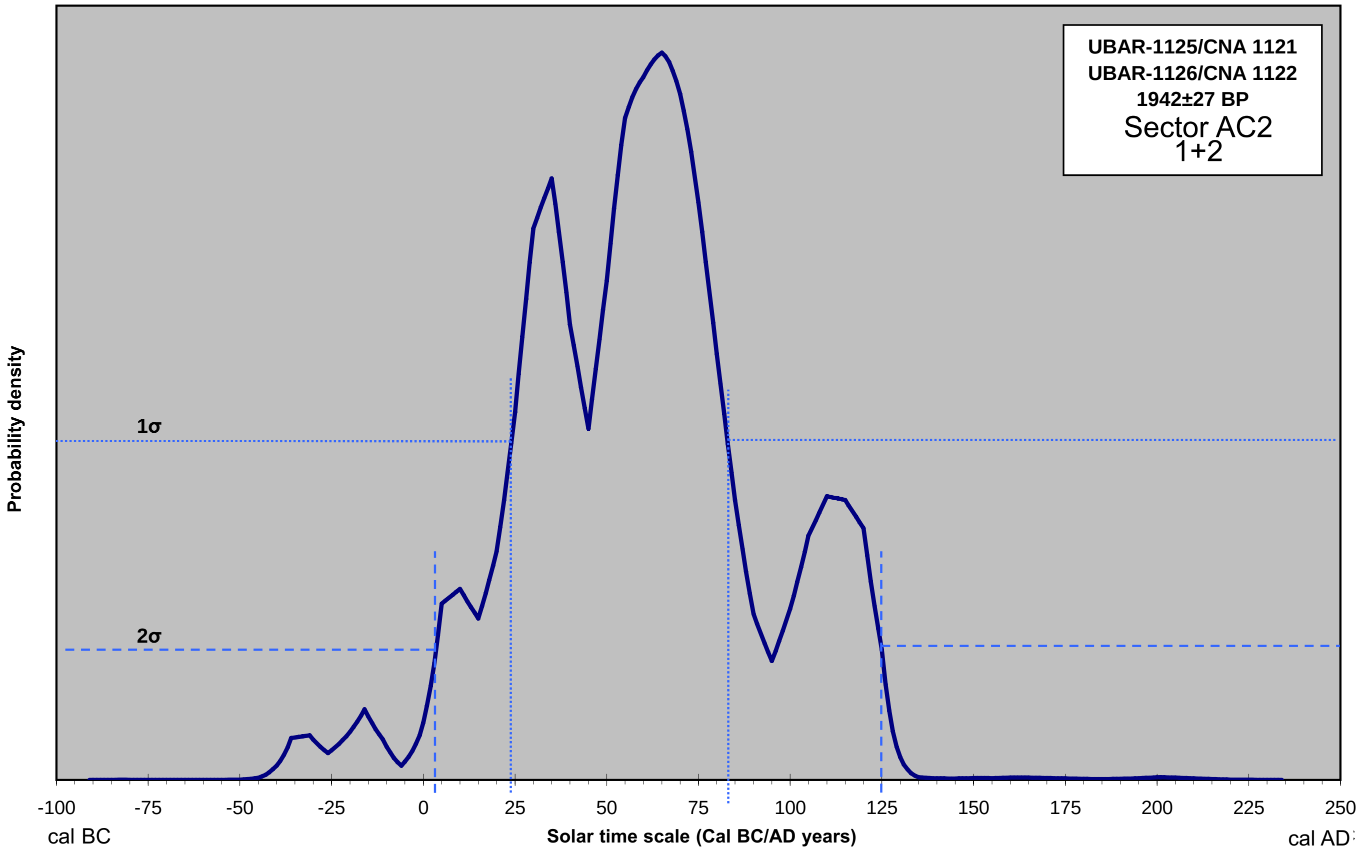

Figura 2a

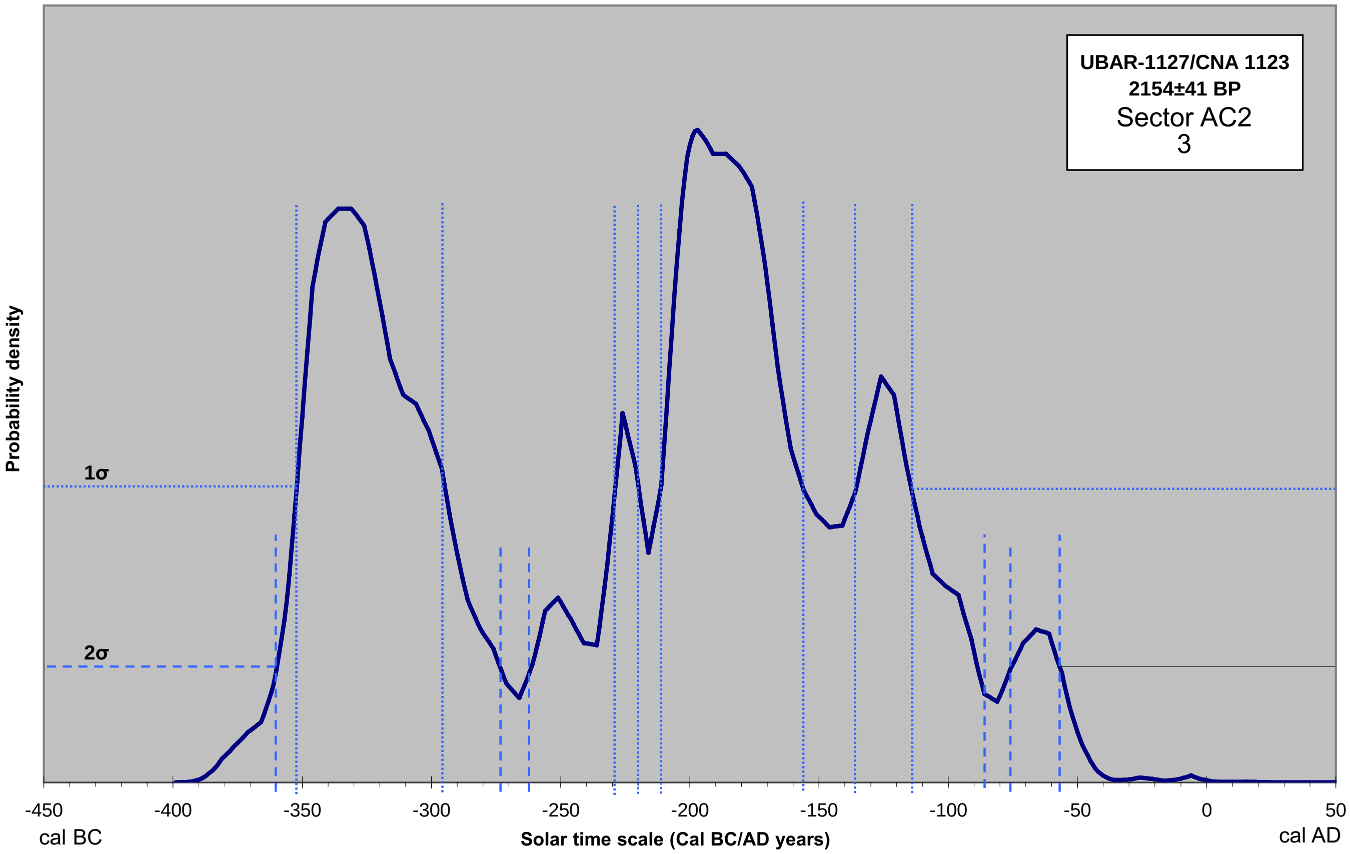

Figure 2b

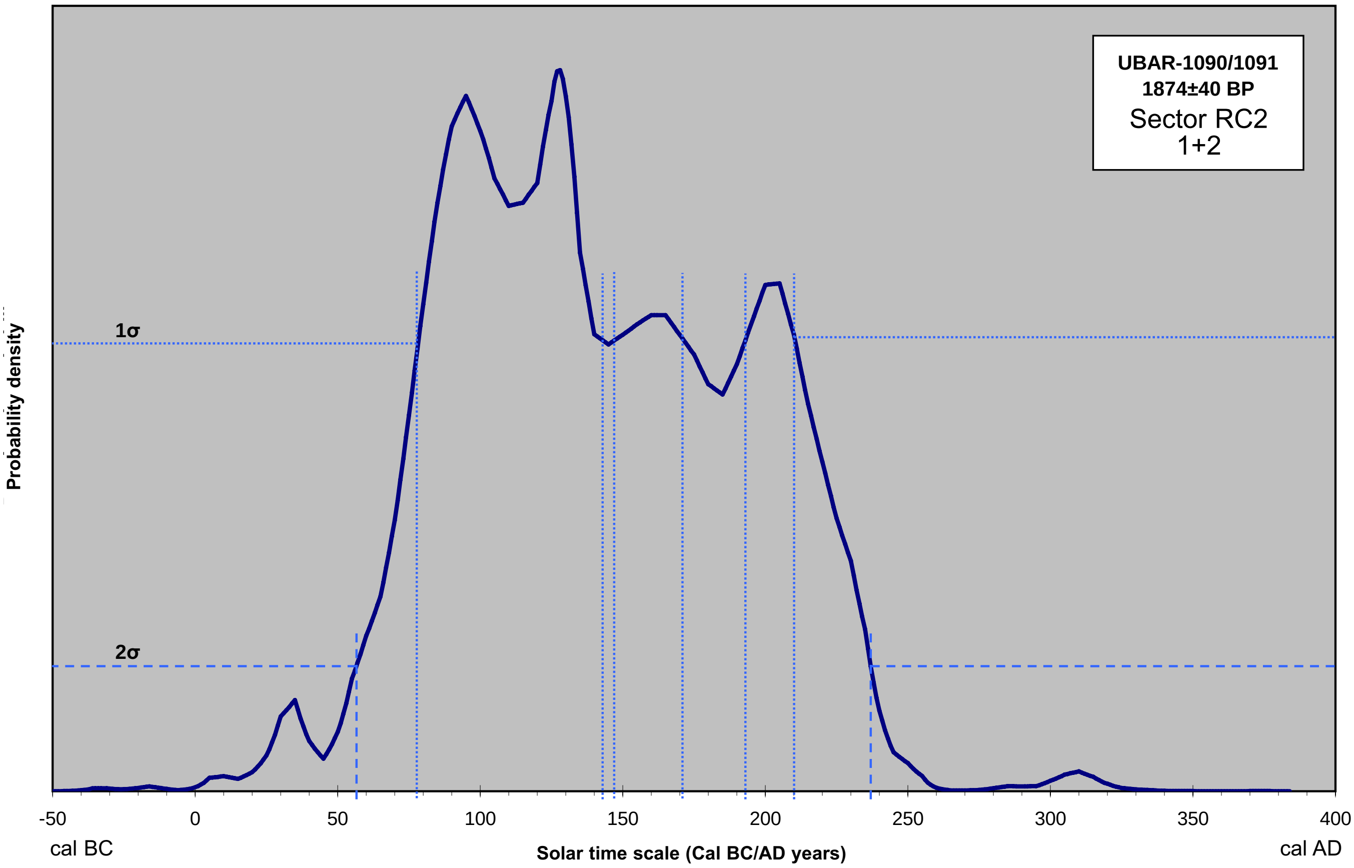

Figure 2c

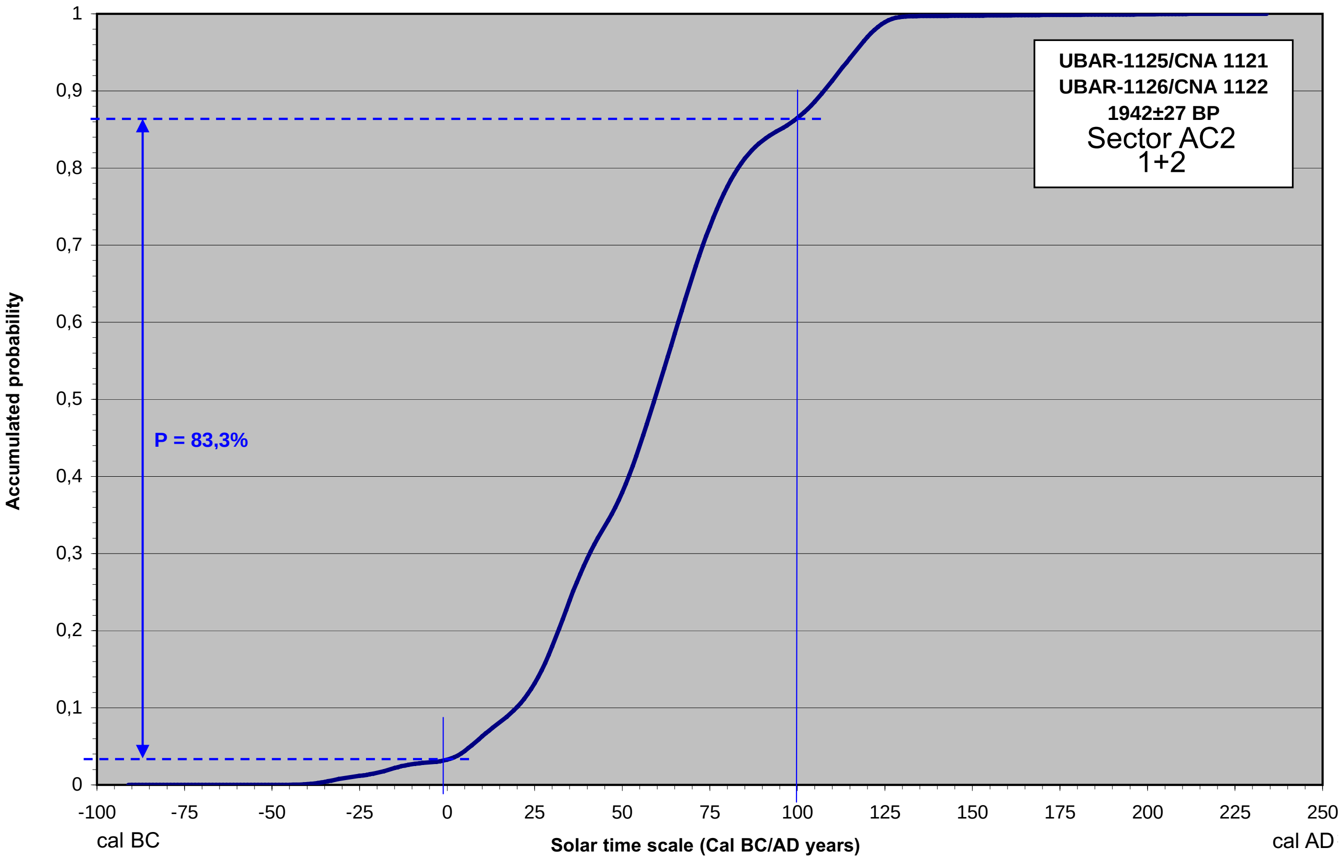

Figure 3 a

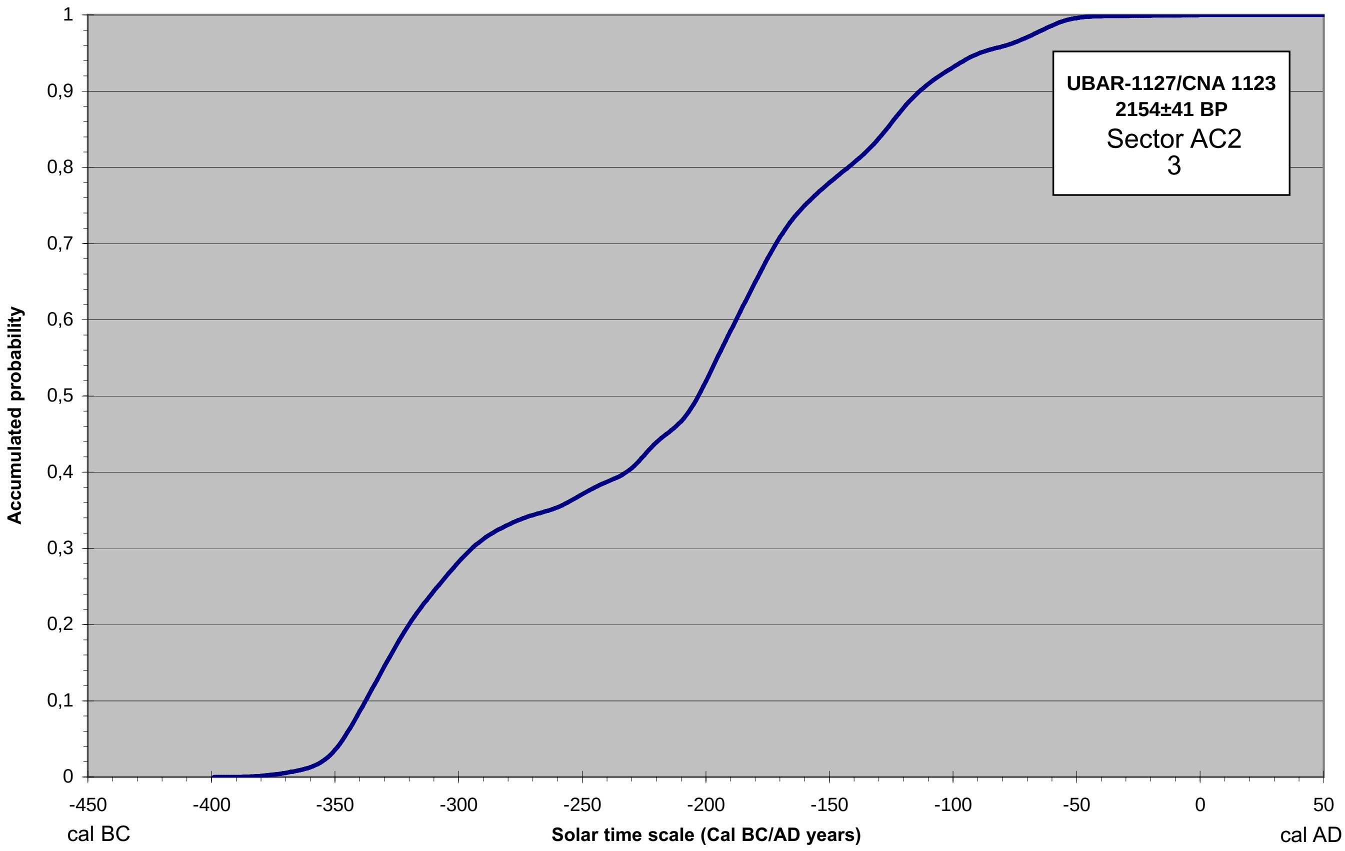

Figure 3 b

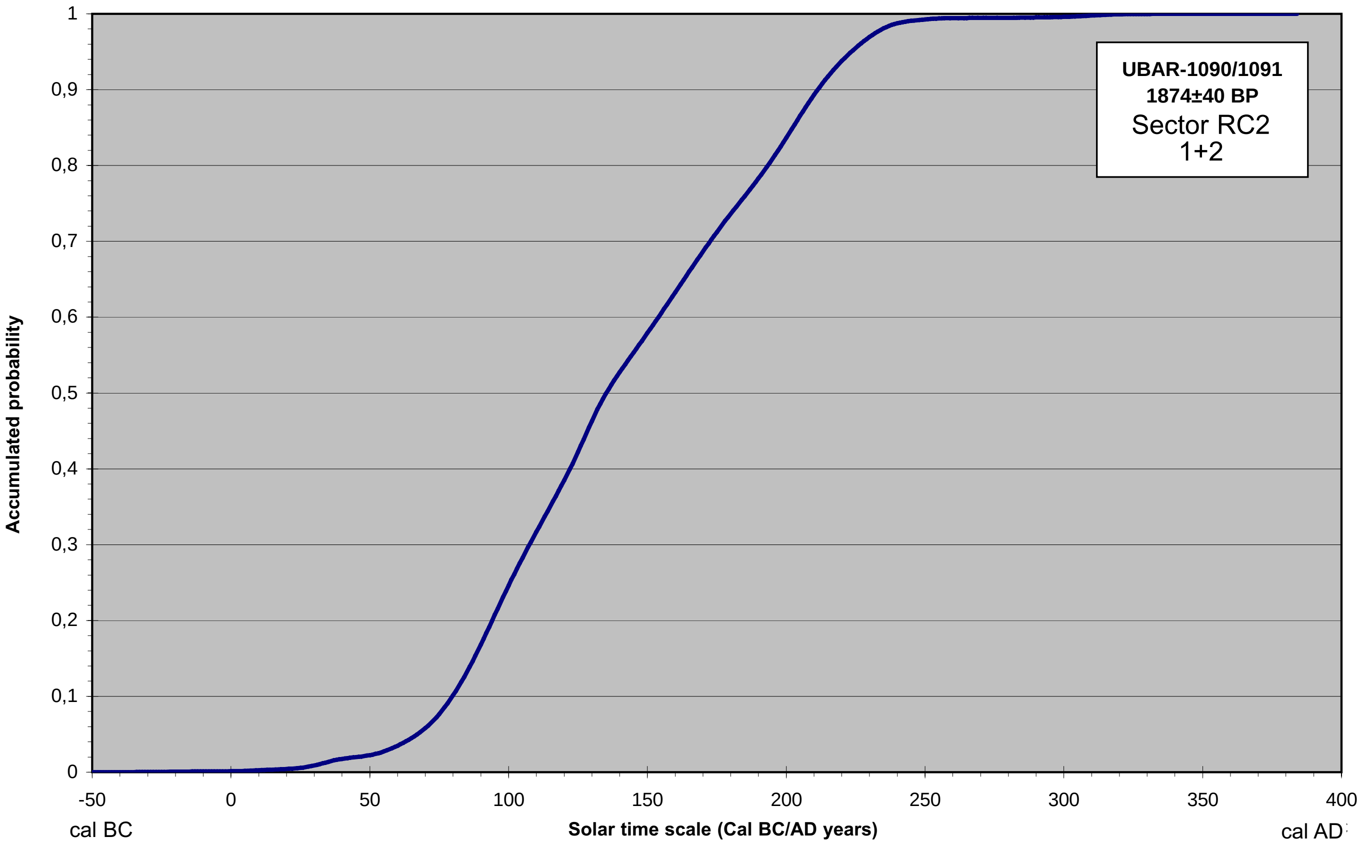
UBAR-1090/1091
1874±40 BP
Sector RC2
1+2
Accumulated probability
1
0,9
0,8
0,7
0,6
0,5
0,4
0,3
0,2
0,1
0
-50
0
50
100
150
200
250
300
350
400
cal BC
Solar time scale (Cal BC/AD years)
cal AD

Figure 3 c

Archaeometrical study of Kushan and Kushan-Sassanian pottery from ancient Termez

Verònica Martínez Ferreras, Josep M. Gurt Esparraguera,
Shakir Pidaev and Evanthia Tsantini

1. Introduction

The study of the **Kushan-Sassanian** pottery recovered at RA and RB sectors from **Tchingiz Tepe** during 2010 mission covers both the archaeological and archaeometrical characterisation. The use of these methodologies is conducted once again to the purpose of obtaining maximum information on the provenance and the technological processes involved in the manufacture of these ceramics. Besides, the study draws on an extensive database already generated by the ERAAUB team from 2006 to date, which comprises several sets of Greco-Bactrian pottery from The Citadel at Termez, Kushan and Kushan-Sassanian pottery from the archaeological sites of Tchinguiz Tepe, Kara Tepe and Ancient Military Quarters at Termez (Tsantini *et al*., 2007; Martínez *et al*., 2008, 2009, 2010; Martínez *et al*., in press) and other Kushan-Sassanian settlements placed in the Surkhan Darya region as Kampyr Tepe and Zar Tepe.

The full archaeometrical characterisation of pottery from **Tchingiz Tepe** will complement and broaden the preliminary archaeological and archaeometrical results of pottery production and commercial distribution in the Surkhan Darya region, in southern Uzbekistan (Tsantini *et al*., 2007; Martínez *et al*., 2008, 2009, 2010). The study will provide knowledge on **provenance** that, in turn, will lead to interpretations of pottery production, distribution and consumption. Archaeometric characterisation will also provide knowledge on the **technological processes** involved in pottery manufacture, such as clay processing, type of modelling, firing temperature and atmosphere, in order to reconstruct the “*chaine opératoire*”. Moreover, archaeometric analysis will lead to the recognition of possible post-depositional alteration and/or contamination processes produced during burial (Martínez *et al*., 2008: 162). Identifying all the above cha-racteristics and processes is the only way to reconstruct the life-cycle of pottery starting from its manufacture, moving to its use through to its discard and finally reaching its deposition in the archaeological layer. Combining and contrasting this information with the archaeological data, such as chronology, typology and context, is the right way to answer fundamental questions related to understanding the ancient societies that manufactured, used and subsequently discarded the pottery in question. For instance: where has it been produced? Where has it been used and how? Why has it been discarded at some point? Where has it spread? How many and which pieces of pottery are local? How many and which pieces of pottery are imported? An integrated evaluation will allow inferences to be drawn about the cultural and technological transfer associated with long-term social interactions between cultures.

2. Study cases and sampling

New 28 pottery fragments from **Termez** (the Kushan and Kushan-Sassanian site of Tchingiz Tepe) have been characterised.

Termez is located in the Surkhan Darya valley, in the Afghano-Tadjic depression, near the Amu Darya (the ancient Oxus River) in southern Uzbekistan (Figure 1). Surkhan Darya valley has a Hercynian basement, reactivated during the Palaeogene and Neogene, which is composed of metamorphic and crystalline rocks from the Baikal fold belt (Cambrian to Devonian). The Mesozoic and Cenozoic sediments filling this basement, basically made up of sandstone, claystone, and siltstone (sheets J-4220 and J-4226a of the Soviet geological maps, 1:200,000), are characterised by specific saline and anhydrite levels related to halocynetic processes.

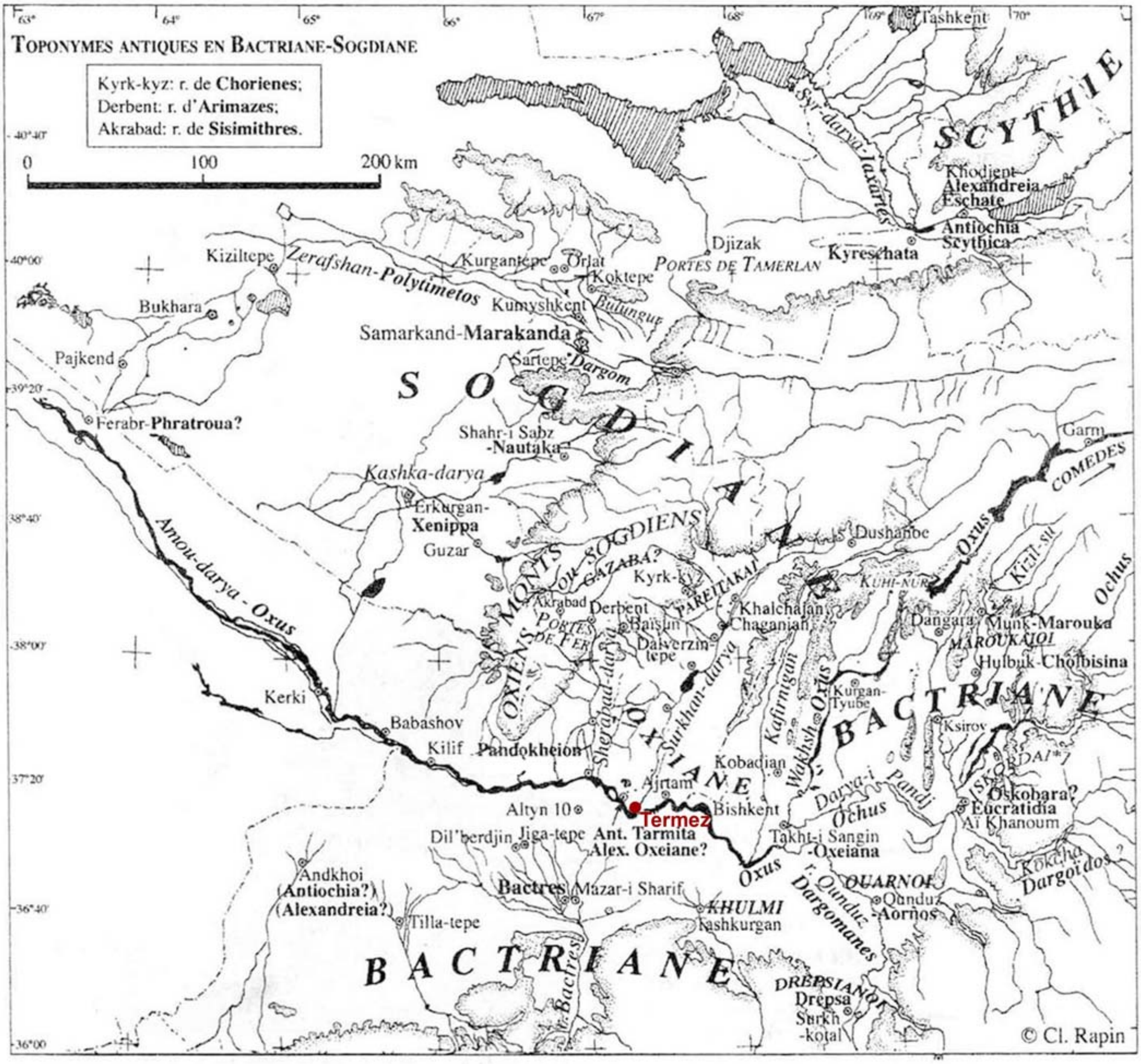

Figure 1: Localization of the studied archaeological sites The cartographic base used corresponds to the figure number 1 (p. 30) published by: Rapin, C. 2007, Nomads and the Shaping of Central Asia: from the Early Iron Age to the Kushan period. After Alexander. Central Asia before Islam (Joe Cribb and Georgina Herrmann edits.) in Proceedings of the British Academy 133, pp. 29-72.

After the conquest of Alexander of Macedonia, Termez was one of the great centres of ancient Bactria. It was a major urban site occupied during the Greco-Bactrian (around 250-150 BC), the Kushan (around 50 BC-250 AD) and Kushan-Sassanian (3rd to 6th century AD) periods, due to its exceptionally important location as an intersection of many intercontinental routes along the Silk Road (Leriche 2007; Leriche and Pidaev 2007, 2008).

Some of the archaeological remains of the Kushan and Kushan-Sassanian period from Termez are located on the hill of **Tchingiz Tepe**, placed on the banks of the Amu Darya, where excavations have uncovered a fortified settlement dated from the 2nd century BC to the 4th century AD by Radiocarbon Dating (Mestres and Rauret 2009, 2010a). At the eastern area of this site, the excavation of several trenches (**sectors RA, RB, RC, RF and RT**) have revealed domestic buildings which seems to correspond to monastic cells of a Buddhist monastery (Achón *et al*., 2008; Ariño, 2009, 2010, this volume; Martínez, this volume). This settlement must be related to the appearance of Buddhism as an important religious element during the Kushan and the Kushan-Sassanian periods, as is confirmed by the number of foundations of Buddhist monasteries (**Kara Tepe, Fayaz Tepe and Tchingiz Tepe**) on the outskirts of the city of Termez (Mkrtyschew, 2007, 2010). As pottery production is concerned, a pottery kiln was recovered at sector RF (Martínez, 2009), near the interior face of the east wall of Tchingiz Tepe, between Tower 5 and Tower 6, that radiocarbon dating has put from the second to the fourth centuries AD (Mestres and Rauret, 2010b).

The analytical results of the Kushan and Kushan-Sassanian pottery from **Tchingiz Tepe** (Table 1), 15 sherds from sector **RA1** (TRZ400-TRZ414) and 13 sherds from sector RB2 (TRZ415-TRZ427) are presented together with previous analytical results obtained on pottery coming from other contemporary archaeological contexts from **Tchingiz Tepe** (sectors RB1, RC and RF) (Tsantini *et al*., 2007; Martínez *et al*., 2008, 2009).

CERAMICS FROM TERMEZ

KUSHAN-SASSANIAN POTTERY FROM TCHINGIZ TEPE

Analytical code	Number of inventory	Site	Type of ceramic
TRZ400	TZ10-RA1-UE1	TCHINGIZ TEPE – RA	Fine common ware, plate, reddish slip
TRZ401	TZ10-RA1-UE6	TCHINGIZ TEPE – RA	Base of common ware, red-slipped on inner and outer surface
TRZ402	TZ10-RA1-UE9	TCHINGIZ TEPE – RA	Rim of fine common ware, cup, red-slipped on inner and outer surface
TRZ403	TZ10-RA1-UE20	TCHINGIZ TEPE – RA	Fine common ware, cup, red-slipped on inner and outer surface
TRZ404	TZ10-RA1-UE24	TCHINGIZ TEPE – RA	Rim of plate, incised decoration and dark brown slip on inner surface
TRZ405	TZ10-RA1-UE25	TCHINGIZ TEPE – RA	Cooking ware, closed rim, shell fragments as temper
TRZ406	TZ10-RA1-UE32	TCHINGIZ TEPE – RA	Jar (possibly an oinochoe), red-slipped on outer surface
TRZ407	TZ10-RA1-UE32	TCHINGIZ TEPE – RA	Plane base of plate, red-slipped on inner surface
TRZ408	TZ10-RA1-UE32	TCHINGIZ TEPE – RA	Cooking ware
TRZ409	TZ10-RA1-UE42	TCHINGIZ TEPE – RA	Base of common ware, red-slipped on inner surface
TRZ410	TZ10-RA1-UE43	TCHINGIZ TEPE – RA	Rim of common ware, plate, incised decoration and dark brown slip on inner surface
TRZ411	TZ10-RA1-UE48	TCHINGIZ TEPE – RA	Rim of common ware, cup, red-slipped on inner and outer surface
TRZ412	TZ10-RA1-UE50	TCHINGIZ TEPE – RA	Rim of common ware, plate, incised decoration, yellow-slipped on inner and outer surface
TRZ413	TZ10-RA1-UE63	TCHINGIZ TEPE – RA	Rim of common ware, cup, red-slipped on inner and outer surface
TRZ414	TZ10-RA1-UE64	TCHINGIZ TEPE – RA	Open rim of common ware, bowl, orange-slipped on inner surface
TRZ415	TZ10-RB2-UE1	TCHINGIZ TEPE RB2	Open rim of common ware, unpainted
TRZ416	TZ10-RB2-UE1	TCHINGIZ TEPE RB2	Small base, common ware, cup, red-slipped on inner and outer surface
TRZ417	TZ10-RB2-UE1	TCHINGIZ TEPE RB2	Rim of common ware, big jar with handle, red-slipped in outer inner surface and rim
TRZ418	TZ10-RB2-UE1	TCHINGIZ TEPE RB2	Open rim of fine common ware, bowl, brownish-grey paste, unpainted
TRZ419	TZ10-RB2-UE4	TCHINGIZ TEPE RB2	Base of fine common ware, red-slipped on inner and outer surface
TRZ420	TZ10-RB2-UE5	TCHINGIZ TEPE RB2	Plane base of common ware, red-slipped on inner and outer surface
TRZ421	TZ10-RB2-UE6	TCHINGIZ TEPE RB2	Rim of common ware, bowl, red-slipped on inner and outer surface
TRZ422	TZ10-RB2-UE8	TCHINGIZ TEPE RB2	Rim of common ware, plate, unpainted
TRZ423	TZ10-RB2-UE8	TCHINGIZ TEPE RB2	Closed rim of common ware, small pot, unpainted
TRZ424	TZ10-RB2-UE9	TCHINGIZ TEPE RB2	Base of fine common ware, grey paste, grey-slipped
TRZ425	TZ10-RB2-UE10	TCHINGIZ TEPE RB2	Base of common ware, yellowish paste, white-slipped
TRZ426	TZ10-RB2-UE10	TCHINGIZ TEPE RB2	Rim of fine common ware, clear brown-slipped on inner surface
TRZ427	TZ10-RB2-UE10	TCHINGIZ TEPE RB2	Rim of fine common ware, reddish-brown slip on inner surface
TRZ088	TZ07-RB-5-38	TCHINGIZ TEPE RB1	Open rim, common ware
TRZ089	TZ07-RB-5-39	TCHINGIZ TEPE RB1	Walls of painted common ware
TRZ090	TZ07-RB-5-40	TCHINGIZ TEPE RB1	Base
TRZ091	TZ07-RB-5-41	TCHINGIZ TEPE RB1	Open rim, common ware
TRZ092	TZ07-RB-5-42	TCHINGIZ TEPE RB1	Closed rim, common ware
TRZ051	TZ07-RC-10-1	TCHINGIZ TEPE – RC	Open rim, slipped common ware
TRZ052	TZ07-RC-10-2	TCHINGIZ TEPE – RC	Open rim, slipped common ware
TRZ053	TZ07-RC-10-3	TCHINGIZ TEPE – RC	Open rim, slipped common ware pintada
TRZ054	TZ07-RC-10-4	TCHINGIZ TEPE – RC	Closed rim, slipped common ware
TRZ055	TZ07-RC-10-5	TCHINGIZ TEPE – RC	Open rim of slipped jar
TRZ056	TZ07-RC-10-6	TCHINGIZ TEPE – RC	Base of slipped common ware
TRZ057	TZ07-RC-10-7	TCHINGIZ TEPE – RC	Open rim, slipped common ware
TRZ058	TZ07-RC-10-8	TCHINGIZ TEPE – RC	Open rim, slipped common ware
TRZ059	TZ07-RC-10-9	TCHINGIZ TEPE – RC	Base of slipped common ware
TRZ060	TZ07-RC-10-10	TCHINGIZ TEPE – RC	Base
TRZ061	TZ07-RC-10-11	TCHINGIZ TEPE – RC	Close rim, cooking ware
TRZ062	TZ07-RC-10-12	TCHINGIZ TEPE – RC	Open rim, slipped common ware
TRZ063	TZ07-RC-10-13	TCHINGIZ TEPE – RC	Base of slipped cup
TRZ064	TZ07-RC-10-14	TCHINGIZ TEPE – RC	Open rim, slipped common ware
TRZ065	TZ07-RC-10-15	TCHINGIZ TEPE – RC	Open rim, slipped common ware
TRZ066	TZ07-RC-10-16	TCHINGIZ TEPE – RC	Open rim, slipped common ware
TRZ073	TZ07-RC-6-23	TCHINGIZ TEPE – RC	Walls of common ware

Table 1: Archaeological context and typological description of the analysed vessels

CERAMICS FROM TERMEZ

KUSHAN-SASSANIAN POTTERY FROM TCHINGIZ TEPE

Analytical code	Number of inventory	Site	Type of ceramic
TRZ074	TZ07-RC-5-24	TCHINGIZ TEPE – RC	Base
TRZ075	TZ07-RC-5-25	TCHINGIZ TEPE – RC	Open rim, slipped common ware
TRZ076	TZ07-RC-5-26	TCHINGIZ TEPE – RC	Open rim, slipped common ware
TRZ077	TZ07-RC-5-27	TCHINGIZ TEPE – RC	Walls of common ware
TRZ078	TZ07-RC-5-28	TCHINGIZ TEPE – RC	Bse of slipped cup
TRZ079	TZ07-RC-5-29	TCHINGIZ TEPE – RC	Walls of common ware
TRZ080	TZ07-RC-5-30	TCHINGIZ TEPE – RC	Open rim, slipped common ware
TRZ081	TZ07-RC-5-31	TCHINGIZ TEPE – RC	Open rim, slipped common ware
TRZ082	TZ07-RC-5-32	TCHINGIZ TEPE – RC	Walls of common ware
TRZ083	TZ07-RC-5-33	TCHINGIZ TEPE – RC	Open rim, common ware
TRZ084	TZ07-RC-5-34	TCHINGIZ TEPE – RC	Closed rim, common ware
TRZ085	TZ07-RC-5-35	TCHINGIZ TEPE – RC	Top
TRZ086	TZ07-RC-5-36	TCHINGIZ TEPE – RC	Base of slipped cup
TRZ087	TZ07-RC-5-37	TCHINGIZ TEPE – RC	Walls of unpainted common ware
TRZ157	TZ08-RC-2-1	TCHINGIZ TEPE – RC	Open rim, painted common ware
TRZ158	TZ08-RC-2-2	TCHINGIZ TEPE – RC	Open rim, slipped common ware
TRZ159	TZ08-RC-2-3	TCHINGIZ TEPE – RC	Open rim of oil lamp
TRZ160	TZ08-RC-2-4	TCHINGIZ TEPE – RC	Base of a slipped cup
TRZ161	TZ08-RC-2-5	TCHINGIZ TEPE – RC	Closed rim, cooking ware
TRZ162	TZ08-RC-3-1	TCHINGIZ TEPE – RC	Base of a cooking ware
TRZ163	TZ08-RC-4-1	TCHINGIZ TEPE – RC	Open rim, cooking ware
TRZ164	TZ08-RC-5-1	TCHINGIZ TEPE – RC	Closed rim, slipped common ware
TRZ165	TZ08-RC-5-2	TCHINGIZ TEPE – RC	Open rim, grey-slipped common ware
TRZ166	TZ08-RC-5-3	TCHINGIZ TEPE – RC	Closed rim, grey-slipped common ware
TRZ167	TZ08-RC-5-4	TCHINGIZ TEPE – RC	High base of common ware
TRZ168	TZ08-RC-5-5	TCHINGIZ TEPE – RC	Angular base of common ware
TRZ169	TZ08-RC-5-6	TCHINGIZ TEPE – RC	Rim of a oil lamp
TRZ170	TZ08-RC-5-7	TCHINGIZ TEPE – RC	Open rim, cooking ware-like african type
TRZ171	TZ08-RC-5-8	TCHINGIZ TEPE – RC	Open rim, cooking ware
TRZ172	TZ08-RC-5-9	TCHINGIZ TEPE – RC	Base of cooking ware
TRZ173	TZ08-RC-18-1	TCHINGIZ TEPE – RC	Open rim, slipped common ware
TRZ174	TZ08-RC-18-2	TCHINGIZ TEPE – RC	Open rim, slipped common ware with incised decoration
TRZ175	TZ08-RC-18-3	TCHINGIZ TEPE – RC	Open rim, slipped common ware
TRZ176	TZ08-RC-18-4	TCHINGIZ TEPE – RC	Open rim, slipped common ware
TRZ177	TZ08-RC-21-1	TCHINGIZ TEPE – RC	Open rim, slipped common ware
TRZ178	TZ08-RC-21-2	TCHINGIZ TEPE – RC	Open rim, slipped common ware
TRZ179	TZ08-RC-21-3	TCHINGIZ TEPE – RC	Closed rim, slipped common ware with incised decoration
TRZ180	TZ08-RC-21-4	TCHINGIZ TEPE – RC	Open rim, slipped common ware with incised decoration (overfired)
TRZ181	TZ08-RC-21-5	TCHINGIZ TEPE – RC	Closed rim of slipped jar with incised decoration in the rim
TRZ182	TZ08-RC-21-6	TCHINGIZ TEPE – RC	Open rim, cooking ware
TRZ183	TZ08-RC-21-7	TCHINGIZ TEPE – RC	Top
TRZ201	TZ08-RC-23-1	TCHINGIZ TEPE – RC	Open rim, red-slipped plate or top
TRZ293	TZ08-RC-5-10	TCHINGIZ TEPE – RC	Cooking ware, open rim, grey paste and reddish surfaces
TRZ294	TZ08-RC-18-5	TCHINGIZ TEPE – RC	Cooking ware, open rim, reddish paste
TRZ295	TZ08-RC-18-6	TCHINGIZ TEPE – RC	Cooking ware, open rim, reddish paste
TRZ296	TZ09-RC2-18-1	TCHINGIZ TEPE – RC	Common ware, open rim, reddish painted on inner and outer surfaces
TRZ297	TZ09-RC2-18-2	TCHINGIZ TEPE – RC	Common ware, plate, incised dec., red painted on inner and outer surfaces
TRZ298	TZ09-RC2-18-3	TCHINGIZ TEPE – RC	Cooking ware, open rim
TRZ299	TZ09-RC2-18-4	TCHINGIZ TEPE – RC	Common ware, open rim, unpainted
TRZ300	TZ09-RC2-21-1	TCHINGIZ TEPE – RC	Common ware, plate, unpainted
TRZ301	TZ09-RC2-21-2	TCHINGIZ TEPE – RC	Common ware, open rim
TRZ302	TZ09-RC2-21-3	TCHINGIZ TEPE – RC	Common ware, painted in internal and external surface
TRZ303	TZ09-RC2-21-4	TCHINGIZ TEPE – RC	Slipped common ware

Table 1: Archaeological context and typological description of the analysed vessels

CERAMICS FROM TERMEZ

KUSHAN-SASSANIAN POTTERY FROM TCHINGIZ TEPE

Analytical code	Number of inventory	Site	Type of ceramic
TRZ304	TZ09-RC2-21-5	TCHINGIZ TEPE – RC	Common ware, incised dec., reddish painted on inner and outer surfaces
TRZ305	TZ09-RC2-25-1	TCHINGIZ TEPE – RC	Open rim of jar
TRZ306	TZ09-RC2-25-2	TCHINGIZ TEPE – RC	Common ware, open rim, incised dec., red painted on inner and outer surfaces
TRZ307	TZ09-RC2-25-3	TCHINGIZ TEPE – RC	Common ware, base of jar, reddish painted on the outer surface
TRZ308	TZ09-RC2-25-4	TCHINGIZ TEPE – RC	Fragment of terracotta, brownish-red paste
TRZ309	TZ09-RC2-28-1	TCHINGIZ TEPE – RC	Cooking ware
TRZ310	TZ09-RC2-28-2	TCHINGIZ TEPE – RC	Common ware, jar, orange-brown painted on inner-outer surfaces
TRZ311	TZ09-RC2-28-3	TCHINGIZ TEPE – RC	Common ware, jar, dark brownish painted on the inner surface
TRZ312	TZ09-RC2-28-4	TCHINGIZ TEPE – RC	Common ware, jar, orange-reddish painted on rim and outer surface
TRZ067	TZ07-5D-17	TCHINGIZ - Prosp	Walls of common ware
TRZ068	TZ07-5D-18	TCHINGIZ - Prosp	Open rim, common ware
TRZ069	TZ07-5D-19	TCHINGIZ - Prosp	Open rim, common ware
TRZ070	TZ07-5D-20	TCHINGIZ - Prosp	Walls of common ware
TRZ071	TZ07-5D-21	TCHINGIZ - Prosp	Walls of common ware
TRZ072	TZ07-5D-22	TCHINGIZ - Prosp	Closed rim, common ware
TRZ184	TZ08-RF-2-1	TCHINGIZ TEPE – RF	Open rim, painted common ware
TRZ185	TZ08-RF-11-1	TCHINGIZ TEPE – RF	Open rim, painted common ware with stamped decoration
TRZ186	TZ08-RF-11-2	TCHINGIZ TEPE – RF	Base of painted common ware
TRZ187	TZ08-RF-11-3	TCHINGIZ TEPE – RF	Rim of cooking ware
TRZ188	TZ08-RF-15-1	TCHINGIZ TEPE – RF	Base of a slipped and overfired cup
TRZ189	TZ08-RF-20-1	TCHINGIZ TEPE – RF	Cooking ware
TRZ190	TZ08-RF-20-2	TCHINGIZ TEPE – RF	Open rim, painted common ware
TRZ191	TZ08-RF-20-3	TCHINGIZ TEPE – RF	Open rim, painted common ware
TRZ192	TZ08-RF-22-1	TCHINGIZ TEPE – RF	Open rim, painted common ware, incised decoration (overfired)
TRZ193	TZ08-RF-22-2	TCHINGIZ TEPE – RF	Open rim, painted common ware
TRZ194	TZ08-RF-22-3	TCHINGIZ TEPE – RF	Open rim, painted common ware with stamped decoration
TRZ195	TZ08-RF-23-1	TCHINGIZ TEPE – RF	Base of painted cup
TRZ196	TZ08-RF-23-2	TCHINGIZ TEPE – RF	Open rim, common ware
TRZ197	TZ08-RF-23-3	TCHINGIZ TEPE – RF	Open rim, common ware
TRZ198	TZ08-RF-23-4	TCHINGIZ TEPE – RF	Walls and rim of painted jar, incised decoration
TRZ199	TZ08-RF-27-1	TCHINGIZ TEPE – RF	Open rim, painted common ware
TRZ200	TZ08-RF-27-2	TCHINGIZ TEPE – RF	Open rim, painted common ware
TRZ202	TZ08-RF-29-1	TCHINGIZ TEPE – RF	Open rim, painted common ware
TRZ291	TZ08-RF-22-4	TCHINGIZ TEPE – RF	Common ware, relief dec., reddish slip on inner and outer surfaces
TRZ292	TZ08-RF-26-1	TCHINGIZ TEPE – RF	Top of cooking ware, clear brown paste

Table 1: Archaeological context and typological description of the analysed vessels

3. The analytical programme and methodology

The archaeometrical study consisted of chemical (XRF), mineralogical (XRD) and petrographic analysis (OM) of 28 sherds from Tchingiz Tepe.

X-Ray Fluorescence (XRF) can determine the exact chemical composition of pottery paste and, when combined with a multivariate statistical treatment, it can show the level of chemical similarity between analysed sherds. In provenance studies, chemical analysis will focus on the identification of specific ceramic productions (reference groups - RGs) that can be archaeologically related to kiln sites or production sites. These RGs represent single pottery productions of a workshop located in a specific area. When the analysed ceramics are unrelated to a specific kiln but related to urban sites (consumption and distribution), the homogeneous groups identified by the chemical analysis are considered paste compositional reference units (PCRUs). The provenance of ceramics from PCRUs will only be assigned when they are chemically associated to an identified RG from a pottery workshop.

For the new samples, XRF was performed on powdered specimens using an Axios-Max advanced Panalytical spectrometer. Major elements (Fe_2O_3, Al_2O_3, P_2O_5, TiO_2, MnO, MgO, CaO, K_2O, SiO_2) were determined by preparing duplicates of glassy pills using 0.3 g of powdered specimen in an alkaline fusion with lithium tetraborate at 1/20 dilution. Trace elements (V, Cr, Co, Ni, Cu, Zn, Ga, Rb, Sr, Y, Zr, Nb, Mo, Sn, Ba, W, Pb, Ce, Th) and Na_2O were determined by powdered pills made from 5 g of specimen mixed with Elvacite agglutinating placed over boric acid in an aluminium capsule and pressed for 60 s at 200 kN in a Herzog press. The loss on ignition (LOI) was determined by firing 0.3 g of dried specimen at 950°C for 3 h. However, XRF analysis carried out in previous years over some of the samples from Termez and Kampyr Tepe considered in this study were performed using a Philips PW 2400 spectrometer with an Rh excitation source. Although the method of sampled preparation is the same and the quantification is fixed by a calibration line performed with the same International Geological Standards (Hein *et al.* 2002), slightly compositional differences are observed in the results obtained from both spectrometers. Major variability occurs in some trace elements as Ba, Rb, V and Cr.

Thin section analysis of ceramics is very useful in studying the petrographic composition of pottery and the various characteristics of the clay matrix. Through comparison with the geological composition of the area, it can give information about the possible geological origin and the type of the raw materials from which the pottery is made. It can also lead to the identification of the possible local or imported character of the raw materials on the basis of their geological compatibility with the zone where the pottery was recovered. Thin section analysis was performed in some selected samples using an Olympus BX41 polarizing microscope working under magnification between 40X and 400X. Each ceramic specimen was impregnated with epoxy resin and mounted using Loctite UV glue and sectioned using a Struers Discoplan TS. The thin sections were finished by hand using a powder abrasive until reaching a thickness of 30 micrometers in which quartz presents a grey-white first order interference colour. Photographs were taken using a digital camera Olympus DP-70 attached to the microscope controlled by specific computer software.

Technological processes on pottery manufacture have been estimated using mineralogical and petrographic analysis, employing **X-ray diffraction (XRD)** and **optical microscopy by thin section analysis.**

X-ray diffraction (XRD) identifies the mineralogical composition of ancient ceramics based on differences between primary phases, firing phases and secondary phases. This will provide information on the paste's raw material, firing conditions (i.e., firing atmosphere and temperature) and possible alteration and contamination processes. Crystalline phases were evaluated using the same powdered specimens prepared for XRF. The measurements were performed using a Siemens D-500 diffractometer working with the Cu Kα radiation (λ=1.5406 Å), and graphite monochromator in the diffracted beam, at 1.2 kW (40 kV, 30 mA). Spectra were taken from 4 to 70°2Θ, at 1°2Θ/min (step size=0.05°2Θ; time=3 s). The evaluation of crystalline phases was carried out using the X'Pert program of Panalytical.

Thin section analysis also provides information on the matrix and aplastic inclusions and it enables inferences to be drawn about technological aspects (e.g., type of clay used, clay mixing, selection of specific inclusions, temper addition and firing temperature).

Technological study will also entail the analysis of the surface treatments of pottery vessels, which serve both as decoration and as a means of reducing their permeability to liquids. We have used the **scanning electron microscope (SEM-EDS**) in order to identify the chemical composition and the microstructure characteristics of the reddish and brownish slips of ceramics from the Hellenistic, Greco-Bactrian, Kushan and Kushan-Sassanian periods and the chemical composition and the firing process followed to obtain the glazed surfaces of the Islamic vessels. Quantitative micro-chemical analysis of the paste and surface slip of several samples were performed using a JEOL JSM-840 Scanning Electron Microscope (SEM) equipped with Secondary Electron (SE) detector and Energy Dispersive X-ray Micro Analyser (EDS). The observations were performed under vacuum at the external surface of the polished sections and the secondary electron image was taken at several magnifications. The acceleration voltage was equal to 20kV and the intensity to 3x10-9 A. The preparation of the samples has been done by fixing the fresh fractures upon a standard metallic base of 1cm diameter with silicon and in order to insure the continuous conductivity between the sample and its base and to avoid the overloading of the surface, the polished sections were covered with silver and then the whole sample was covered with carbon.

4. Ceramics from the early Kushan and Kushan-Sassanian periods.

4.1. Tchingiz Tepe (Termez): Integrated results of archaeometrical analysis

ERAAUB's analytical database comprises 135 (Table 1) sherds coming from several trenches excavated at four different sectors of Tchingiz Tepe (RA, RB, RC and RF) (Figure 2). Fifteen sherds (TRZ400 to TRZ414) were recovered at several stratigraphical units of RA sector, placed in contact with the eastern line of the fortification, in front of the Tower 7 (Martínez, this volume). The works in this trench have revealed the presence of monastic cells from a Kushan-Sassanian settlement and a previous occupation which is still undated. From these sherds, 13 are common wares and two are cooking wares (TRZ405 and TRZ408).

At the north of sector RA, more monastic buildings dated between the 3th and the end of the 4th century AD were recovered at sector RC. These rooms are placed in parallel to the eastern wall, between Tower 4 and Tower 5. From sector RC, 78 common and cooking wares from different archaeological levels (TRZ051 to TRZ060, TRZ163 to TRZ166; TRZ073 to TRZ087; TRZ157 to TRZ183; TRZ201; TRZ293 to TRZ312), analysed in previous works (Martínez *et al*., 2008, 2009, 2010), have been compared to the archaeometrical results obtained for ceramics from RA sector. From these sherds, 12 correspond to cooking wares (TRZ161, 162, 163, 170, 171, 172, 182, 293, 294, 295, 298 and 309) and two are tops (TRZ085, 183).

Between RA and RC sectors, a pottery kiln was discovered and excavated in 2008 in sector RF, placed between Tower 5 and Tower 6 of the eastern wall of Tchingiz Tepe. Archaeometrical analyses were also performed over 26 pottery sherds recovered in surface (TRZ067 to TRZ072) or inside the kiln structure (Martínez *et al*., 2009). They comes from levels of accumulation of materials which corresponded to the collapse of the kiln structures or strata formed by household trash when the kiln no longer performed its primary function but was used as a trash heap instead (TRZ184 to TRZ200, 202, 291 and 292). Three of these sherds correspond to cooking wares (TRZ187, 189 and 192).

The rest of analysed sherds comes from two different trenches (RB1 and RB2) excavated at sector RB, placed at the southern-east area of Tchingiz Tepe, in front of Tower 9. They are 5 ceramics from sector RB1 (TRZ088 to TRZ092), dated from the 2nd century BC (Martínez *et al*., 2008; Mestres and Rauret, 2009), and 13 sherds from sector RB2 (TRZ415 to TRZ427) (Ariño, this volume).

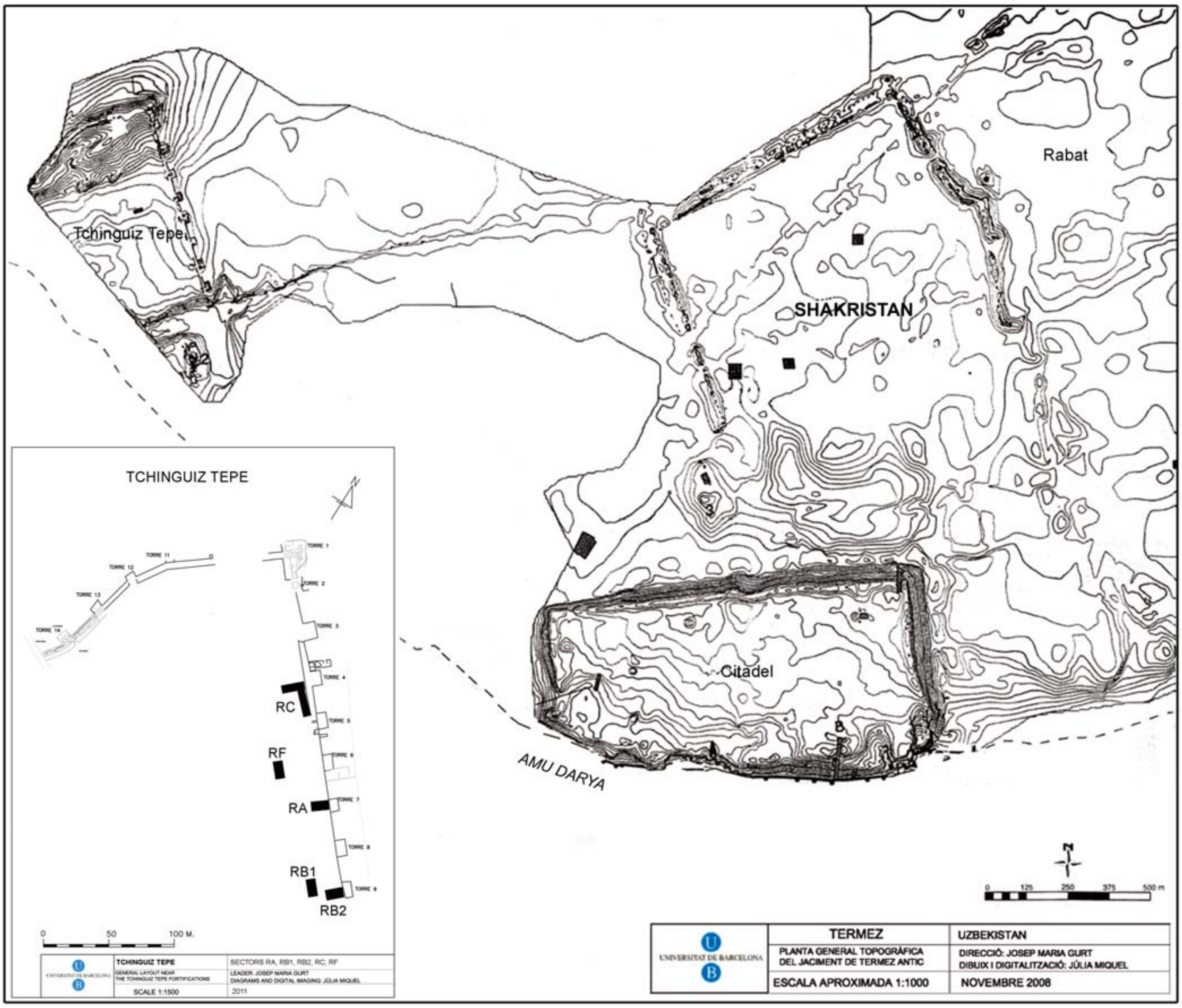

Figure 2: General layout of part of the archaeological site of Termez with indication of the location of Tchinguiz Tepe site and the excavated sectors (RA, RB1, RB2, RC and RF).

The chemical concentrations of 135 pottery sherds from **Tchingiz Tepe (TT)** determined by XRF (Table 2) were treated statistically according to the proposals of Aitchison (1986) and Buxeda (1999). One of the most important steps for the statistical evaluation of the chemical data is to calculate somehow the variability in the data set. One of the common ways is to calculate the Compositional Variation Matrix (CVM) (Buxeda, 1999; Buxeda and Kilikoglou, 2003), which includes the total variation and the variability that each element is introducing in the data set.

The CVM has been calculated over the 135 ceramic individuals using the subcomposition: Fe_2O_3 (as total Fe), Al_2O_3, TiO_2, MgO, CaO, Na_2O, K_2O, SiO_2, Th, Nb, Zr, Y, Sr, Ce, Ga, Zn, Cu and Ni. Some elements have not been considered: Mo, Sn, Ba, Rb, V and Cr because can introduce a false high variability in the data set due to analytical imprecision; Co and W because their values might have been altered during sample preparation process and P_2O_5, Pb and MnO because they are very susceptible to suffer postdepositional contaminations. Finally, Th values have not been used in the statistical treatment because it usually suffers strong interferences due to the high Sr values produced during XRF analysis, leading to the underestimation of Th values.

The Compositional Variation Matrix (CVM) shows a vt = 0.480 (Table 3). This value is moderately high and could indicate a relative polygenic origin of the data set. The main variability is introduced by the elements: CaO ($^{\tau}$·CaO = 4.977), Sr ($^{\tau}$·Sr = 1.530), Na_2O_3 ($^{\tau}$·Na_2O_3 = 1.048), Ce ($^{\tau}$·Ce = 0.860), Cu ($^{\tau}$·Cu = 0.787), Th ($^{\tau}$·Th = 0.747), K_2O ($^{\tau}$·K2O = 0.727) and MgO ($^{\tau}$·MgO = 0.707).

lc	Fe2O3	Al2O3	MnO	P2O5	TiO2	MgO	CaO	Na2O	K2O	SiO2	Ba	Rb	Th	Nb	Pb	Zr	Y
TRZ400	6.42	16.34	0.1	0.23	0.675	3.99	8.865	1.17	3.69	56.04	0.0931	0.0128	0.0012	0.0014	0.0023	0.0147	0.0027
TRZ401	5.735	14.46	0.095	0.36	0.66	3.07	8.075	1.475	3.515	58.02	0.0675	0.0106	0.0012	0.0014	0.0023	0.0168	0.0028
TRZ402	6.915	16.98	0.1	0.19	0.715	3.635	10.03	1.37	3.49	55.65	0.0621	0.0133	0.0014	0.0015	0.0022	0.0149	0.0027
TRZ403	6.275	16.01	0.1	0.2	0.695	3.755	8.835	1.465	3.345	57.39	0.0506	0.0123	0.0012	0.0015	0.0029	0.0157	0.0027
TRZ404	6.46	16.3	0.11	0.195	0.685	3.825	10.82	2.045	2.79	56.81	0.0550	0.0082	0.0012	0.0014	0.0015	0.0149	0.0027
TRZ405	3.075	8.54	0.05	0.165	0.405	1.695	23.52	1.09	2.27	38.62	0.0318	0.0066	0.0006	0.0009	0.0010	0.0127	0.0018
TRZ406	5.795	15.23	0.095	0.22	0.655	3.715	10.61	1.37	3.125	56.97	0.0495	0.0116	0.0012	0.0014	0.0016	0.0156	0.0027
TRZ407	6.315	16.27	0.105	0.2	0.685	3.715	9.185	1.485	3.395	56.34	0.0576	0.0127	0.0012	0.0014	0.0019	0.0143	0.0026
TRZ408	6.225	17.32	0.04	0.35	0.805	2.245	2.395	2.015	3.13	64.17	0.0387	0.0129	0.0012	0.0015	0.0019	0.0194	0.0035
TRZ409	6.11	15.32	0.11	0.375	0.645	3.54	11.13	1.695	3.225	53.74	0.0582	0.0110	0.0011	0.0014	0.0023	0.0145	0.0026
TRZ410	6.54	16.29	0.12	0.195	0.67	3.615	11.18	1.495	3.045	56.21	0.0660	0.0123	0.0013	0.0015	0.0010	0.0151	0.0027
TRZ411	6.775	16.65	0.11	0.18	0.7	3.5	9.515	1.55	3.23	56.9	0.0607	0.0125	0.0014	0.0015	0.0021	0.0153	0.0028
TRZ412	6.025	15.81	0.095	0.19	0.65	4.23	11.52	1.255	3.17	54.17	0.0523	0.0126	0.0012	0.0014	0.0014	0.0140	0.0026
TRZ413	6.845	16.94	0.11	0.19	0.72	4.14	10.15	1.415	3.195	55.85	0.0575	0.0117	0.0013	0.0015	0.0027	0.0157	0.0027
TRZ414	6.065	15.24	0.1	0.18	0.66	3.045	8.42	1.46	3.165	55.29	0.0485	0.0108	0.0011	0.0013	0.0024	0.0142	0.0025
TRZ415	6.475	15.58	0.12	0.19	0.66	3.435	9.61	1.71	3.23	55.2	0.0556	0.0120	0.0012	0.0014	0.0022	0.0144	0.0026
TRZ416	6.34	15.72	0.11	0.215	0.68	3.275	9.26	1.635	3.4	56.06	0.0541	0.0122	0.0013	0.0015	0.0025	0.0150	0.0026
TRZ417	5.88	15.1	0.1	0.235	0.61	3.75	12.24	1.515	3.365	51.71	0.0463	0.0119	0.0011	0.0014	0.0025	0.0139	0.0025
TRZ418	6.08	15.35	0.11	0.19	0.665	3.345	9.43	1.675	3.185	58.05	0.0612	0.0101	0.0011	0.0014	0.0021	0.0153	0.0026
TRZ419	6.225	15.81	0.11	0.25	0.68	3.475	7.98	1.58	3.24	57.4	0.0573	0.0118	0.0012	0.0014	0.0025	0.0151	0.0027
TRZ421	6.06	15.73	0.1	0.24	0.67	3.55	9.46	1.49	3.385	55.75	0.0540	0.0122	0.0011	0.0014	0.0023	0.0149	0.0027
TRZ422	6.31	16.05	0.11	0.25	0.67	3.615	10.06	1.42	3.45	54.89	0.0541	0.0125	0.0012	0.0015	0.0027	0.0145	0.0028
TRZ423	5.505	14.13	0.11	0.205	0.625	2.785	10.33	1.655	3.035	54.35	0.0549	0.0108	0.0012	0.0013	0.0021	0.0145	0.0025
TRZ424	6.545	16.59	0.11	0.27	0.69	3.535	9.4	1.74	2.98	57.55	0.0596	0.0105	0.0012	0.0014	0.0024	0.0145	0.0027
TRZ425	6.41	16.18	0.1	0.19	0.685	3.55	11.03	1.405	3.255	55.71	0.0636	0.0126	0.0013	0.0015	0.0024	0.0149	0.0027
TRZ426	6.23	15.41	0.12	0.18	0.645	3.27	12.79	1.48	2.91	56.1	0.0604	0.0117	0.0011	0.0014	0.0015	0.0145	0.0026
TRZ427	6.295	16.11	0.1	0.22	0.68	3.69	9.86	1.6	3.015	58.51	0.0506	0.0111	0.0012	0.0015	0.0017	0.0162	0.0026

lc	Sr	Ce	Ga	V	Zn	Cu	Ni	Cr
TRZ400	0.0473	0.0067	0.0020	0.0130	0.0100	0.0026	0.0050	0.0094
TRZ401	0.0484	0.0068	0.0018	0.0104	0.0089	0.0027	0.0043	0.0079
TRZ402	0.0366	0.0073	0.0021	0.0142	0.0105	0.0036	0.0058	0.0124
TRZ403	0.0353	0.0064	0.0020	0.0124	0.0118	0.0032	0.0049	0.0089
TRZ404	0.0302	0.0059	0.0020	0.0127	0.0101	0.0034	0.0051	0.0094
TRZ405	0.0530	0.0037	0.0011	0.0101	0.0066	0.0022	0.0020	0.0063
TRZ406	0.0360	0.0063	0.0019	0.0117	0.0100	0.0032	0.0048	0.0092
TRZ407	0.0322	0.0062	0.0020	0.0133	0.0100	0.0028	0.0053	0.0095
TRZ408	0.0389	0.0069	0.0021	0.0251	0.0087	0.0020	0.0036	0.0175
TRZ409	0.0417	0.0054	0.0019	0.0128	0.0100	0.0035	0.0051	0.0091
TRZ410	0.0370	0.0065	0.0021	0.0129	0.0110	0.0038	0.0054	0.0101
TRZ411	0.0365	0.0065	0.0021	0.0130	0.0098	0.0036	0.0054	0.0097
TRZ412	0.0416	0.0059	0.0020	0.0139	0.0102	0.0035	0.0051	0.0095
TRZ413	0.0322	0.0071	0.0021	0.0121	0.0105	0.0039	0.0053	0.0100
TRZ414	0.0463	0.0066	0.0018	0.0110	0.0091	0.0032	0.0047	0.0079
TRZ415	0.0501	0.0064	0.0018	0.0114	0.0088	0.0032	0.0046	0.0085
TRZ416	0.0369	0.0062	0.0019	0.0119	0.0092	0.0036	0.0050	0.0082
TRZ417	0.0502	0.0064	0.0018	0.0130	0.0098	0.0033	0.0048	0.0095
TRZ418	0.0383	0.0056	0.0018	0.0116	0.0079	0.0025	0.0048	0.0094
TRZ419	0.0356	0.0069	0.0019	0.0123	0.0098	0.0028	0.0045	0.0088
TRZ421	0.0392	0.0069	0.0019	0.0122	0.0095	0.0030	0.0044	0.0080
TRZ422	0.0418	0.0071	0.0020	0.0121	0.0092	0.0032	0.0047	0.0085
TRZ423	0.0541	0.0061	0.0017	0.0115	0.0084	0.0029	0.0043	0.0083
TRZ424	0.0343	0.0063	0.0020	0.0137	0.0091	0.0030	0.0049	0.0091
TRZ425	0.0361	0.0064	0.0020	0.0117	0.0095	0.0031	0.0053	0.0096
TRZ426	0.0297	0.0063	0.0019	0.0129	0.0095	0.0029	0.0049	0.0095
TRZ427	0.0316	0.0063	0.0019	0.0115	0.0100	0.0030	0.0048	0.0091

Table 2: Table 2: The normalised chemical composition of the analysed ceramic material from **Tchinguiz Tepe** (TRZ400 to TRZ427)

(TT)	Fe_2O_3	Al_2O_3	TiO_2	MgO	CaO	Na_2O	K_2O	SiO_2	Th	Nb	Zr	Y	Sr	Ce	Ga
$\tau_{.i}$	0.523	0.541	0.565	0.707	4.977	1.048	0.727	0.581	0.747	0.599	0.649	0.598	1.530	0.860	0.550
$vt/\tau_{.i}$	0.919	0.887	0.850	0.679	0.096	0.458	0.660	0.826	0.642	0.801	0.740	0.803	0.314	0.559	0.872
$r\ v,\tau$	0.999	0.999	0.998	0.994	-0.629	0.996	0.998	0.997	0.996	0.998	0.996	0.997	0.916	0.998	0.999
vt	0.480														

(TT)	Zn	Cu	Ni
$\tau_{.i}$	0.642	0.787	0.651
$vt/\tau_{.i}$	0.748	0.610	0.737
$r\ v,\tau$	0.998	0.990	0.993
vt			

Table 3: Compositional Variation Matrix (CVM) calculated upon the 133 ceramics from the Kushan period sampled at sectors RA, RB, RC and RFof Tchingiz Tepe and two clay samples, one from ***Tchingiz Tepe*** (G-TRZ-28) and the other from the area of Ancient Military Cuarters (G-TRZ-27)(Termez).

The variability introduced by CaO is clearly linked to some differences in the calcareous character of the material, although most of individuals were produced using calcareous clays whereas few correspond to low calcareous pastes. Nonetheless the variability introduced by CaO and Sr could be the result of the crystallisation of secondary calcite inside the pores of some vessels (Buxeda and Cau, 1995; Cau, Day, Montana, 2002), as it has been observed at TRZ148 by thin section analysis (Martínez *et al*., 2009). The variability introduced mathematically by Cu cannot be trusted as it can easily present postdepositional alterations. However, in the case of MgO and Ce the variability must be due to slightly differences in the chemical concentration between sherds, probably related to different raw materials. In the case of Th, this is a trace element that may suffer interference caused by high Sr contents that involve their undervaluation and its concentration may not correspond to the real value.

Finally, some of the variability introduced by Na_2O can be explained by the existence of a characteristic postdepositional alteration related to the formation of the Na-zeolite analcime($Na[AlSi_2O_6]\cdot 6H_2O$), as it has been already detected in previous archaeometric works we have carried out on the pottery of Termez (Tsantini *et al*., 2007; Martínez *et al*., 2008, 2009, 2010). The crystallisation of this secondary phase in some specimens can lead to the K_2O variability. Furthermore, relevant number of the previously analysed sherds by SEM-EDS exhibit NaCl crystals (Martínez *et al*., 2008). The crystallization of both minerals must be related to the same alteration and/or contamination process occurred during burial at a dessert environment, rich in salt efflorescences stemming from the emergence of salts originated in Mesozoic salt beds, due to halo-cinetic processes (Sánchez del Corral, 2009). For these reasons, Na_2O, K_2O, Th, Sr and Cu were excluded of the statistical evaluation of the chemical data.

Repeating the same statistical routine considering only Fe_2O_3 (as total Fe), Al_2O_3, TiO_2, MgO, CaO, SiO_2, Nb, Zr, Y, Ce, Ga, Zn and Ni, the vt resulted of the new CVM is more lower (vt = 0.3402). A total variation of that range indicates a relative homogeneous data set which, in geochemical terms, points towards a relative similar geochemical origin of the raw materials used for the production of most of the analysed individuals, without this necessarily meaning that all of them belong into the same pottery production or the same pottery production area. Then, the sub-composition considered were transformed into logratios following the consideration of Aitchison (1986) and Buxeda (1999) on compositional data, where Ga was used as divisor, as according to the CVM, it was the element less contributing to the chemical variability (Buxeda and Kilikoglou, 2003).

The chemical results of the 135 sherds and two clay samples (**G-TRZ27 and G-TRZ28**) are summarized in the dendrogram of Figure 3, resulting from the cluster analysis performed using the Square Euclidean distance and the centroid algorithm with S-plus2000 (MathSoft, 1999). Based on their chemical similarity, sherds are grouped into several groups which have already been identified in previous studies (Martínez *et al*., 2008, 2009). These groups comprise cooking wares (TT-A, TT-B, TT-C and TT-D) or both common and cooking wares (TT-E and TT-G). The new specimens incorporated in the present study are part of the group TT-A or they appear isolated because of their chemical differences compared to other samples.

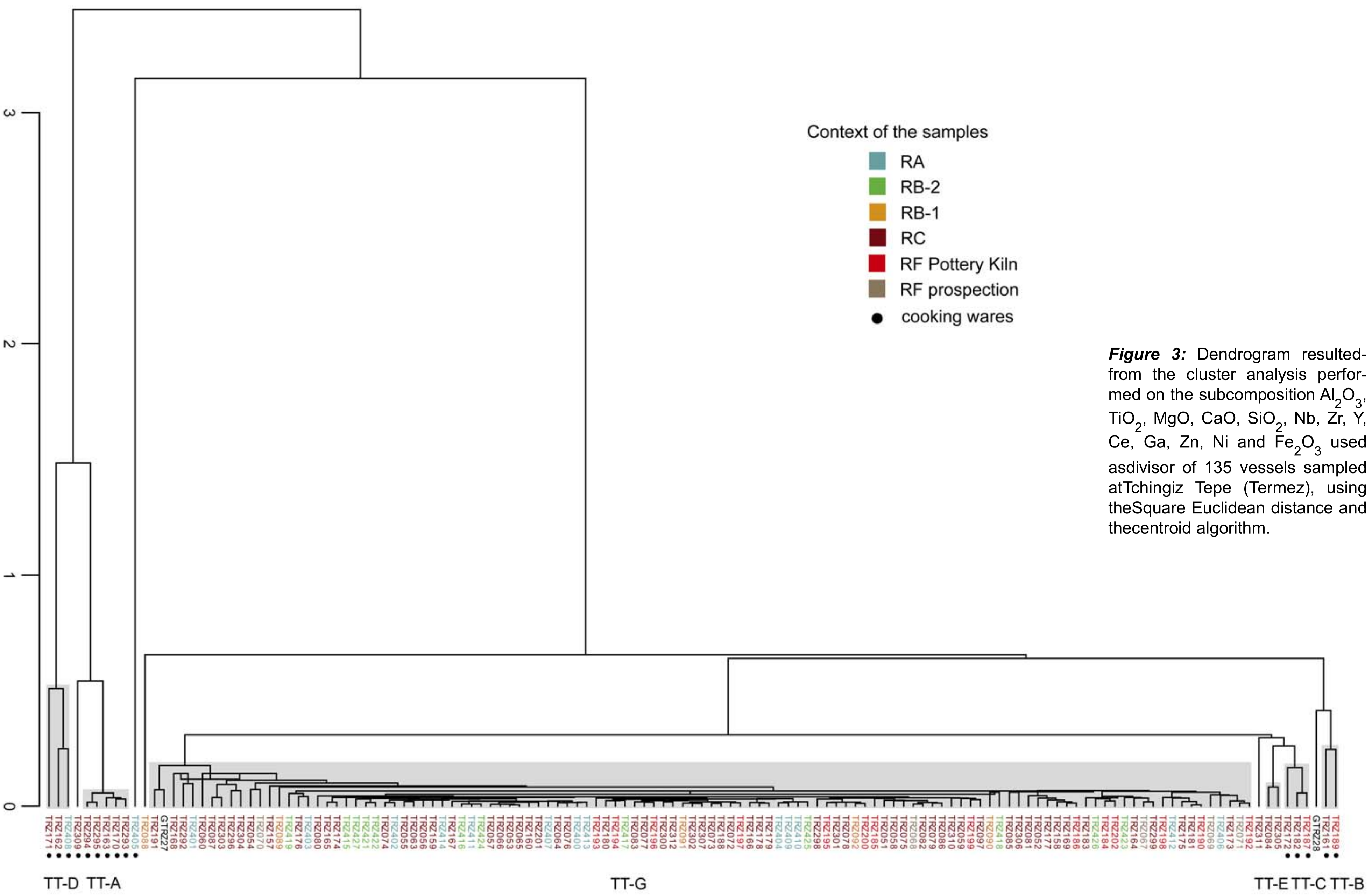

Figure 3: Dendrogram resulted from the cluster analysis performed on the subcomposition Al_2O_3, TiO_2, MgO, CaO, SiO_2, Nb, Zr, Y, Ce, Ga, Zn, Ni and Fe_2O_3 used asdivisor of 135 vessels sampled atTchingiz Tepe (Termez), using theSquare Euclidean distance and thecentroid algorithm.

At the left side of the dendrogram, 5 cooking wares from RC sector (TRZ163, TRZ170, TRZ293, TRZ294 and TRZ295) are joined at TT-A group, which was already identified in previous studies (Martínez et al. 2010). These cooking wares are low calcareous and present Al2O3, TiO2, SiO2, Nb, Zr, Y and Ce high relative values respect to the rest of the material. All these sherds present the same typological characteristics (Figure 4) and their chemical differences compared to the rest of the analysed material in this dendrogram are important enough to indicate that they correspond to one single production, TT-A. In chemical and typological terms, TRZ309 is relatively similar to pottery from TT-A group but differs because it presents higher values in Sr and lower in Ce. The mean chemical composition and the standard deviation of TT-A group and the cooking ware TRZ309 are given in Table 4.

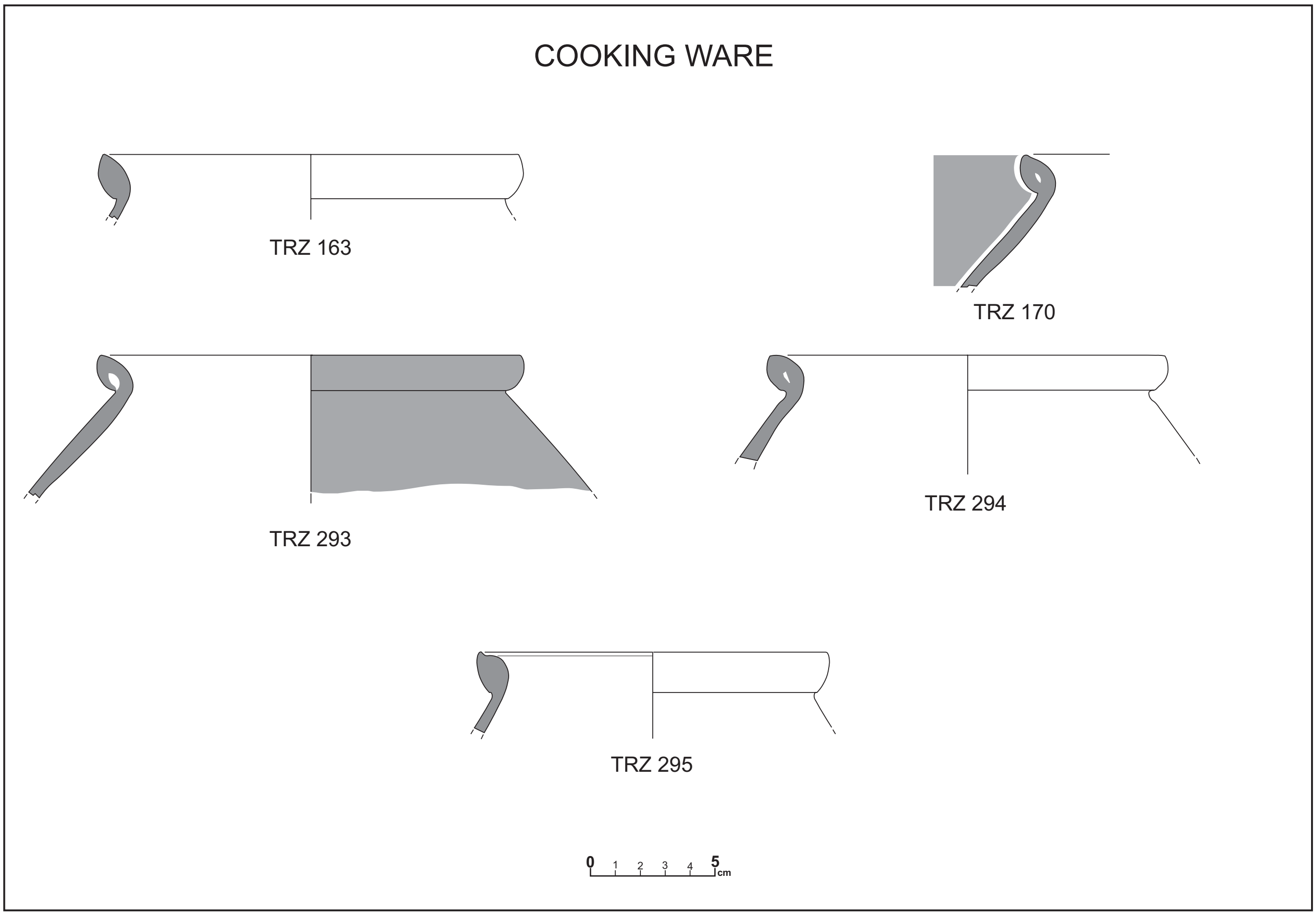

Figure 4: Typology of vessels from group **TT-A.**

	TT-A (n=5)		**TT -B** (n= 2)		**TT -C** (n= 3)		**TT -D** (n= 3)		**TT -E** (n= 2)		**TRZ309**	**TRZ405**	**TRZ088**	**TRZ311**	**G-TRZ27**	**G-TRZ28**
	m	**sd**	**m**	**sd**	**m**	**sd**	**m**	**sd**	**m**	**sd**	**nc**	**nc**	**nc**	**nc**	**nc**	**nc**
Fe_2O_3 (%)	6.37	0.19	5.56	0.20	6.16	0.23	5.98	0.35	5.99	0.12	6.42	3.87	6.63	6	6.15	5.51
Al_2O_3 (%)	18.31	0.36	13.98	1.16	16.86	0.42	16.75	0.76	16.12	0.47	17.40	10.76	16.70	15.39	15.27	13.02
TiO_2 (%)	0.79	0.01	0.59	0.04	0.74	0.02	0.76	0.05	0.72	0.02	0.78	0.51	0.72	0.68	0.66	0.67
MgO (%)	3.93	0.03	2.87	0.06	3.18	0.44	2.32	0.23	3.09	0.06	3.70	2.13	3.56	4.39	4.19	2.74
CaO (%)	1.16	0.15	21.27	4.43	6.25	0.50	3.29	1.24	6.21	0.49	2.30	29.62	8.29	6.42	14.27	15.03
Na_2O (%)	1.55	0.09	1.94	0.02	1.56	0.86	1.64	0.35	1.72	0.00	1.50	1.37	1.92	1.50	0.82	0.96
K_2O (%)	4.26	0.05	3.60	0.56	3.59	0.11	3.50	0.28	4.15	0.39	4.24	2.86	3.64	3.64	3.11	2.75
SiO_2 (%)	69.37	0.55	50.03	2.43	61.48	0.62	65.55	1.10	61.75	1.54	63.42	48.64	58.23	61.68	55.03	58.88
Ba (ppm)	432	9	408	13	469	78	336	50	540	45	528	400	608	492	629	454
Rb (ppm)	146	4	121	7	158	5	136	8	127	9	149	**83**	132	101	141	127
Th (ppm)	15	1	15	1	14	1	13	1	12	2	15	8	14	13	18	18
Nb (ppm)	19	1	14	0	17	0	14	1	17	1	19	12	16	16	18	20
Zr (ppm)	199	2	140	4	172	4	189	8	166	1	186	160	156	152	150	193
Y (ppm)	34	1	23	0	26	2	29	6	25	1	33	22	24	26	28	25
Sr (ppm)	151	9	527	77	364	23	363	52	476	237	196	668	421	539	292	216
Ce (ppm)	82	5	53	9	74	9	63	9	62	10	68	47	32	48	59	54
Ga (ppm)	20	1	17	1	19	0	19	2	17	0	20	14	18	16	18	16
V (ppm)	128	4	100	7	220	14	170	74	106	10	132	127	96	92	120	95
Zn (ppm)	127	2	103	1	116	5	93	6	70	7	138	83	93	106	107	88
Cu (ppm)	33	1	28	4	20	2	21	1	25	0	38	27	35	31	36	35
Ni (ppm)	50	2	40	3	45	2	31	5	46	1	57	25	52	46	50	42
Cr (ppm)	95	6	61	1	226	32	123	48	78	2	98	79	78	80	81	70

Table 4: The mean chemical composition (m) and the standard deviation (sd) using normalised data of TT-A, TT-B, TT-C, TT-D, TT-E chemical groups and the raw normalised-chemical composition (nc) of the ceramic outliers TRZ309, TRZ311, TRZ405 and TRZ088 from **Tchingiz Tepe** and of the two clay samples (G-TRZ-27 and G-TRZ-28) fromTermez

From a petrographic point of view, cooking wares from **TT-A** group (TRZ163, TRZ170, TRZ293, TRZ294, TRZ295 and TRZ309) are characteristics of a medium-fine fabric (Figure 5a). Clay matrix is Fe rich, semi-vitrified. Groundmass is relatively abundant and fine whereas coarser inclusions (≤ 0.5 mm) are scarce. Fragments of quartz, muscovite, k-feldspars, plagioclase, quartz-mica schist and mica-schist are predominant; fragments of quartzite and chert are dominants; nodules of micritic calcite are frequent; amphibole, epidote and white mica are common; biotite, amphiboles, epidote and volcanic rocks are common to occasional; garnet is few (Martínez *et al*., 2010: 349).

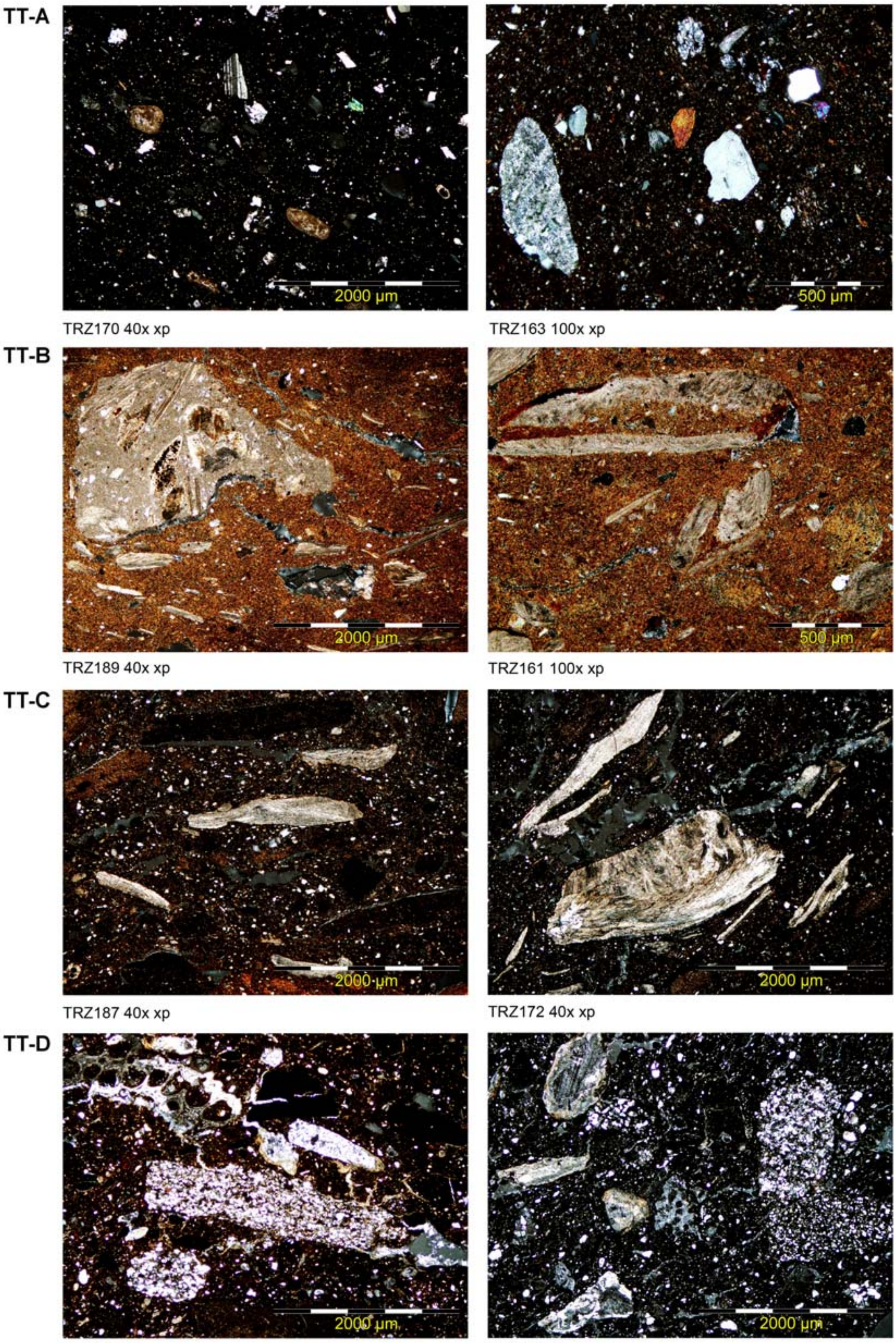

TRZ170 40x xp
TRZ163 100x xp
TRZ189 40x xp
TRZ161 100x xp
TRZ187 40x xp
TRZ172 40x xp
TRZ162 40x xp
TRZ171 40x xp

Figure 5: Microphotographs by crossed polars (xp) of the cooking wares from Tchingiz Tepe belongs to chemical groups **TT-A**, **TT-B**, **TT-C** and **TT-D**.

Previous mineralogical study through XRD analysis of low calcareous ceramics from **TT-A** group showed three different firing categories according to the presence and/or absence of some crystal phases (Martínez *et al*., 2010: 356). TRZ294, TRZ295 and TRZ309 were well fired and the Equivalent Firing Temperature (EFT) has been fixed around (850/900-950ºC). TRZ163 was fired at relatively high firing temperature (950/1000°C) whereas TRZ293 and TRZ170 were possibly over fired and the EFT has been established between 1050°C and 1100°C.

At the right side of the dendrogram of Figure 3, chemical group **TT-B** (Figure 3) is composed of two cooking wares (TRZ161 from s.u. 2 of RC grid and TRZ189 from s.u. 20 of RF grid) with similar typological characteristics (Figure 6). They present relative chemical similarity between them as both have very high CaO and low SiO_2, Zr and Cr values within the analysed sherds from Tchingiz Tepe (Table 4). The high calcareous component is provided by the presence of shell fragments as dominant aplas-tic inclusions, as evidenced by macroscopic and microscopic analysis. Apart of that, other chemical differences respect to the rest of the individuals of this data set leads us to consider them both as two variants of the same pottery production.

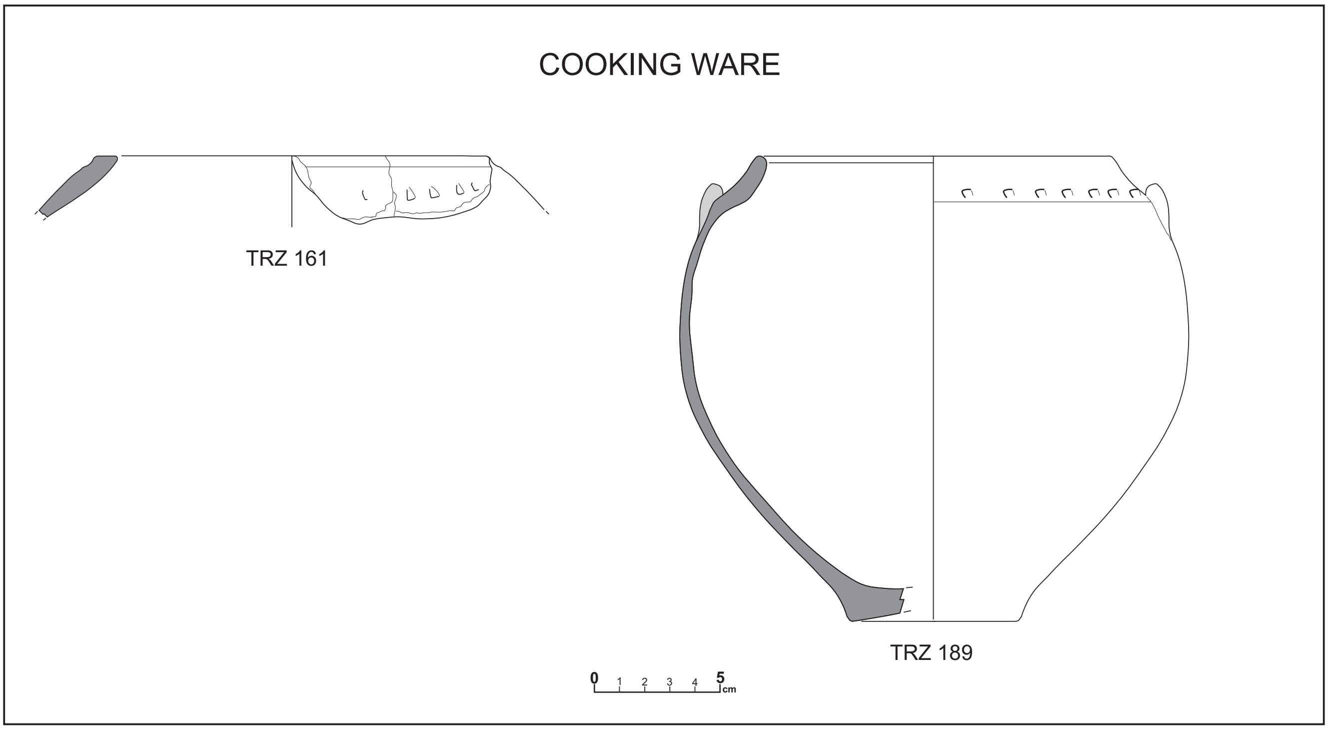

Figure 6: Typology of vessels from group **TT-B.**

In petrographical terms, the cooking wares TRZ161 and TRZ189 from **TT-B** chemical group correspond to a coarse fabric with dominant shell-fragments inclusions (Figure 5b). Clay matrix is Fe-rich and Ca-rich due to the presence of shell fragments and fossils, poorly vitrified. Groundmass is relatively abundant and fine. Coarser inclusions (≤ 1.5 mm) are relatively abundant and besides shell fragments they are constituted of calcareous sedimentary rock fragments (fine-grained sandstone) and quartz-mica schist together with occasional volcanic-glass (Martínez *et al*., 2010: 350).

Previous mineralogical analysis by XRD of calcareous cooking wares (TRZ161 and TRZ189) from TT-B group showed the existence of only primary phases, which indicates an EFT around 800-850ºC (Martínez *et al*., 2010: 357).

A third group of cooking wares from Tchingiz Tepe already identified is **TT-C** (Martínez *et al*., 2008, 2009). Sherds of this group appear at the right side of the dendrogram of Figure 3, linked together at small ultrametrical distance. Two of them (TRZ172 and TRZ182) come from sector RC (s.u. 5 and 21 respectively) and the third (TRZ187) comes from s.u. 11 of the sector RF (Figure 7). As has been demonstrated in previous studies (Martínez *et al*., 2010: 338), this group is border calcareous with significant high values in Rb, V and Cr compared to the rest of the analysed material (Table 4). Particularly, the very high Cr concentration regarding to the rest of the ceramic material was taken as indication of the possible foreign origin of this production. From a macroscopic and microscopic point of view, these three vessels present calcareous shell fragments as dominant aplastic inclusions.

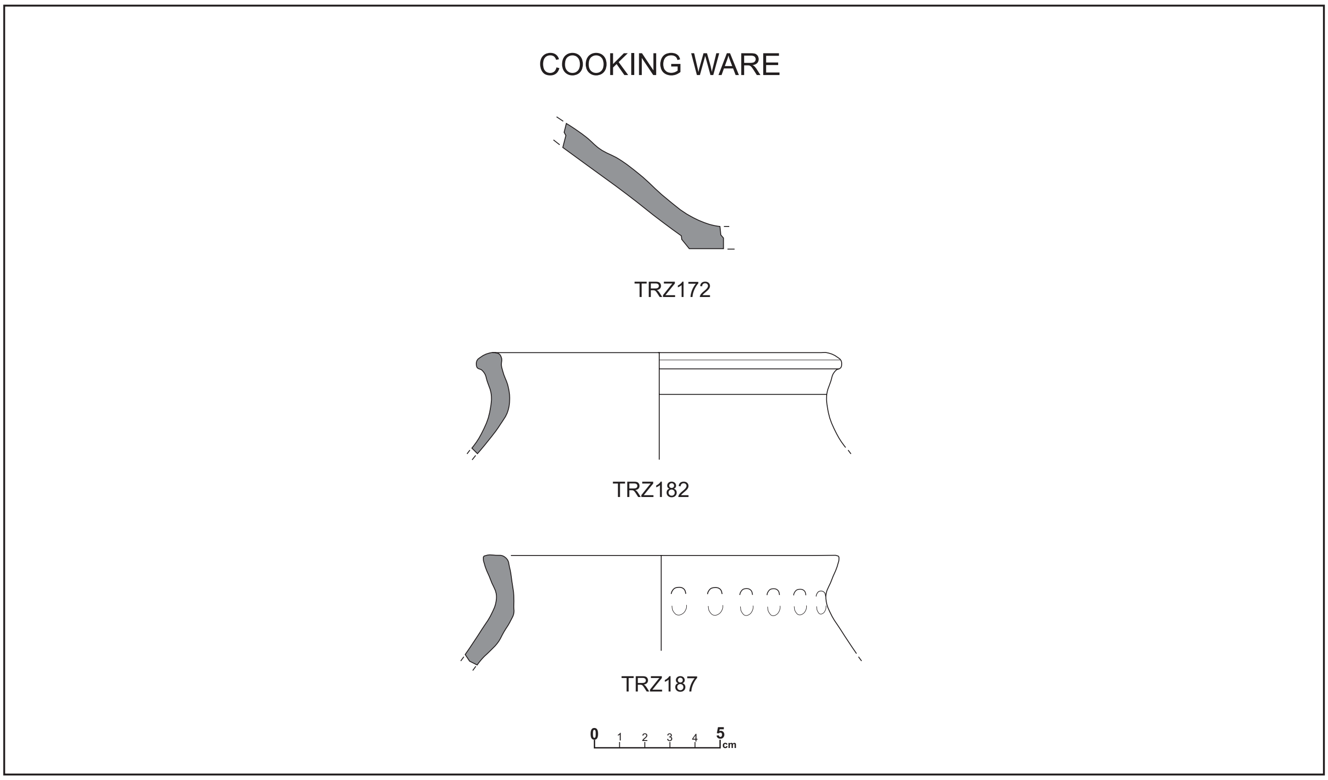

Figure 7: Typology of vessels from group **TT-C.**

The main petrographic characteristic of the coarse fabric **TT-C** (Martínez *et al*., 2010: 351) is the presence of shell fragments which measures 3 mm as maximum long axis dimension (Figure 5c). In the three samples there are also frequent microfossils, some of which have been decomposed during the firing process becoming micritic calcite (Cau *et al*., 2002). However, several differences in the type of aplastic inclusions point at the existence of various sub-fabrics. Clay matrix is Fe-rich and Ca-rich due to the presence of shell and fossils, poorly vitrified. Groundmass is relatively abundant, more scarce and fine in TRZ172 and TRZ182. Coarser inclusions (≤ 3 mm) are relatively abundant. Calcareous microfossils and shell fragments are predominant in all cases whereas amphiboles and volcanic rocks are commons. However, TRZ182 and TRZ187 contain also sedimentary rocks such as sandstones and siltstones, together with metamorphic rocks such as quartz-mica schist.

According to XRD analysis, the three individuals belong to **TT-C** group correspond to two different mineralogical categories associated to two different Equivalent Firing Temperatures (Martínez *et al*., 2010: 358). On the one hand, TRZ172 and TRZ187 both are characterised by the presence of clear primary phases which indicates a low firing temperature (800/850°C). On the other hand, the absence of illite-muscovite and the presence of firing phases in the diffractogram of TRZ182 points to a EFT around 1050°C and 1100°C.

At the left side of the dendrogram of Figure 3, the cooking ware TRZ408 from s.u. 32 from RA sector (Figure 8) links together with two cooking wares (TRZ162 from s.u. 3 and TRZ171 from s.u. 5 sampled at RC sector) identified in previous studies as **TT-D** chemical group (Martínez *et al*., 2008, 2009).

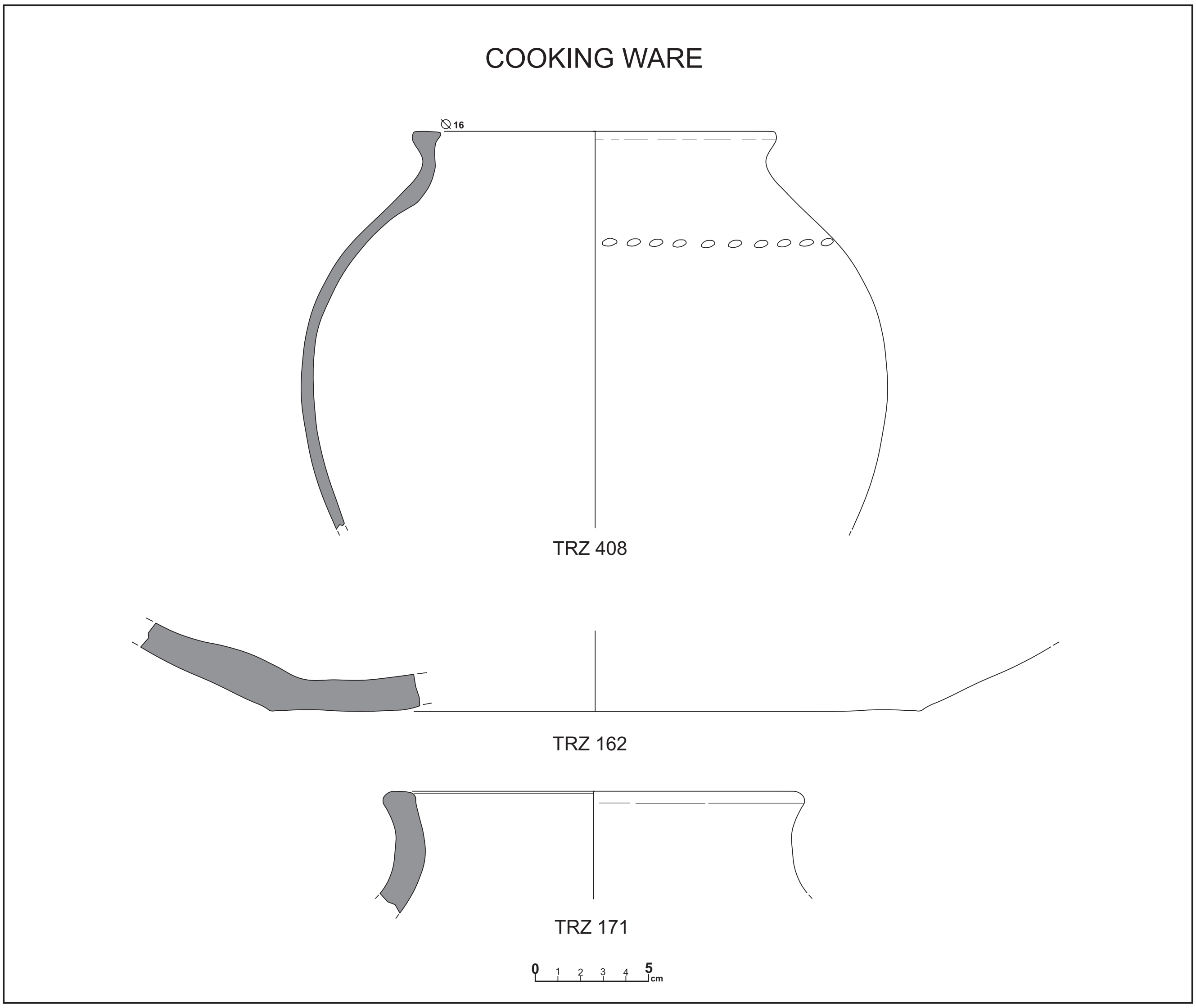

Figure 8: Typology of vessels from group **TT-D.**

Although the existence of slight chemical differences between them, they are low calcareous and pres-ent the lowest MgO, Ba and Ni relative concentrations regarding to the rest of the material. The mean chemical composition and the standard deviation of the group **TT-D** is given at Table 4. The pet-rograph-ic examination of TRZ162 and TRZ171 also sustains that they can be variants of the same ceramic pro-duction (Martínez *et al*., 2010: 351). Clay matrix is Fe-rich and Ca-rich in both cases, semi-vitrified (Figure 5d). Groundmass is moderately abundant, homogeneous with low optical activity whereas coarser inclusions (≤ 2.5 mm) are relatively abundant. In the case of sample TRZ172, sedimentary rock fragments (sandstone and siltstones), calcareous microfossils and shell fragments are predominant while chert fragments and quartz, muscovite, plagioclase, amphibole and epidote crystals are frequent. In the case of **TRZ171**, sandstones and secondary micritic calcite derived from calcareous shell frag-ments are very common (Cau *et al*., 2002). Nevertheless, no cherts, plagioclases, amphiboles nor epi-dotes are present. In mineralogical terms, XRD analysis has evidenced a very high firing temperature (Figure 9), between 1050°C and 1100°C, for these three vessels (Martínez *et al*., 2010: 359). Similarity in morphological characteristics and macroscopic composition of pastes of these three cooking wares points to the same origin.

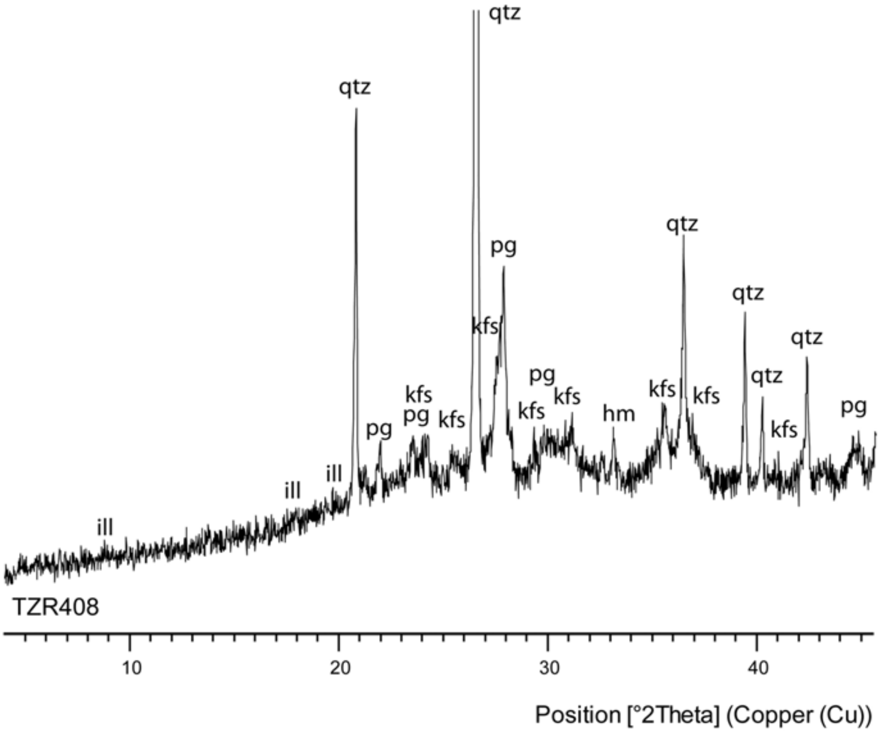

Figure 9: Diffractograms of the individuals TRZ408 representing the chemical group ***TT-D***; hm: hematite, ill: illite-muscovite, kfs: k-feldspar, pl: plagioclase, qtz: quartz.

Two samples appear associated in the dendrogram of Figure 3. They form a new chemical group which could be related to the previous identified TT-E group (Martínez *et al*., 2008, 2009). This group is composed of two jars, TRZ084 from s.u. 5 and TRZ305 from s.u. 25 both from sector RC (Figure 10). The significant similarities of their chemical composition, such as the low concentrations in Th and Zn, point to a similar origin. Another jar (TRZ311) from sector RC (s.u. 28), with dark brownish slip, presents similar chemical composition with this group. It is joined at small ultrametrical distance but dif-fers because of the lower values in Ce and Zr and higher in Zn. The mean chemical composition and standard deviation of TT-E chemical group and TRZ311 is given at Table 4. Petrographic examination of TRZ084 points toward a local origin of the raw materials. Clay matrix is Fe-rich and Ca-rich, semi-vitrified. Groundmass is abundant whereas coarser inclusions (≤ 1.5 mm) are relatively abundant. Predominant inclusions are quartz-mica schist fragments and quartz and muscovite crystals together with dominant plagioclase, k-feldspar and few quartzite fragments and amphibole, epidote and biotite crystals (Figure 11).

As showed in previous studies (Martínez *et al*., 2010: 359), diffractogram resulted of XRD analysis of sample TRZ311 is characterised of a low fired ceramic (800-850ºC) because of the presence of only primary phases (quartz, calcite, illite-muscovite, k-feldspar, plagioclase and few hematite. However, TRZ084 and TRZ305 are characteristics of well fired ceramics because of the presence of primary and firing crystalline phases in its initial phase of formation. The EFT of this fabric has been estimated around 850/900°C.

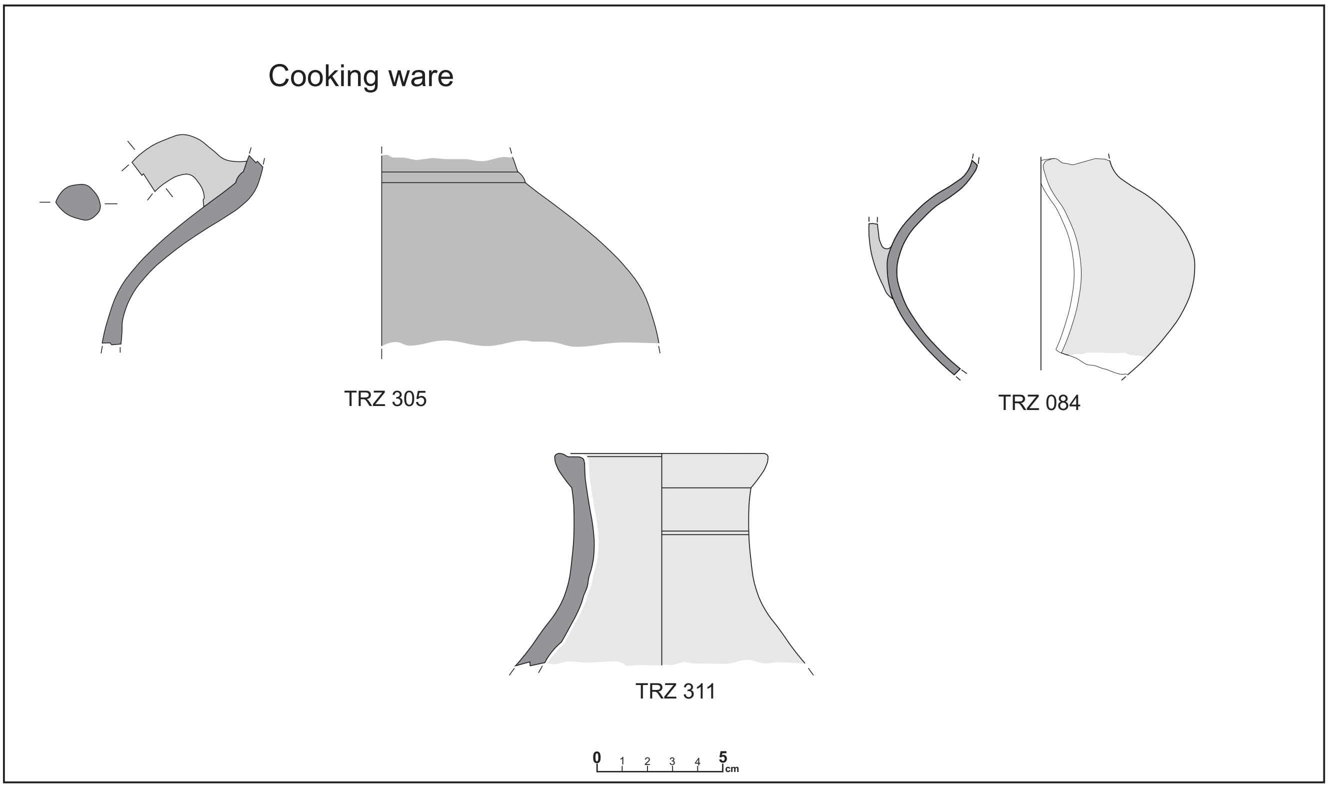

Figure 10: Typology of vessels from group **TT-E.**

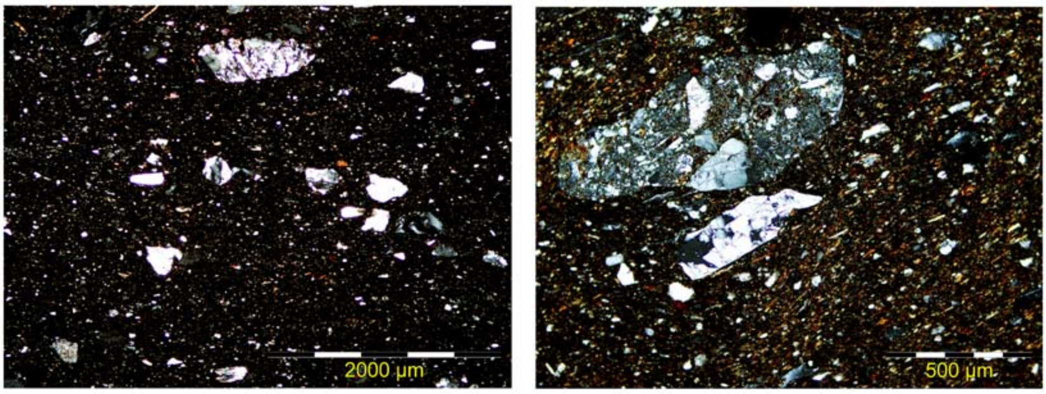

TRZ084 40x xp

TRZ084 100x xp

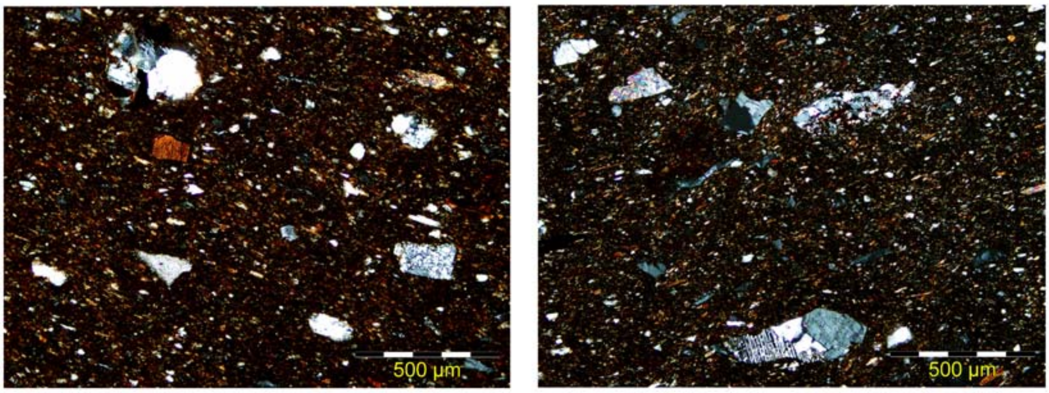

TRZ084 100x xp

TRZ084 100x xp

Figure 11: Microphotographs by crossed polars (xp) of the common wares from Tchingiz Tepe belongs to chemical groups ***TT-E.***

The cooking ware **TRZ405** sampled at s.u. 25 from sector RA and a base of a decorated common ware **TRZ088** sampled at s.u. 5 from sector RB1 (Figure 12) appear isolated in the dendrogram of Figure 3. On the one hand, **TRZ405** presents the highest CaO and Sr values and the lowest TiO_2, MgO, Rb, Th, Nb, Y and Ga concentrations within the analysed sherds from Tchingiz Tepe. The calcareous component is mainly provided by the presence of calcareous shell fragments as dominant aplastic inclusions. Even though its chemical composition is relatively similar to cooking wares from TT-B chemical group, it can not be clearly classified into this production. XRD analysis shows that the cooking ware TRZ405 was fired at low firing temperature (Figure 13) because of the presence of only primary phases as quartz, calcite, aragonite, k-feldspar, plagioclase, illite-muscovite and hematites together with the initial formation of gehlenite. That indicates an EFT around 800-850/900ºC. On the other hand, the common ware **TRZ088** stays isolated because of the high Na_2O and Ba values and the low Ce and V contents. The mean chemical composition and standard deviation of TRZ405 and TRZ088 are given at Table 4.

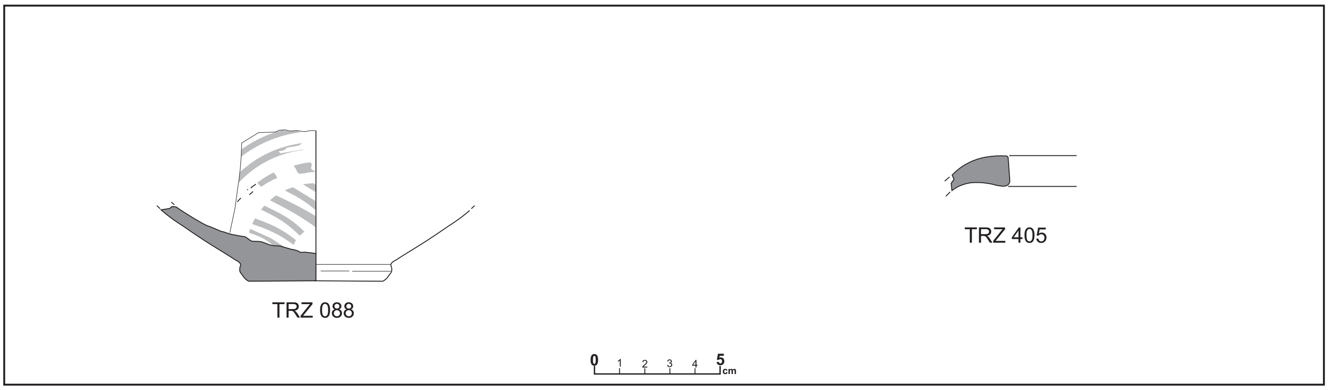

Figure 12: Typology of the pottery outliers from sector RB1 (TRZ088) and sector RA (TRZ405) from Tchingiz Tepe.

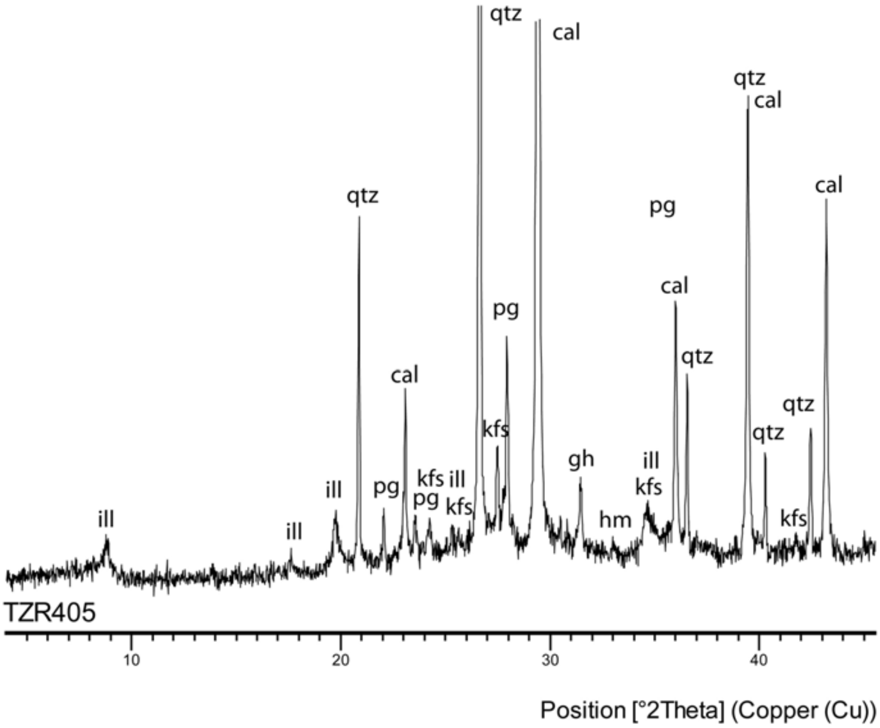

Figure 13: Diffractograms of the outlier TRZ405; cal: calcite, gh: gehlenite, hm: hematite, ill: illite-muscovite, kfs: k-feldspar, pl: plagioclase, qtz: quartz.

The main group TT-G, placed at the centre of the dendrogram of Figure 3, is composed by 114 calcareous pottery sherds (TRZ051, 52, 53, 54, 55, 56, 57, 58, 59, 60, 63, 64, 65, 66, 67, 68, 69, 70, 71, 72, 73, 74, 75, 76, 77, 78, 79, 80, 81, 82, 83, 85, 86, 87, 89, 90, 91, 92, 157, 158, 159, 160, 164, 165, 166, 167, 168, 169, 173, 174, 175, 176, 177, 178, 179, 180, 181, 183, 184, 185, 186, 188, 190, 191, 192, 193, 194, 195, 196, 197, 198, 199, 200, 201, 202, 292, 296, 297, 298, 299, 300, 301, 302, 303, 304, 306, 307, 310, 312, 400, 401, 402, 403, 404, 406, 407, 409, 410, 411, 412, 413, 414, 415, 416, 417, 418, 419, 421, 422, 423, 424, 425, 426 and 427) from sectors RA, RB1, RB2, RC and RF with significant chemical similarities. They are 13 sherds from sector RA, 4 samples from sector RB1 and 12 wares from sector RB2, 63 vessels from sector RC and 22 sherds from sector RF. According to the CVM calculated for this group, considering the chemical composition Fe_2O_3 (as total Fe), Al_2O_3, TiO_2, MgO, CaO, SiO_2, Nb, Zr, Y, Ce, Ga, Zn and Ni, the very low total variation (vt = 0.0517) indicates, in mathematical terms, that all these vessels correspond to a monogenetic data set and they probably represent local pottery productions (Buxeda and Kilikoglou, 2003).

To visualize the distribution of vessels from **TT-G** group, we present a new dendrogram in Figure 14 resulting from the cluster analysis performed over 114 vessels and two clays (G-TRZ-27 and G-TRZ-28) from Termez. This statistical treatment has been performed using the Square Euclidean distance and the centroid algorithm by S-plus2000 (MathSoft, 1999) using Al_2O_3 as divisor in the logratio transformation. In this cluster, most of the common wares belonging to TT-G chemical group appear associated in a short ultrametrical distance at the central area of the dendrogram forming several chemical subgroups. Taking into account that all common wares sampled at the kiln site (RF) of Tchingiz Tepe, except the slipped cup TRZ191, are classified into the central area of **TT-G** chemical group, we can associate all these vessels, with high probability, to the ceramic productions of this pottery workshop recovered at Tchingiz Tepe (Martínez, 2009). They correspond to a large variety of types (bowls, plates, cups, jars, tops and oil lamps) distributed in seven subgroups which must correspond to several pottery productions inside this workshop along its period of activity (Figure 14). However, keeping in mind the low total variation of this set of vessels, sherds from the seven subgroups can be considered as the Reference Group (RG) of this specific workshop located at sector RF of Tchingiz Tepe.

At the left side of the dendrogram of Figure 14, 11 common wares from sectors RB1 (TRZ089, TRZ090, TRZ092 from s.u. 5), RB2 (TRZ418 from s.u. 1), RC (TRZ078, TRZ0298, TRZ0301, TRZ0310 from u.s. 5, 18, 21 and 28 respectively) and RF (TRZ070, TRZ195 from s.u. 20, TRZ200 from s. u. 27) are joined in **TT-G1** subgroup (Figure 15a). It is formed by different types of slipped and unslipped common wares (3 plates, 3 bowls, 2 jars, 2 cups, 1 base), from contexts dated from the second quarter of the 3rd century AD to the last quarter of the 4th century AD (Mestres and Rauret, 2010a, 2010b). Only some vessels from RB1 group (TRZ89, TRZ090, TRZ091 and TRZ092) come from a context dated by C14 at the last quarter of the 2nd century BC (Mestres and Rauret, 2009). This indicates that the oldest pottery located at Tchingiz Tepe is compatible, in chemical terms, with the local productions identified for the Kushan and Kushan-Sassanian periods, when the pottery kiln of sector RF was working. This could confirm the presence of local pottery production in this area during the Greco-Bactrian period, although any pottery kiln has been found.

Two tops from RC sector (TRZ085 from s.u. 5 and TRZ183 from s.u. 21) are joined in subgroup **TT-G2** because of the similar chemical composition (Figure 15a). The production of these tops has been fixed by C14 analysis between the second quarter and the end of the 3rd century AD (Mestres and Rauret, 2010a).

Subgroup **TT-G3** is composed of a large variety of slipped and unslipped common wares (jars, bowls and plates) from sectors RA (TRZ406), RB2 (TRZ417, TRZ423 and TRZ426), RC (TRZ164, TRZ173, TRZ180, TRZ299, TRZ300, TRZ302 and TRZ312) and RF (TRZ067, TRZ070, TRZ184, TRZ192 and TRZ202). We must to mention that non cup can be assigned to this subgroup (Figure 15a). The slipped plate TRZ192 (s.u. 22) from sector RF comes from a specific archaeological context dated by C14 around the second quarter of the 2nd century AD. This vessel marks the *terminus post quem* of this pottery production whereas some bowls and plates coming from sector RC (TRZ164 from s.u. 5, TRZ 173 and TRZ299 from s.u. 18, TRZ180, TRZ300 and TRZ302 from s.u. 21) fixe the *terminus ante quem* at the first quarter of the 4th century AD (Mestres and Rauret, 2010a, 2010b).

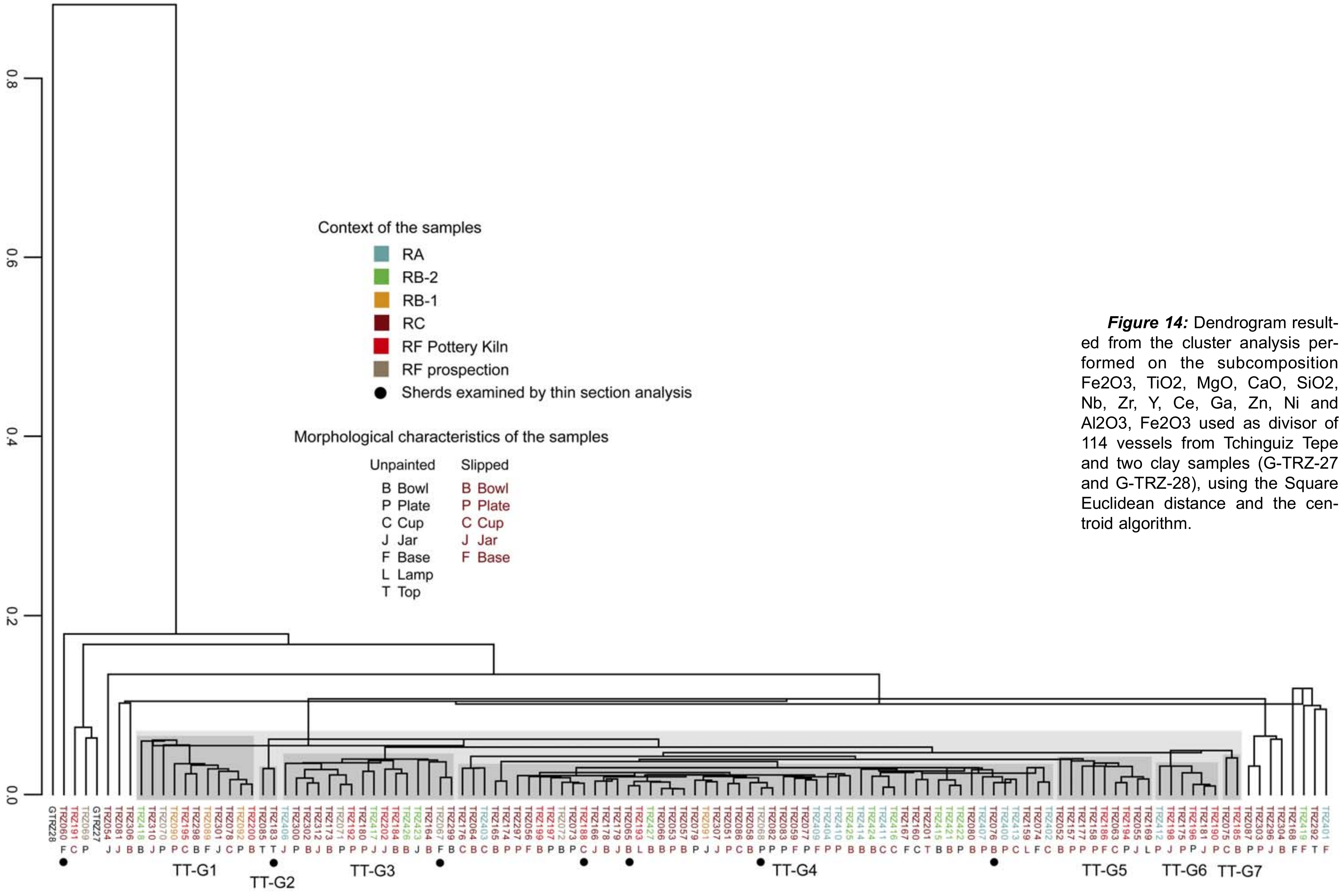

Figure 14: Dendrogram resulted from the cluster analysis performed on the subcomposition Fe2O3, TiO2, MgO, CaO, SiO2, Nb, Zr, Y, Ce, Ga, Zn, Ni and Al2O3, Fe2O3 used as divisor of 114 vessels from Tchinguiz Tepe and two clay samples (G-TRZ-27 and G-TRZ-28), using the Square Euclidean distance and the centroid algorithm.

Most of common wares from TT-G group present very similar chemical composition and they appear joined in subgroup **TT-G4**. It is formed by slipped and unslipped vessels from all sectors excavated at Tchingiz Tepe (RA, RB1, RB2, RC and RF). The oldest pot from this subgroup is an unslipped jar from s.u. 5 from sector RB1 (TRZ091), dated at the last quarter of the 2nd century BC (Figure 15a). At sector RA, slipped plates (TRZ400, 404, 407, 410) and slipped cups (TRZ402, 411, 413) are predominant together with one bowl (TRZ414). The rest of the vessels from RB2, RC and RF correspond to a large variety of slipped and unslipped common wares, predominantly plates and bowls together with few cups, jars and 2 oil lamps. This large and wide ranged production can be dated by C14 between the second quarter of the 2nd century AD to the first quarter of the 4th century AD. The oldest archaeological contexts in which this production is present are the s.u 22 (TRZ193) and the s.u. 23 (TRZ197) from sector RF. However, most of the vessels from subgroup TT-G4 come from sector RC and they are generally dated between the second quarter of the 3rd century AD and the first quarter of the 4th century AD (Mestres and Rauret, 2010a, 2010b).

Subgroup **TT-G5** shows a similar chemical composition with subgroup TT-G4. It is composed of 9 ves-sels from sectors RC (TRZ052, TRZ055, TRZ063, TRZ157, TRZ158, TRZ169 and TRZ177) and RF (TRZ186 and TRZ194). As is the previous case, these vessels can be assigned to a large chronological sequence, indicating a long lasting production (Figure 15a). One unpainted plate (TRZ194) from sector RF fixes the *terminus post quem* of this pottery production at the second quarter of the 2nd century AD. At sector RC, one painted plate comes from a stratigraphical context dated at the second quarter of the 3rd century AD vessels recovered at sector RC whereas a lamp (TRZ169) is dated at the second half of the 3rd century AD. The earliest chronology is given by two slipped plates (TRZ157 and TRZ158) from s.u. 2 from sector RC, dated at the last quarter of the 4th century AD (Mestres and Rauret, 2010a, 2010b).

A similar situation is observed for subgroup **TT-G6** (Figure 15a), which groups 3 common wares from sector RF (TRZ190, TRZ196 and TRZ198), one plate (TRZ175) and one jar (TRZ181), both slipped, from sector RC and one slipped plate from sector RA (TRZ412). They can be also assigned to a large chronological period from the second quarter of the 2nd century AD to the last quarter of the 4th century AD.

A last subgroup (**TT-G7**) is formed by one slipped cup (TRZ075) from sector RC and one slipped bowl (TRZ185) from sector RF (Figure 15a). We only have an absolute chronology for this group, provided by the archaeological context s.u. 5 from RC sector, which is dated during the second half of the 3rd century AD and the beginning of the 4th century AD.

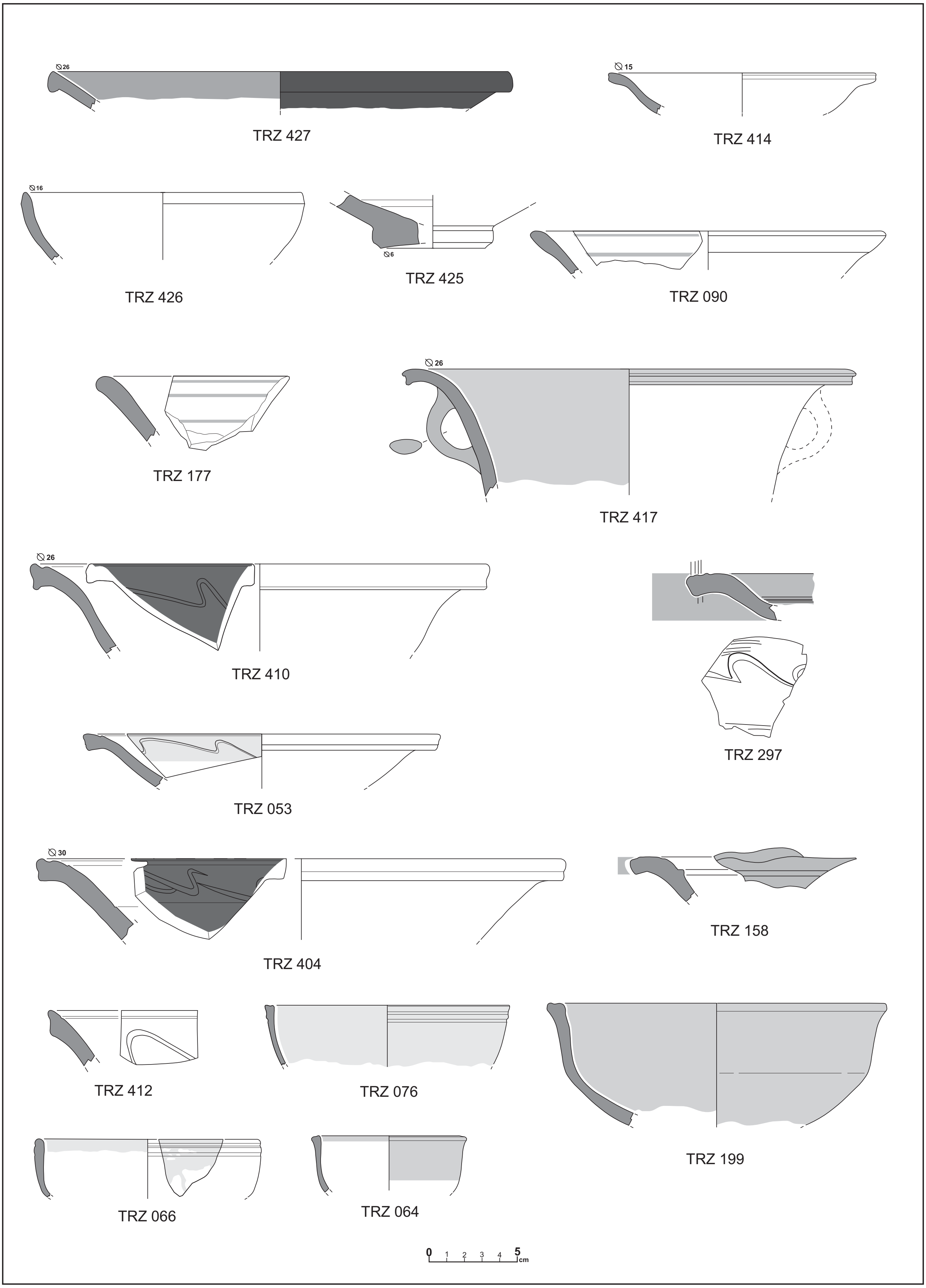

Figure 15a: Typology of vessels from group **TT-G.**

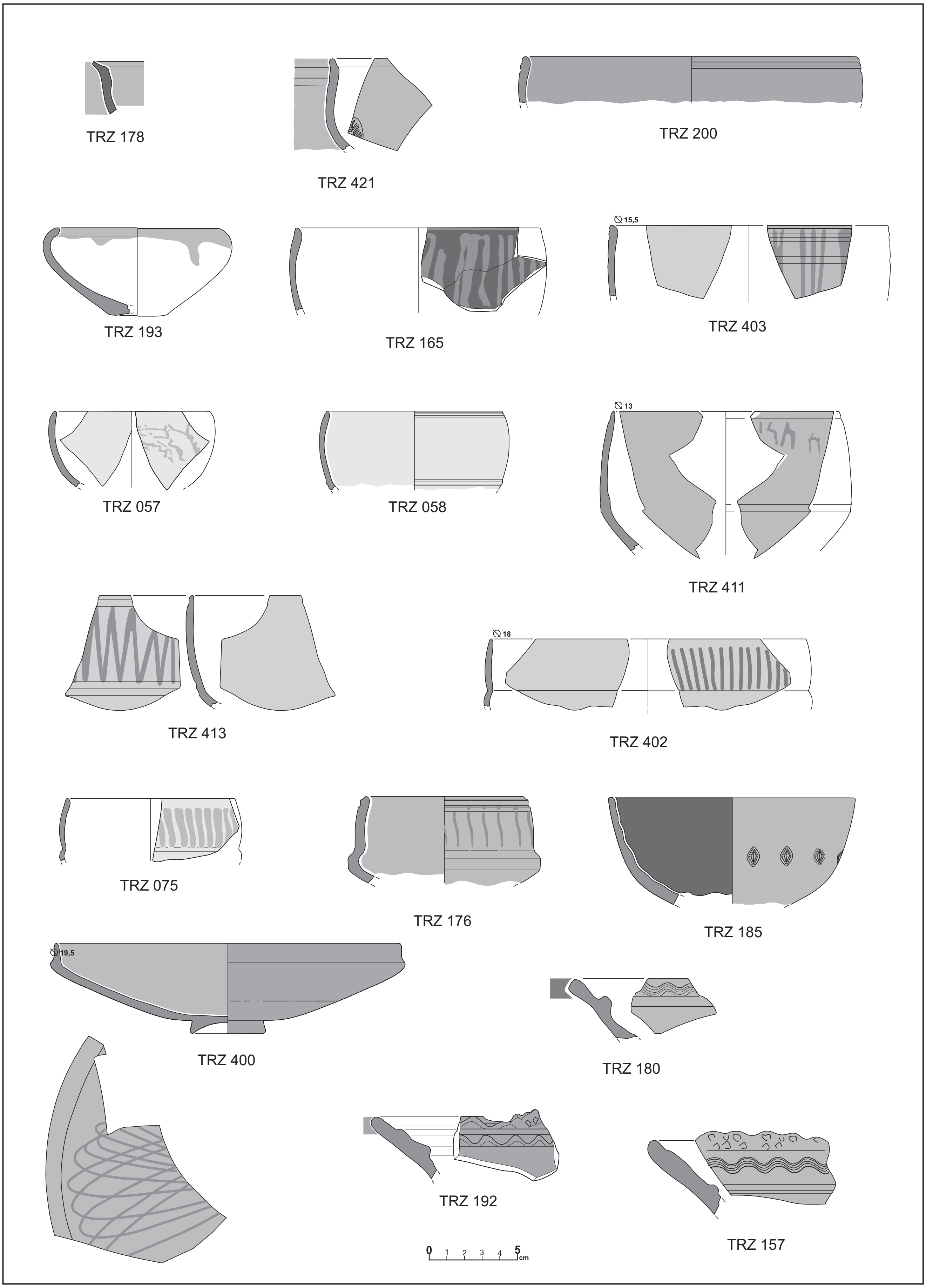

Figure 15a: Typology of vessels from group **TT-G.**

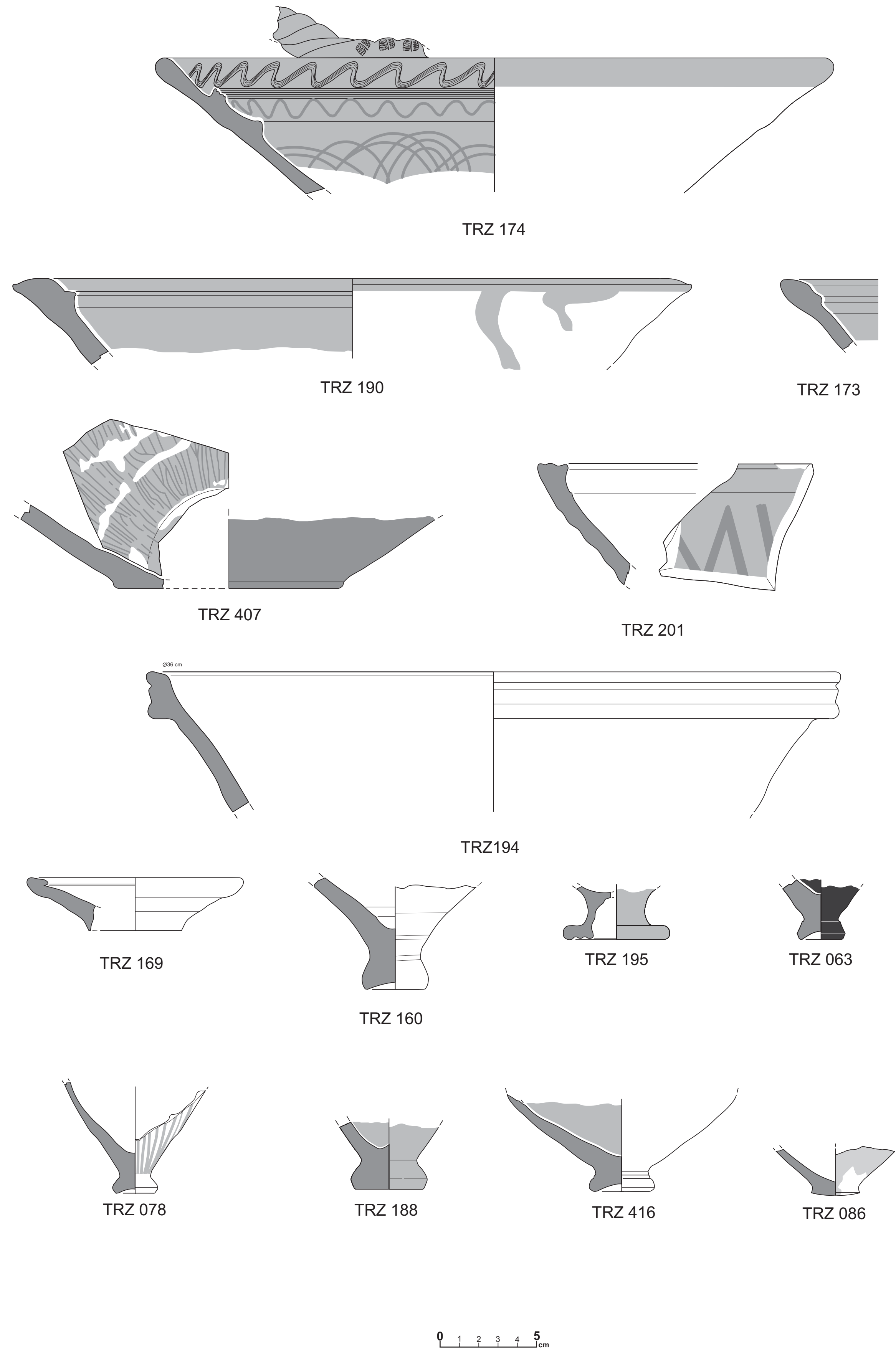

Figure 15a: Typology of vessels from group **TT-G.**

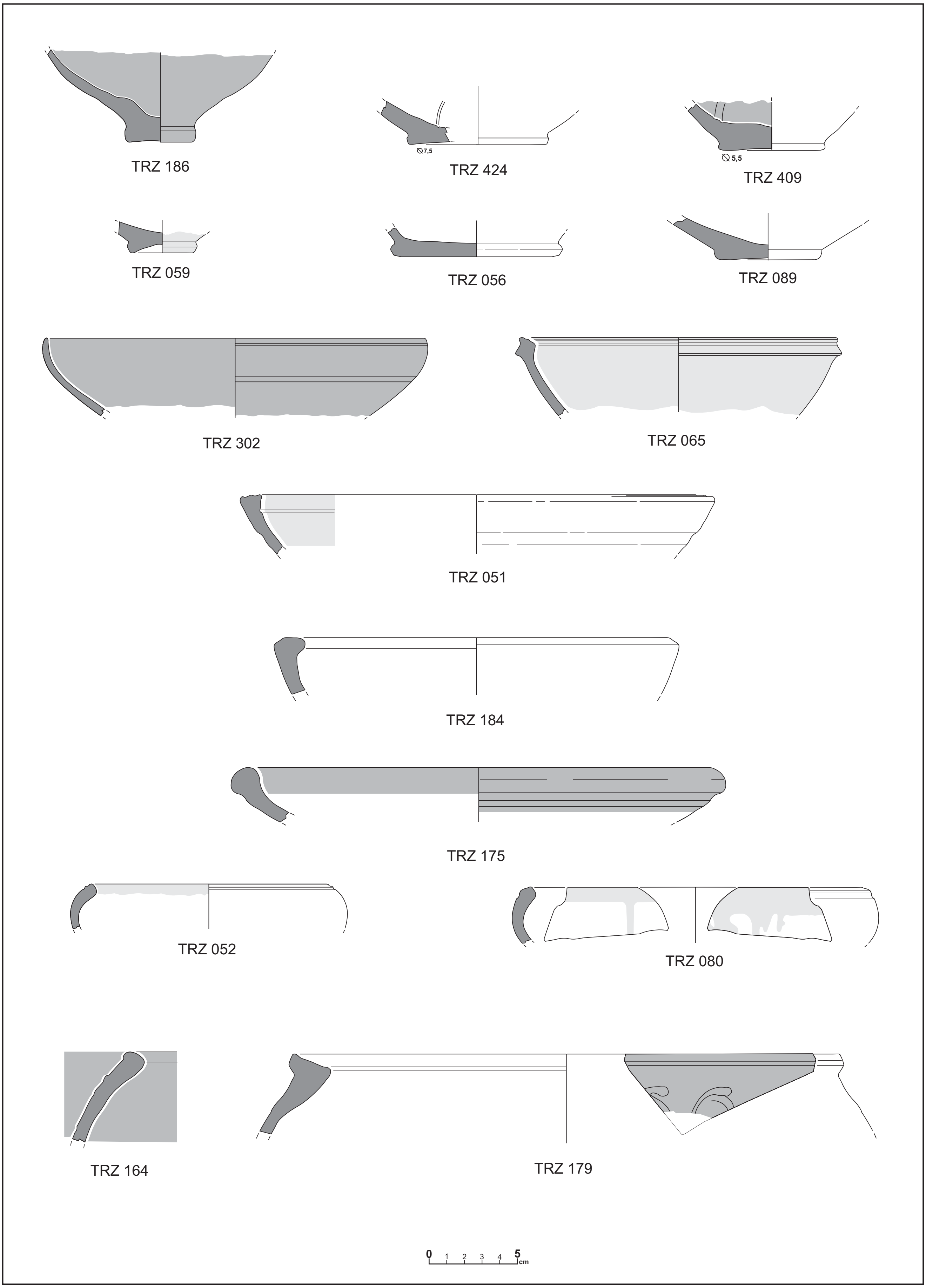

Figure 15a: Typology of vessels from group **TT-G.**

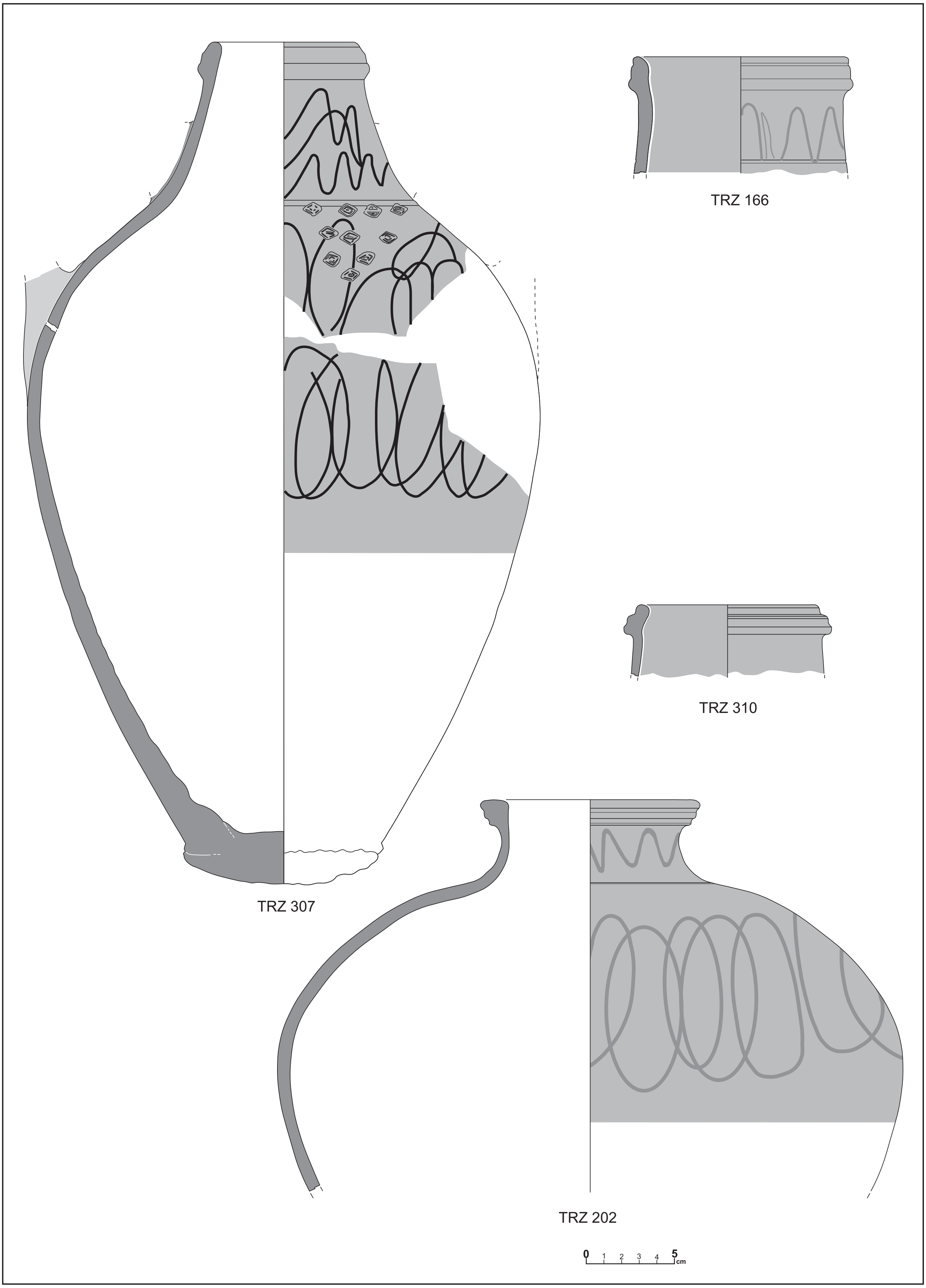

Figure 15a: Typology of vessels from group **TT-G.**

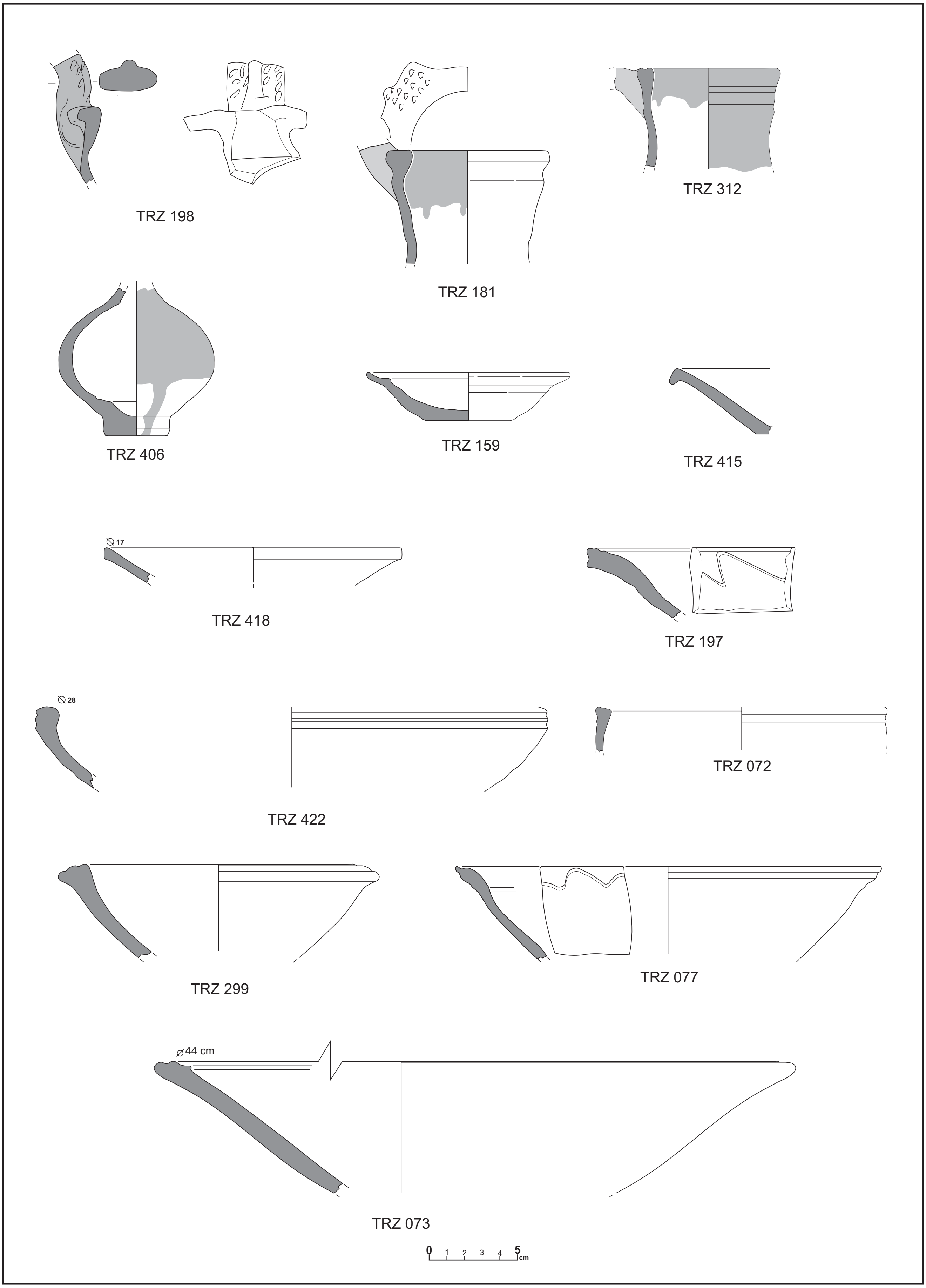

Figure 15a: Typology of vessels from group **TT-G.**

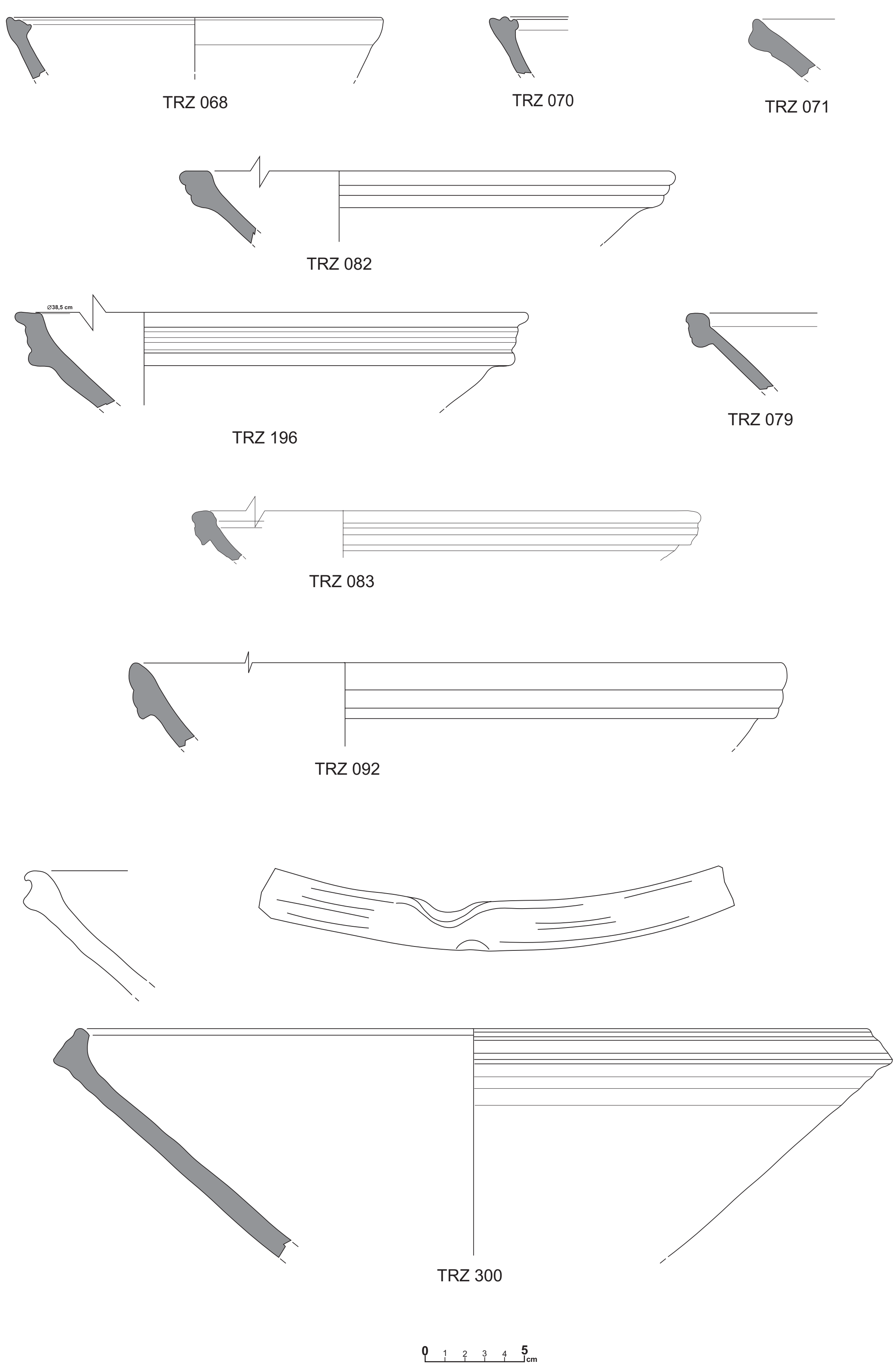

Figure 15a: Typology of vessels from group **TT-G.**

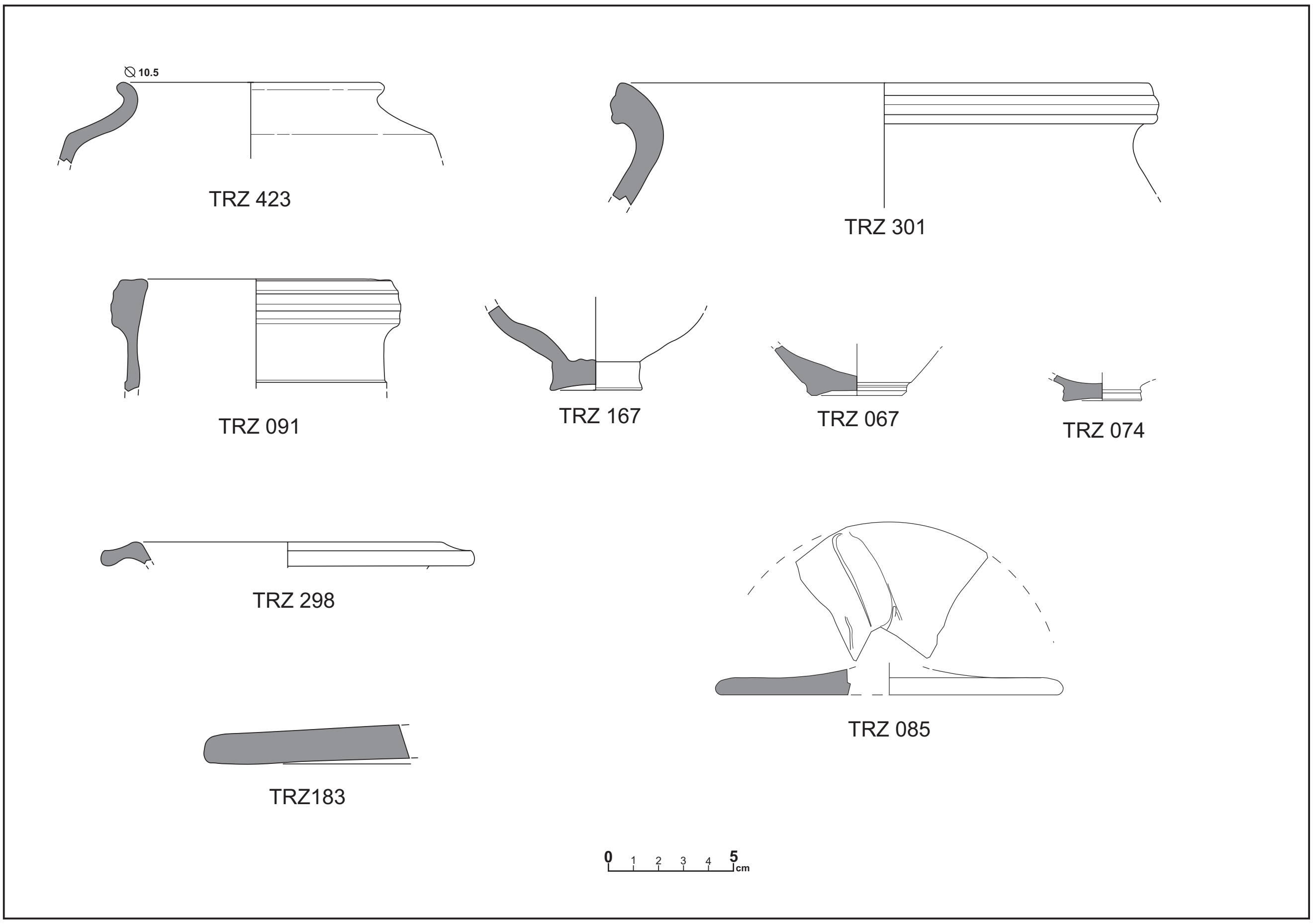

Figure 15a: Typology of vessels from group **TT-G*****.***

Few common wares placed at both sides of the dendrogram are joined to the major group at relative higher ultrametrical due to slightly chemical differences (TRZ054, TRZ060, TRZ069, TRZ081, TRZ087, TRZ168, TRZ191, TRZ292, TRZ296, TRZ303, TRZ304, TRZ306, TRZ401 and TRZ419). However, keeping in mind the very low total variation we can consider these vessels as local productions possibly manufactured in other pottery workshops of the area which used similar raw materials (Figure 15b). The mean chemical composition and the standard deviation of **TT-G** (formed by samples from TT-G1, TT-G2, TT-G3, TT-G4, TT-G5, TT-G6 and TT-G7) group and normalised chemical composition of the local ceramic outliers previously cited are given in Table 5.

As clay source concerns, vessels from TT-G group shares more similar chemical composition with the sample **G-TRZ27** which corresponds to reddish clay from the alluvial plane surrounding the south-east façade of Tchingiz Tepe. Chemical differences of clay **G-TRZ28** are important enough to consider that clay deposits partially covering the geological basement (sandstone) of Tchingiz Tepe were no used on pottery manufacture. Both are calcareous but G-TRZ27 contains higher Fe_2O_3, Al_2O_3, MgO, Ba, Rb, Sr, Ce, V, Zn and Ni values whereas G-TRZ28 presents higher SiO_2 relative concentration.

The slow diversity between sherds from TT-G group is also evidenced by the petrographic analysis. Two main petrographical fabrics have been identified according mainly to certain differences in frequency and dimensions of non-plastic inclusions and the presence or absence of some petrographic components. Seven sherds from sectors RC and RF have been examined (TRZ060, 65, 67, 68, 76, 183, 188).

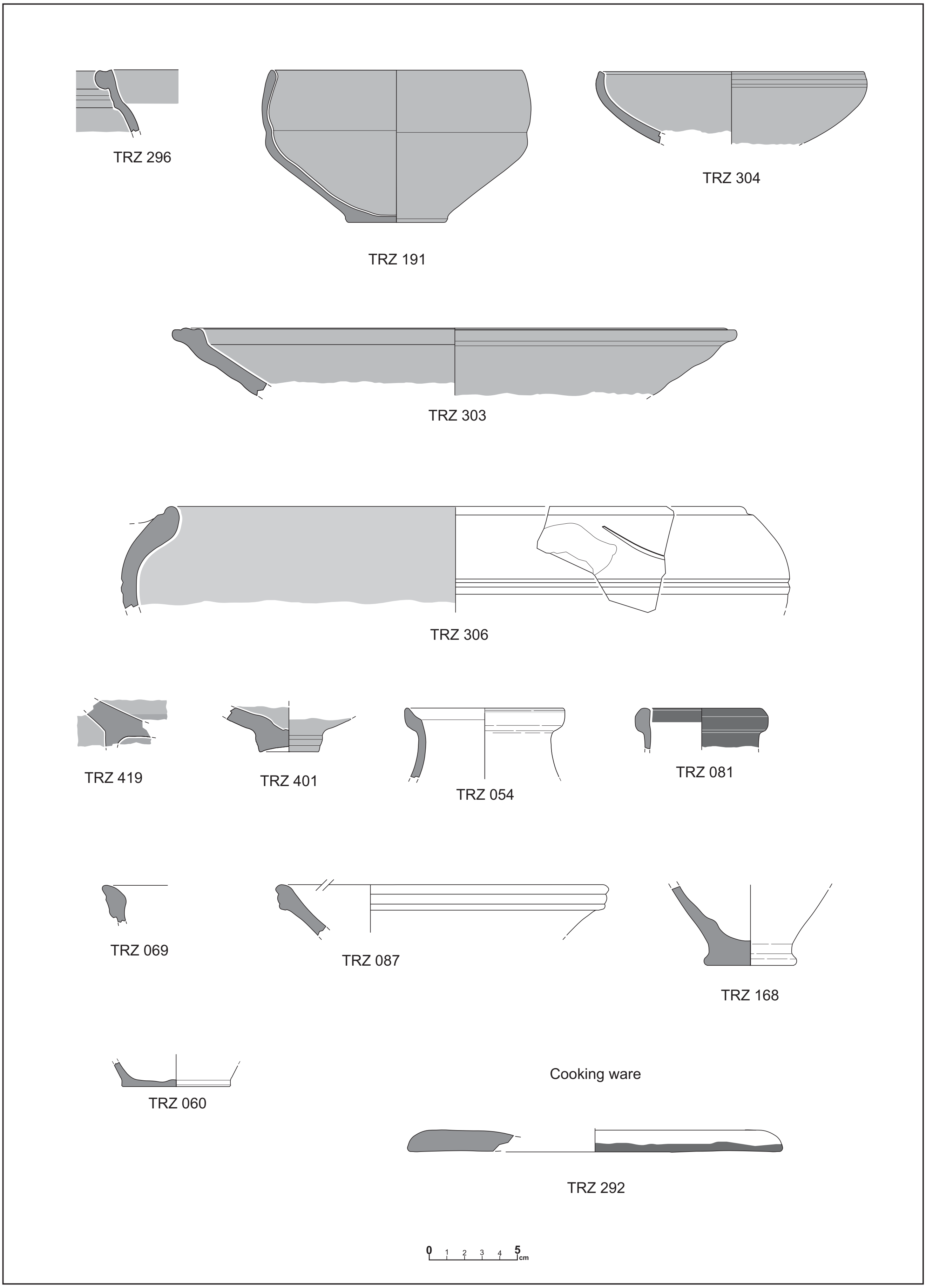

Figure 15b: Typology of vessels from group **TT-G** with slight different chemical composition.

	TT-G (n=100)		TRZ054	TRZ060	TRZ069	TRZ081	TRZ087	TRZ168	TRZ191	TRZ292	TRZ296	TRZ303	TRZ304	TRZ306	TRZ401	TRZ419
	m	sd	nc	nc	nc	nc	nc	nc	nc	nc	nc	nc	nc	nc	nc	nc
Fe_2O_3 (%)	6.10	0.39	5.80	6.19	5.91	6.49	6.41	6.54	6.11	6.04	6.16	6.54	6.08	6.07	6.02	6.44
Al_2O_3 (%)	15.60	0.86	15.57	15.98	15.04	16.48	16.14	16.47	15.43	16.84	15.64	16.22	15.54	15.32	15.17	16.35
TiO_2 (%)	0.66	0.04	0.67	0.66	0.65	0.66	0.68	0.72	0.64	0.73	0.67	0.68	0.68	0.68	0.69	0.70
MgO (%)	3.55	0.40	4.42	3.99	4.15	3.91	3.55	3.24	4.01	3.74	4.45	3.97	3.83	3.84	3.22	3.59
CaO (%)	9.57	2.72	9.36	10.77	13.28	11.01	10.91	8.45	14.47	1.14	9.78	11.08	11.24	10.20	8.47	8.26
Na_2O (%)	1.44	0.24	1.27	1.17	1.50	1.37	1.46	1.40	1.30	1.60	1.38	1.37	1.25	1.48	1.55	1.63
K_2O (%)	3.31	0.34	3.20	3.36	2.90	3.28	3.42	3.90	3.65	4.27	3.38	3.37	3.55	3.14	3.69	3.36
SiO_2 (%)	56.13	3.21	59.46	57.65	56.30	56.54	57.15	59.01	54.11	65.44	58.27	56.49	57.56	59	60.88	59.38
Ba (ppm)	536	86	501	436	659	582	610	644	504	438	447	486	502	577	708	593
Rb (ppm)	124	13	110	110	118	144	136	144	130	143	121	129	131	129	111	122
Th (ppm)	14	2	12	11	14	17	14	14	13	14	11	13	12	13	12	12
Nb (ppm)	15	1	14	13	16	15	15	16	16	18	17	16	17	17	15	14
Zr (ppm)	150	12	162	132	160	151	151	157	137	188	146	147	152	165	176	156
Y (ppm)	25	2	24	23	25	27	26	26	23	32	26	25	27	27	29	28
Sr (ppm)	364	75	351	348	371	313	379	311	500	153	389	407	440	339	508	369
Ce (ppm)	61	8	62	53	61	88	43	65	54	82	46	44	50	77	71	72
Ga (ppm)	18	1	16	16	18	20	19	18	18	19	18	18	18	19	19	20
V (ppm)	108	21	106	86	96	111	106	105	101	118	106	103	102	83	109	127
Zn (ppm)	101	10	92	87	94	105	100	88	106	119	107	105	108	99	93	102
Cu (ppm)	32	5	26	27	33	38	36	36	34	34	30	37	33	37	28	29
Ni (ppm)	49	5	40	42	50	51	54	58	51	45	46	48	49	49	45	47
Cr (ppm)	83	24	70	61	69	73	74	85	75	83	79	77	74	82	83	91

Table 5: The mean chemical composition (m) and the standard deviation (sd) using normalised data of **TT-G1**, **TT-G2** and **TT-G3** chemical subgroups and the raw normalised chemical composition (nc) of the local ceramic outliers from TT-G group TRZ054, TRZ060, TRZ069, TRZ081, TRZ087, TRZ168, TRZ191, TRZ292, TRZ296, TRZ303, TRZ304, TRZ306, TRZ401 and TRZ419 from **Tchingiz Tepe**

Common wares TRZ060, TRZ065, TRZ068 and TRZ076 forms the petrographic fabric *F-TT-G1*, which clay matrix is Fe-rich mixed with calcareous clays and semi-vitrified. Groundmass is relatively abundant and very fine whereas coarser inclusions (≤ 0.5 mm) are scarce (Figure 16). Quartz, quartzite

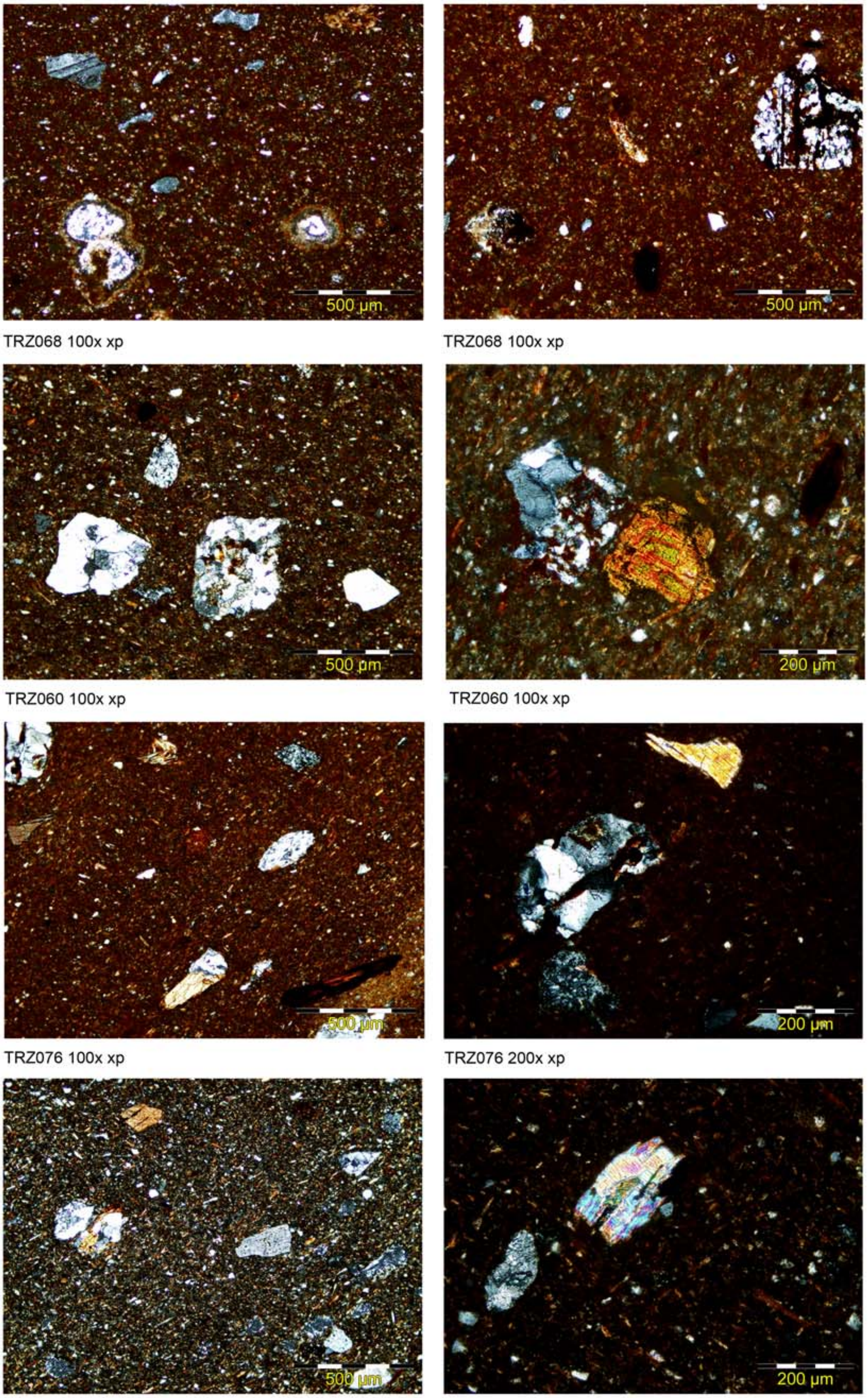

TRZ068 100x xp

TRZ068 100x xp

TRZ060 100x xp

TRZ060 100x xp

TRZ076 100x xp

TRZ076 200x xp

TRZ065 100x xp

TRZ065 200x xp

Figure 16: Microphotographs by crossed polars (xp) of the common wares TRZ060, TRZ065, TRZ068 and TRZ076 from the petrographic fabric **F-TT-G1**

and quart-mica schist are predominant; muscovite lames, plagioclase and k-feldspar are dominant; chert, amphibole, calcareous microfossils and nodules of micritic calcite are frequent; biotite lames are common; phyllite and sandstone fragments together with amphibole, epidote, garnet and volcanic rocks are few. The slipped cup TRZ188 and the over fired base TRZ067 both from sector RF are medium coarse wares with identical rock components but inclusions are slightly coarser with regard to vessels from subfabric F-TT-G1 (Figure 17). They can be considered as variants of the same subfabric.

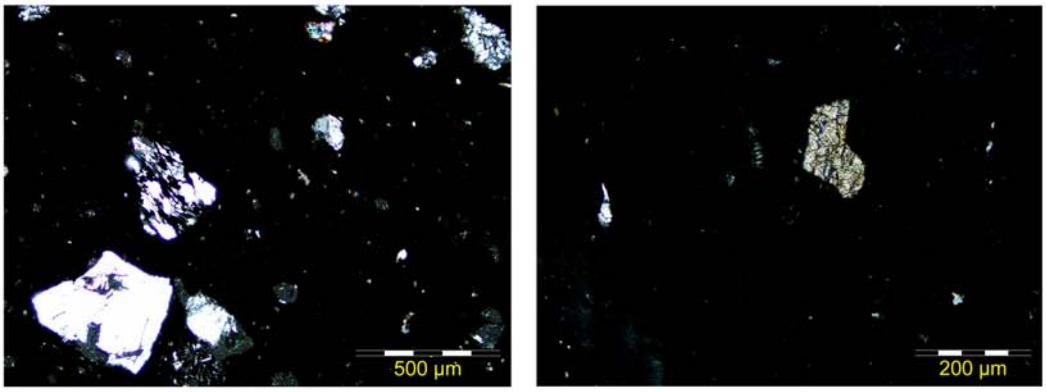

TRZ188 100x xp TRZ188 200x xp

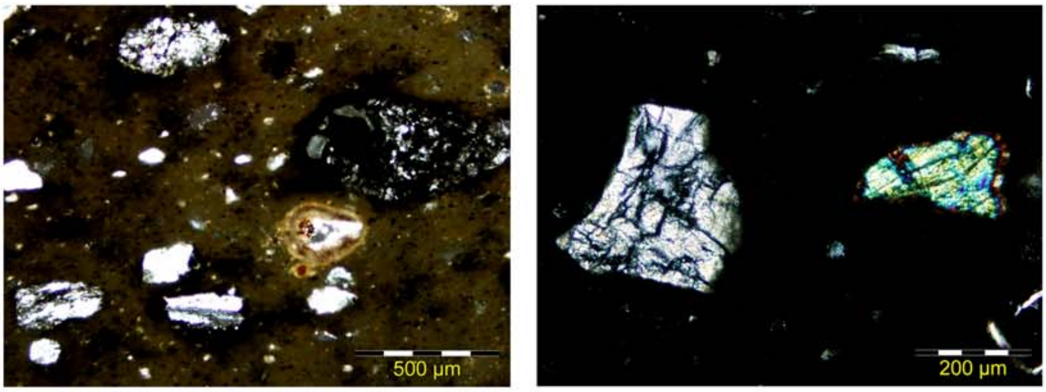

TRZ067 100x xp TRZ067 200x xp

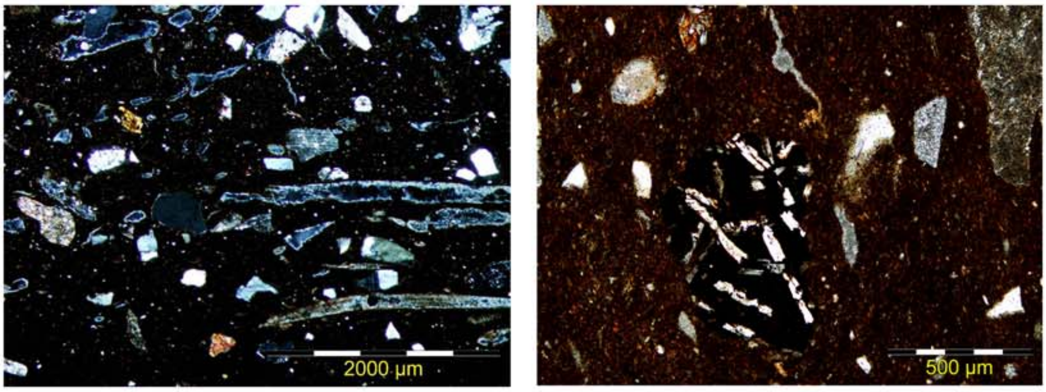

TRZ085 40x xp TRZ085 100x xp

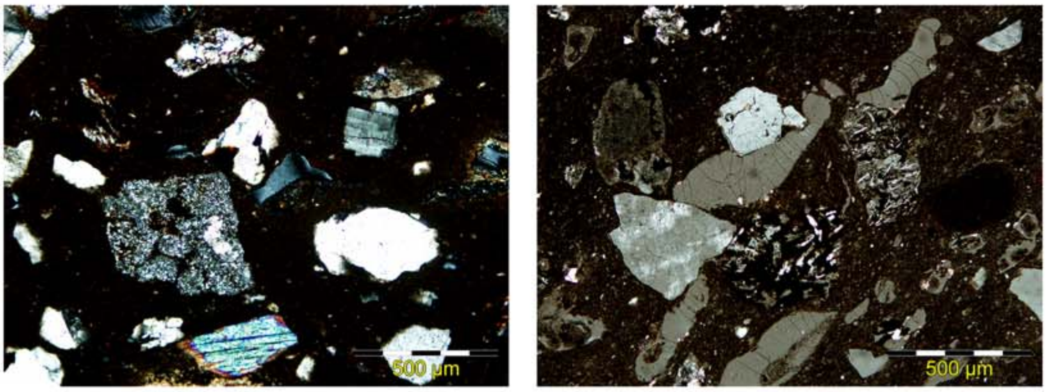

TRZ183 100x xp TRZ183 100x xp

Figure 17: Microphotographs by crossed polars (xp) of the TRZ067 and TRZ188 (which are variants of the petrographic fabric **F-TT-G1** and of the tops **TRZ085** and **TRZ183** from the petrographic fabric **F-TT-G2**

The tops **TRZ183** (from s.u. 21) and **TRZ085** (from s.u. 5) of sector RC belong to the medium-coarse fabric ***F-TT-G2***. The clay is rich in iron oxides but TRZ085 includes more rests of carbonates that can be the consequence of calcareous shell decomposition, latter altered to secondary micritic calcite (Cau *et al*., 2002). Groundmass is relatively abundant, very fine and coarser inclusions (≤ 500-700µm) are abundant. Quartz-mica schist fragments, quartz crystals and shell fragments are predominant; muscovite lames and plagioclase and k-feldspar crystals are dominant; phyllite, amphibole and epidote are common; sandstones, chert, biotite, basalt and volcanic rocks are common to occasional (Figure 17).

The main petrographical components observed in all these samples are general in all defined subfabrics and, as already indicated, the differences are related to the proportion and size of the aplastic particles. Apart of the presence of quartz, quartzite, quartz-mica schist and sandstone, volcanic rocks are present in all these fabrics together with amphiboles and epidotes. These are characteristic elements of pottery produced at Tchingiz Tepe together with abundant white mica lames. Few differences are observed in the case of both tops (TRZ085 and TRZ183), which are also characterised by the pres-ence of calcareous fossils and shell fragments.

.

Because of that, the chemical and petrographic variability between sherds from TT-G group, consid-ered the RG of the Kiln site (sector RF) of Tchingiz Tepe, must correspond to variants of the pottery pro-duction inside this workshop along its period of activity. In any case, the geo-chemical and petrograph-ic similarity between vessels dated at the Greco-Bactrian period and vessels from the Kushan-Sassanian period is indicative of a constant persisting over the time: the use of very similar raw mate-rials from local sources and the persistence of standardised technological processes in pottery making.

According to the mineralogical analysis through XRD carried out last year (Martínez *et al*., 2010: 360), the individuals representing the group **TT-G** can be divided into four mineralogical categories. The first contains the individuals TRZ080, TRZ089, TRZ166, TRZ179, TRZ184, TRZ191, TRZ202, TRZ414 and TRZ423. It is characterised by the presence of primary mineral phases and the total absence of clear firing phases (Figure 18). The EFT estimated for this category is 800-850°C, which corresponds to a low firing temperature.

In the second category, the coexistence of primary phases, like calcite, illite-muscovite and alkaline feldspars, and firing phases in the initial phase of development, like gehlenite and pyroxenes, can be observed (Figure 18). Therefore, the EFT of this category is around 850-900°C. This category is configured by TRZ051, TRZ052, TRZ054, TRZ055, TRZ057, TRZ064, TRZ068, TRZ085, TRZ086, TRZ160, TRZ164, TRZ169, TRZ178, TRZ186, TRZ302, TRZ303, TRZ304, TRZ400, TRZ401, TRZ412, TRZ415, TRZ416, TRZ417, TRZ419 and TRZ422.

In the third category, the development of the firing phases is much more advanced. The absence of calcite and the existence of small peaks of illite-muscovite in the diffractograms of the individuals in this category indicate a EFT between 900-950/1000°C (Figure 18).The individuals that belong to this mineralogical fabric are: TRZ053, TRZ058, TRZ063, TRZ065, TRZ066, TRZ070, TRZ077, TRZ078, TRZ092, TRZ157, TRZ158, TRZ173, TRZ174, TRZ175, TRZ181, TRZ190, TRZ192, TRZ193, TRZ195, TRZ196, TRZ197, TRZ198, TRZ199, TRZ201, TRZ296, TRZ297, TRZ301, TRZ307, TRZ310, TRZ312, TRZ402, TRZ403, TRZ406, TRZ407, TRZ409, TRZ411, TRZ413, TRZ418, TRZ421, TRZ424, TRZ425 and TRZ427.

Finally, the last mineralogical category is characterised by the advanced decomposition of illite-muscovite and gehlenite and the high degree of decomposition of calcite with the parallel clear increment of the pyroxenes as a firing phase of a high temperature (Figure 19). Consequently, this fabric represents over fired ceramics. Its ETF can be estimated in the rang between 1000-1050/1110°C and it includes TRZ056, TRZ059, TRZ060, TRZ067, TRZ069, TRZ071, TRZ072, TRZ073, TRZ074, TRZ075, TRZ076, TRZ079, TRZ081, TRZ082, TRZ083, TRZ087, TRZ090, TRZ091, TRZ165, TRZ167, TRZ168, TRZ176, TRZ177, TRZ180, TRZ183, TRZ185, TRZ188, TRZ194, TRZ200, TRZ300, TRZ306, TRZ404, TRZ410, and TRZ426. Moreover, TRZ056, TRZ069, TRZ071, TRZ079, TRZ083, TRZ183, TRZ200, TRZ404 and TRZ410 present also analcime ($Na[AlSi2O6]\cdot 6H2O$) in their diffractogram (Figure 19).

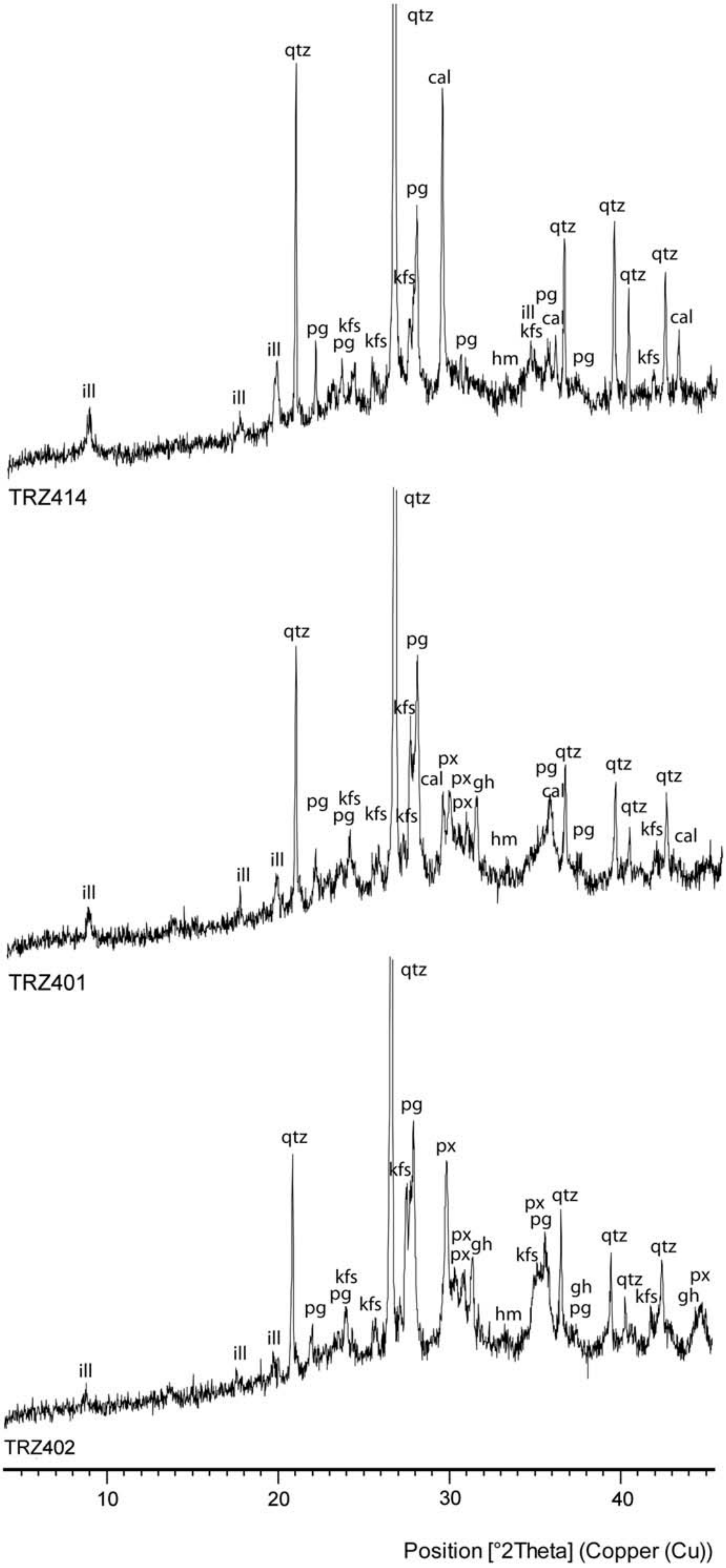

Figure 18: Diffractograms of the individuals TRZ414, TRZ401 and TRZ402 representing the chemical group **TT-G**; cal: calcite, gh: gehlenite, hm: hematite, ill: illite-muscovite, kfs: k-feldspar, pl: plagioclase, px: pyroxene, qtz: quartz

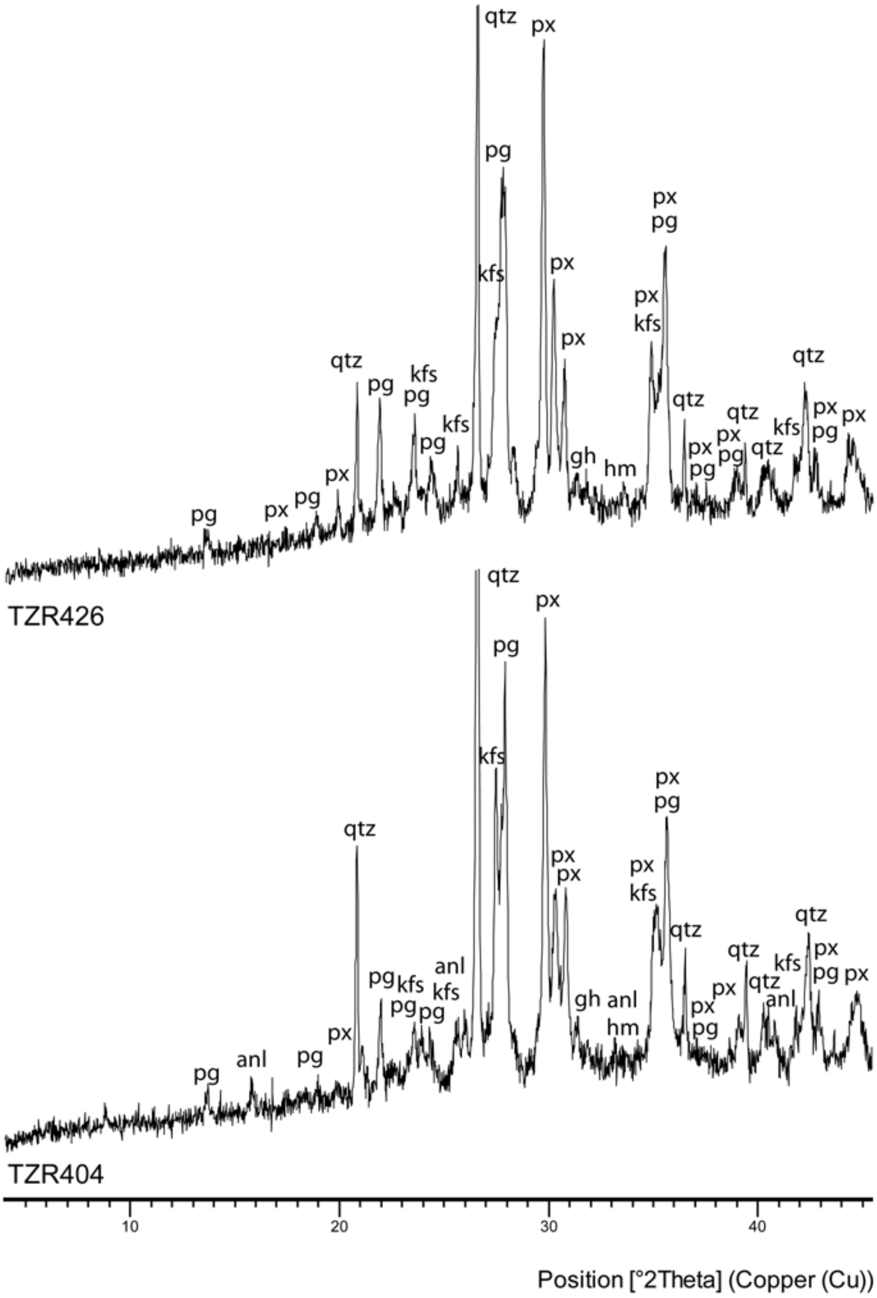

Figure 19: Diffractograms of the individuals TRZ426 and TRZ404 representing the over fired vessels from chemical group **TT-G**; anl: analcime, cal: calcite, gh: gehlenite, hm: hematite, ill: illite-muscovite, kfs: k-feldspar, pl: plagioclase, px: pyroxene, qtz: quartz

4.2. Tchingiz Tepe (Termez). Pottery production and distribution

We can conclude that the knowledge related to pottery production and pottery distribution in Tchingiz Tepe in ancient times has been largely increased. The combination of a detailed stratigraphic evaluation, which makes possible to establish specific ceramic contexts, together with the use of radiocarbon dating and a systematic archaeometrical program of pottery analysis, has allows to identify a clear Reference Group ascribed to several common wares productions from the pottery workshop found at sector RF. Radiocarbon analysis that are in progress will provided new absolute dates for contexts from sectors RA and RB2, which will provide more precise chronologies for the pottery recovered at Tchingiz Tepe.

As provenance study is concerned it is important to mention the existence of clearly differentiated productions of cooking wares. They have been grouped in TT-A, TT-B, TT-C, TT-D chemical and petrografic groups which can be related to a local or regional origin.

Cooking wares from group **TT-A** can be considered as a local production because the inclusions present in these pastes are clearly compatible with the geological formations of the area. These particles are also identical to the inclusions identified in the pastes of the common wares grouped in group **TT-G**, the RG assigned to the pottery workshop located at sector RF in Tchingiz Tepe. The predominant components of these pastes are crystals of quartz, plagioclase, k-feldspar and muscovite derived of granitic rocks and crystalline schist from the Paleozoic basement of the Surkhan Darya valley. Lames of biotite and crystals of amphibole and epidote identified in these pastes can probably derive from granitic rocks. As a particular feature, we must to emphasize the regular presence of common-few crystals of olivine and clinopyroxene. Basalt is also observed as a common aplastic inclusion in the paste of the tops TRZ085 and TRZ183 from group TT-G. The source of these volcanic rocks could be placed in the Lower Carboniferous volcanic formations present in the Tien Shan mountain system and its southern foothill, the Gissar-Alai mountain system, situated at the northern area of Termez. Fragments of sedimentary rocks (sandstone and chert) can be assigned to Mesozoic and Cenozoic formations filling this basin. These continental and marine deposits consists of shale, grey sandstone and limestone with shallow sea fauna, which are elements also observed in some of the previous petrographic fabrics identified (**TTG-B**, **TTG-C** and **TTG-D**).

Cooking wares from groups **TT-B**, **TT-C** and **TT-D** exhibit limestone with shells fragments as a main petrographic component. These calcareous inclusions must come from maritime sediments deposited during the Mesozoiz and Cenozoic age that cover areas of Gissar Mountains. Some of these fabrics also contain sandstone and siltstone (TT-C and TT-D), which is another component characteristic of Mesozoiz and Cenozoic sediments of this area. In this regard, we must conclude that cooking wares from groups **TT-B**, **TT-C** and **TT-D** correspond to regional pottery productions placed, probably, at the Surkhan Darya valley.

As technological study is concerned, cooking wares used and produced at the Kushan and Kushan-Sassanian periods follow different technological patterns. Local productions are medium-coarse fabrics which common temper are rock fragments. In contrary, the regional cooking wares are characterised by the only presence of big shell fragments. In both cases, is clear that potters have manipulated paste composition, adding coarse temper into the fine iron rich clay paste, to obtain cooking wares with specific functional properties. Using this technological modification, potters made these pots more suitable for cooking, because coarse non plastic tempering offers high resistance to thermal stress and heat impact.

Common wares from the Kushan-Sassanian period were produced using calcareous alluvial clays mixed with very small rock fragments from the local geological formations. The compositional similarity detected in pottery production in Tchingiz Tepe point to the existence of a long lasting local/regional ceramic tradition. During more than four centuries, is attested the procurement and choice of raw materials available in similar geochemical sources and very standardised technological process in pottery making (pastes, firing conditions, forms and surface treatments).

Bibliography

Achón, O., Ariño, E., García, D., Gurt, J.M., Sala, R., 2008, Archaeological work at Tchingiz Tepe: Verifying the results of geophysical surveying using radar, en J.M. Gurt, S. Pidaev, A.M. Rauret and S. Stride (eds.), IPAEB: Preliminary Report of the work of the International Pluridisciplinary Archaeological Expedition to Bactria, Vol. 2, Barcelona, pp. 75- 139.

Aitchison, J., 1986, The Statistical Analysis of Compositional Data, Chapman and Hall, London.

Ariño, E., 2009, Archaeological record: Sector RC (Tchingiz Tepe), en J.M. Gurt and S. Pidaev (eds.), IPAEB: Preliminary Report of the work of the International Pluridisciplinary Archaeological Expedition to Bactria, Vol. 3, Barcelona, pp. 7-110.

Ariño, E., 2010, Archaeological record: Sector RC (Tchingiz Tepe), in J.M. Gurt and S. Pidaev (eds.), IPAEB: Preliminary Report of the work of the International Pluridisciplinary Archaeological Expedition to Bactria 2009, Vol. 4, Barcelona, pp. 7-120.

Buxeda i Garrigós, J., 1999, Alteration and Contamination of Archaeological Ceramics: The perturbation problem, Journal of Archaeological Science, 26, pp. 295-313.

Gurt, J.M., 2009, Archaeological record: Sector AC, military camp (former barracks), in J.M. Gurt, S. Pidaev, A.M. Rauret and S. Stride (eds.), IPAEB: Preliminary Report of the work of the International Pluridisciplinary Archaeological Expedition to Bactria 2008, Vol. 3, Barcelona, pp. 187-217.

Leriche, P., 2007, Bactria, Land of a Thousand Cities, in J. Cribb and G. Herrmann (eds.), After Alexander. Central Asia before Islam, Proceedings of the British Academy, Oxford University Press Inc, New York, pp. 121-153.

Leriche, P., Pidaev, Sh., 2007, Termez in Antiquity, in J. Cribb and G. Herrmann (eds.), After Alexander. Central Asia before Islam, Proceedings of the British Academy, Oxford University Press Inc, New York, pp. 179-211.

Leriche, P., Pidaev, Sh., 2008, Termez sur Oxus. Cité-capitale d'Asie Centrale, Maisonneuve & Larose, París.

Martínez Ferreras, V., 2009, Archaeological record: Sector RF (Tchingiz Tepe), in J.M. Gurt, S. Pidaev, A.M. Rauret and S. Stride (eds.), IPAEB: Preliminary Report of the work of the International Pluridisciplinary Archaeological Expedition to Bactria 2008, Vol. 3, Barcelona, pp. 111-184.

Martínez Ferreras, V., 2010, Archaelogical excavation of Sector AC2 at Ancient Military Quarters (Termez), in J.M. Gurt and S. Pidaev (eds.), IPAEB: Preliminary Report of the work of the International Pluridisciplinary Archaeological Expedition to Bactria, vol. 4, Barcelona, pp. 125- 221.

Martínez Ferreras, V., Tsantini, E., Gurt i Esparraguera, J.M., Pidaev, S., 2008, Archaeometrical study of the ceramics coming from the archaeological site of Termez in Uzbekistan, in J.M. Gurt, S. Pidaev, A.M. Rauret and S. Stride (eds.), IPAEB: Preliminary Report of the work of the International Pluridisciplinary Archaeological Expedition to Bactria, Vol. 2, Barcelona, pp. 141-194.

Martínez Ferreras, V., Tsantini, E., Gurt i Esparraguera, J.M., Pidaev, S., 2009, Provenience and Technological study of the ceramics coming from the archaeological sites of Termez, Kampyr Tepe and Zar Tepe in Uzbekistan, in J.M. Gurt, S. Pidaev, A.M. Rauret and S. Stride (eds.), IPAEB: Preliminary Report of the work of the International Pluridisciplinary Archaeological Expedition to Bactria, Vol. 3, Barcelona, pp. 231-248.

Martínez Ferreras, V., Tsantini, E., Gurt i Esparraguera, J.M., Pidaev, S., 2010, Archaeometrical study of archaeological ceramics. Extension of provenance and technological analysis with new materials from ancient Termez, Kampyr Tepe and Tchurobkurgan sites in J.M. Gurt and S. Pidaev (eds.), *IPAEB: Preliminary Report of the work of the International Pluridisciplinary Archaeological Expedition to Bactria*, Vol. 4, Barcelona, pp. 291-418.

Martínez Ferreras, V., Tsantini, E., Gurt i Esparraguera, J.M., Pidaev, S., in press, Archaeometrical study of the ceramic technology in Termez (Uzbekistan). Potery making in the ancient Bactria province during and following the Hellenistic period, 10th European Meeting of Ancient Ceramics. The British Museum and The University College of London.

Mestres i Torres, J.S., Rauret i Dalmau, A.M., 2009, Report on Radiocarbon Dating, in in J.M. Gurt, S. Pidaev, A.M. Rauret and S. Stride (eds.), *IPAEB: Preliminary Report of the work of the International Pluridisciplinary Archaeological Expedition to Bactria 2008*, Vol. 3, Barcelona, pp. 349-357.

Mestres i Torres, J.S., Rauret i Dalmau, A.M., 2010a, Report on Radiocarbon Dating /1, in J.M. Gurt and S. Pidaev (eds.), *IPAEB: Preliminary Report of the work of the International Pluridisciplinary Archaeological Expedition to Bactria 2009*, Vol. 4, Barcelona, pp. 243-257.

Mestres i Torres, J.S., Rauret i Dalmau, A.M., 2010b, Report on Radiocarbon Dating /2, in J.M. Gurt and S. Pidaev (eds.), *IPAEB: Preliminary Report of the work of the International Pluridisciplinary Archaeological Expedition to Bactria 2009*, Vol. 4, Barcelona, pp. 259-274.

Mkrtyschew, T., 2007, Buddhism and Features of the Buddhist Art of Bactria-Tokharistan, in J. Cribb and G. Herrmann (eds.), *After Alexander. Central Asia before Islam*, *Proceedings of the British Academy*, 133, Oxford, pp. 475-485.

Mkrtyschew, T., 2010, El arte budista en Bactria, in S. Hansen, A. Wieczorek and M. Tellenbach (eds.), *Alejandro Magno. Encuentro con Oriente. Catálogo de la exposición*, Regensburg, pp. 215-227.

Rtweladse, E.V., 1994, Kampyr Tepe: Structures, written documents and coins, *Bulletin of the Asia Institute. New Series*, 8, pp. 141-154.

Rtweladse, E.V., 2009a, *Civilizations, states and cultures of Central Asia*, Forum of Culture and Arts of Uzbekistan Foundation (Fund Forum Uz), University of World Economy and Diplomacy, Tashkent.

Rtweladse, E.V., 2009b, Alejandría Oxiana, in S. Hansen, A. Wieczorek, M. Tellenbach (eds.), *Alejandro Magno. Encuentro con oriente. Catálogo de la exposición*, Regensburg, pp. 173-179.

Tsantini, E., Martínez, V., Gurt i Esparraguera, J. M., 2007, Results of all the available archaeological and archaeometrical information on the excavation of Kara Tepe, in J.M. Gurt, S. Pidaev, A.M. Rauret and S. Stride (eds.), *IPAEB: Preliminary Report of the work of the International Pluridisciplinary Archaeological Expedition to Bactria*, Vol. 1, pp. 67-90.

Proposal on the preliminar scientific study of the construction materials of Termez, for the identification of the preservation state and study of suitable conservation treatment and rehabilitation process

E. Tsantini, V. Martinez, J.M. Gurt, S. Pidaev

Introduction

The site of Ancient Termez is located in southern Uzbekistan, on the banks of the Amu Darya River, on the Afghan border. Termez is a major urban site occupied at least since the Hellenistic period and up to the Mongol conquest. The archaeological site includes the urban complex, with two fortified enclosures -Citadel and Thingiz Tepe- and the Buddhist monastery of Kara Tepe. The Buddhist complex of Fayaz Tepe and Zurmala are located near the old town.

The average annual rainfall at this area is 147.3 mm and it can be classified within the category of arid o semi-arid region. Nevertheless, as all arid or semi-arid environment, this area is also characterised by brusque temperature changes and high variation between the lowest and highest temperatures, not only between the different seasons but also between day and night during the same day.

Another characteristic is the luck of vegetation that has two main consequences. The first is that, the windblown, that is normally strong at the deserted zones (precisely because of the absence of vegetation), finds no resistance dragging away all the sand and solid atmospheric compounds (like salty particles very common in this kind of environments), and the second is, that the rainfall finds no obstacles neither, as there are no vegetation to absorb the water, thus it can create strong water flows (mainly during winter) that drags away all kind of sediments that it finds in its way, as well. That is why the unrecovered constructions at all the archaeological complexes at the site of Termez are already covered by superficial formations that are the result of natural weathering processes. To the above weathering processes also can be added the human action and the deterioration of the constructions due to historic use.

On the other hand, the recovered constructions are made of a natural local raw material that is very sensitive to any climate changes and to any mechanical o chemical weathering process. In most Central Asian sites of the Kushan and Sassanian period, walls structures are made from *pakhsa*, which is in fact a mud brick (compressed clay and clayey sand). As *paksha* is hand made, therefore the percentage of clay and sand may vary, affecting the degree of compression, consequently, the weathering processes are not necessarily affect at the same degree the whole building complex, neither affect at the same way the different buildings (selective weathering). The problems with these structures, in fact, begin before excavation, as specific burial conditions can disintegrate the *pakhsa* structures.

The construction with mud bricks and the almost absolute absence of rock structures (that have been only punctually found at socially or religiously important contexts, for example the rock column bases at Kara Tepe or Thcinguiz Tepe religious areas), that are much more resistant and easily restorable, is not the only difficulty can be found at this archaeological site, but also the existence of wall painting laying directly upon a thin calcareous cement (*intonaco*) that has been straight applied upon the raw mud brick structures, without any mortar background. This technological peculiarity makes the paintings much less durable and easily affected by any deterioration

.

Viewable weathering processes affecting the buildings and the decorations

Chemical weathering:

At Termez region, *chemical weathering* is limited practically to processes related to the salt and gypsum transfer and migration, *redox* processes that can lead to crystallization of secondary minerals ($CaSO_4$, NaCl etc.) which a part of the modification of the chemical and mineralogical composition finally modifies the physical properties of the buildings, debilitating the mud bricks producing superficial crack and ruptures and a superficial erosions, as well, like powdering, exfoliation, scaling, spalling of the surface and its partial detachment that can lead to total loss of the material. In the case of the wall paintings the superficial salt erosions can lead to the absolute loss of the pigments or its detachment from the background (Figure 1). All these chemical weathering profiles are inherited from more humid paleoenvironments.

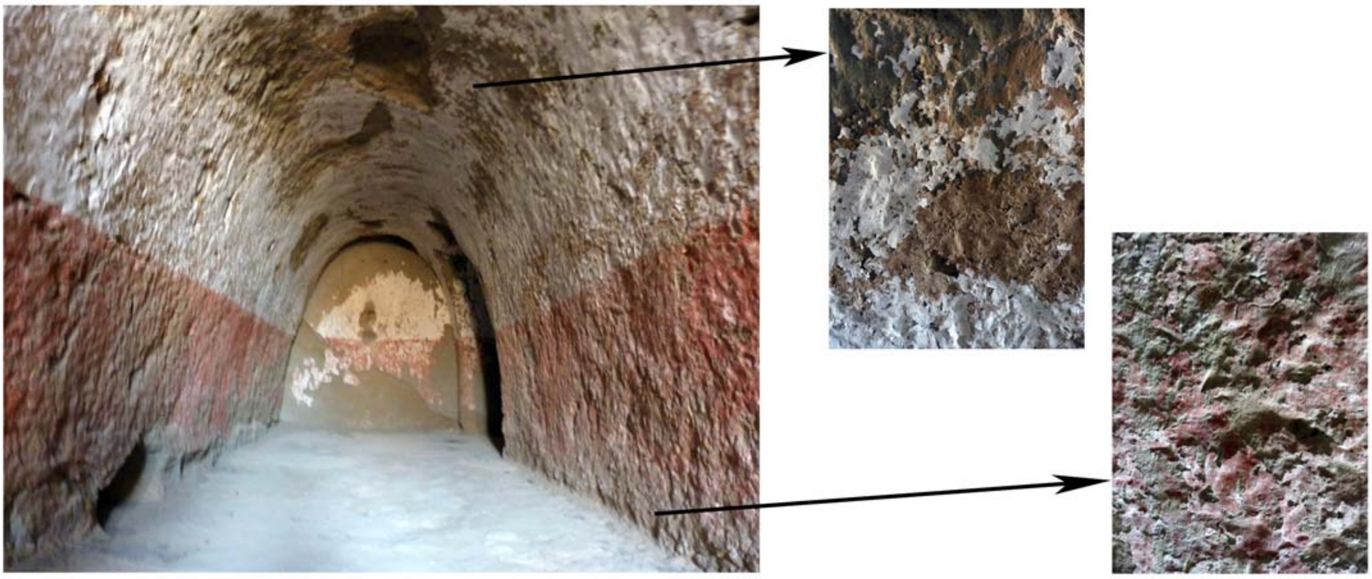

Figure 1: Examples of salt erosion

Mechanical weathering:

Mechanical weathering at Termez is preferably related to (Figure 2):

Figure 2: Some examples of mechanical weathering processes

1. Wind action:

As it has been already mentioned before, windblown that is strong at the deserted area of Termez (because of the absence of vegetation), finds no resistance dragging away all the sand and solid atmospheric compounds (like salty particles which are common in this kind of environments) that continuously bombed against the surface of the mud brick structure producing holes, and capillary cavities (*alveoli and alveoli-like weathering)* that then lead to cracks and loss of material due to the additional action of other weathering processes that are mentioned below.

2. Thermoclasty:

The continuous and brusque temperature changes at arid and semi-arid environments force the material to expand and shtick roughly and continuously, which create cracks and ruptures that then lead to the absolute falling down of the structures.

3. Haloclasty:

In simple *halioclastia* water seeps into cracks and evaporates depositing salt crystals on the surface of the structures then heated up the deposited salt crystals will expand putting pressure on the rest of the structure which can be cracked or fragmented. It is normally associated with arid climates where strong heating causes strong evaporation and therefore salt crystallization (also can occur along the coast, of course). Salt crystallization may also take place when solutions decompose rocks (for example, limestone and chalk) to form salt solutions of sodium sulfate or sodium carbonate, of which the moisture evaporates to form their respective salt crystals. However, at Termez, the mechanic action of the wind that makes capillary superficial cavities or small superficial holes accelerates this phenomenon retroactively.

4. Rainsplash:

Raindrop impact generates the initial particles mobilization and leads to the superficial deposition upon the mud brick walls.

Finally, it has to be stressed out that*alveoli and alveoli-likedifferential weathering* is very frequent in arid and semi-arid regions that leads to differential cementation or deposition and localized variation of the physical properties and of the permeability.

Analytical methodology and experimental study proposed for the identification of the raw material used for construction of walls and wall painting and for the identification of their preservation states

For both the study of the mud brick structure and the wall paintings we propose the full identification of their composition and characterisation of their technological aspects. We suggest also the experimental identification of the mechanical properties of the *pakhsa* structure, its mechanical and thermal properties, and the calculations of Attemberg's Limits in order to calculate water absorption (liquid and plastic limits) and finally, the calculation of the linear shrinkage without any treatment thus to understand its behaviour. Unfortunately, we cannot do that for the wall paintings, as the samples that are required for the experimental study are too big.

Following, in a second phase, the same mechanical, thermal properties and the Attemberg's limits and Linear Shrinkage will be studied treating the original mad brick with different non aggressive natural organic substances that will be described in the following section of this report. The analytical methodology followed for this first study phase will be the following:

A. Petrographic analysis (OM):

Petrographic analysis by OM will be used for the full identification of the character and origin of the raw materials applied for the mud-bricks fabrication. Via this technique the rock fragments present in the structure, its matrix and all its compositional and optical aspects will be studied. On the base of the petrographic study, the character and the possible origin of the raw materials can be identified. This technique is suitable to identify if there are abundant well crystallised contamination of secondary minerals in the structure (any well crystallised salt contamination) or not, as well.

The petrographic study will be carried out by the observation of thin-sections prepared from the transversal section of a sample of a mud brick using an *Olympus BX-41* polarising microscope working under magnification between 40X and 400X. Each ceramic specimen will be impregnated with epoxy resin and mounted using Loctite UV glue and sectioned using a *Struers Discoplan TS*. The thin sections will be finished by hand using a powder abrasive until reaching a thickness of 30 micrometers in which quartz presents a grey-white first order interference colour. The observations will be carried out with Olympus BX41 microscope equipped with objectives of x4, x10, x20, 40 working between 40 and 400 magnifications. Photographs will be taken using a digital camera Olympus DP-70 attached to the microscope controlled by specific computer software.

B. X-Ray Diffraction (XRD):

XRD analyses will be used complementary to the patrographic study to identify the mineralogical composition of the raw materials of the mud bricks and will used as a basic methodology to identify the correspondent minerals of the pigments and the white preparation of the wall paintings. This technique is specially suitable for the identification of the crypto-crystalline phases present in the mud bricks, that cannot be identified by OM. Considering that there might be contamination of zeoliths due to chemical action of the salt that are normally crypto-crystalline, the mineralogical analysis will be well complement the petrographic study. Regarding to the characterisation of the wall paintings, this is the most suitable technique to use for the full mineralogical identification of the pigments and the background without being essential to apply OM study.

The XRD analysis will be were carried out by using 1gr of powdered sample. Measurements will performed using a *PANanalyticalX'pert Pro MPD X-ray powder diffractometer*working with the Cu Ka radiation (l=1.5406 Å), and graphite monochromator in the diffracted beam, at 1.2 kW (40 kV, 30 mA).

Spectra will be taken from 4 to 70°2Q, at 1°2Q/min (step size=0.05°2Q; time=3 s). The evaluation of crystalline phases was carried out using the DIFFRACT/AT program by Siemens, which includes the Joint Committee of Powder Diffraction Standards (JCPDS) data bank incorporated into the soft wear of *PANanalyticalX'pert Pro*.

C. Scanning Electron Microscopy Equipped with X-Ray Energy Dispersive Detector for micro-chemical analysis:

Scanning Electron Microscopy Equipped with X-Ray Energy Dispersive Detector for microchemical analysis will be used complementary to the above two techniques, both in the case of the mud bricks and the mural paintings, in order to study the microstructure and to identify secondary well crystallised mineral precipitations that are not abundant in the material. Therefore this technique together with OM will be really useful to identify the soluble salt precipitation in the building material and evaluate realistically its extension. It will be applied also to confirm the composition of the pigments in the case of the wall paintings by microchemical analysis.

For this study *a JEOL JSM-840Scanning Electron Microscope (SEM) equipped with Secondary Electron (SE) detector and Energy Dispersive X-ray Micro Analyser (EDS)* will be used. The observations will be performed under vacuum at the external surface of the fresh fractures and the secondary electron image will be taken at different magnifications, also X-ray microanalysis will be performed. The experimental condition will be the following: acceleration voltage will be equal to 20kV and the intensity to $3x10^{-9}$ A. Both fresh fractures and polished sections will be used for the study. The preparation of the samples will be done by fixing the fresh fractures upon a standard metallic base of 1cm diameter with silicon and in order to assure the continuous conductivity between the sample and its base and to avoid the overloading of the surface, the fresh fractures will be covered with silver and then the whole sample will be covered with carbon to avoid superficial electrical overload. In the case of the polished section the same preparation process will be followed upon the resin impregnated cross section of the samples.

D. Experimental Study of the Mechanical Resistance and Thoughtless and Hardness:

The mechanical and thermal properties are directly related to microstructure and the characteristics of materials that depend on the raw materials have been used and the production processes. All these aspects affect the techno-functional sufficiency of the product.

The mechanical properties which will be tested are the **mechanical resistance** (TRS), **hardness** (H), **toughness** (Kk), thermal expansion and cooling retraction and thermal shock resistance (ktrs). The techno-functional aspects together with the above mentioned methodologies to study the composition and character of the material will be useful to fully describe the technological suitability of the material. By understanding the physical properties of the bricks, suitable organic substances might be added to improve its physical properties and long lasting resistance.

First, for the **TRS** tests fragments from a mud brick will be cut down into small briquettes of 3-4 cm length, 1cm width and at least 0.5 cm of thickness. All their surfaces will be polished (60 mm and 320 μm) until they become absolutely parallels. To check the precision of the technique we will prepare and test 3 briquettes from one single mud brick that we have already sampled.

The TRS will be tested with a motorised INSTRON 1195 instrument exerting four point pressures (5N/sec). In this way, there is a compression applied at the upper part of the briquette and at the same time tension (by stretching) at the lower part of the briquette, when the pressure is high enough the fracture will start from the lower part of the briquette and propagate to the upper surface. Finally, the detector will detect the maximum force (N) at the exact moment before the fracture has been taken place. After the experiment the TRS will be calculated according to the following equation:

$$TRS= [3Pf \times (S_1\text{-}S_2)]/2bd^2$$

The same experiment with motorised INSTRON 1195 instrument exerting four point pressure (5N/sec) upon another briquettes already sectioned at the lower surface (a small and thin section about 1mm profound called single edge notched beam will be produced before testing). By recording the maximum pressure the **toughness** will be calculated by the equation:

$$K_{ic} = \frac{3P_f(S_1 - S_2)}{2bd^2}$$

The broken fragments of the tested for briquettes will be used to test the **Hardness**. The experiment this time will be performed with a simple mechanic press exerting a pressure correspondent to 30kg with a pyramid shaped diamond at the surface of the samples (with parallel sites) for 10 sec. Consequently the diamonds will mark the surface and according to the length of the diagonals of the mark, the Hardness will be estimated by the equation:

$$Hv=1.8544[P/d^2] \text{ o: } d=[d_1+d_2]/2$$

Where d_1 i d_2 are the lengths of the diagonal marks on the surface.

As for the **thermal properties,** it is known that materials change their physical properties by the increase of temperature (T°). Therefore, in this project the following kind of thermal properties will be calculated: **Thermal Expansion** and **Thermal Shock Resistance** (*Rs*).

Most of the solids are expanded when they heated and contracted when they cool down. The change of the size by temperature is given by the equation:

$$\frac{l_f - l_0}{l_0} = \alpha_l (T_f - T_0)$$

$$\frac{\Delta l}{l_0} = \alpha_l \Delta T$$

Where l_f is the final length of the object l_0 is the initial and T_f is the max. temperature and T_0 is the initial, finally α_1 is the lineal coefficient of thermal expansion. **Thermal expansion** will be calculated experimentally by heating of a rectangular sample and measuring the change of length according to the change of temperature (*ΔT*). For statistical reasons to reduce errors, 3 samples will be prepared. As thermal expansion not only affects the length but all the volume of a material, by the same experiment the volumetric thermal expansion coefficient (α_v) will be also calculated applying the following equation:

$$\frac{\Delta V}{V_0} = \alpha_V \Delta T$$

$$\frac{(V_f - V_0)}{V_0} = \alpha_V (T_f - T_0)$$

Where V_f is the final volume and V_0 is the initial one.

On the other hand, **Thermal Shock Resistance** is an ability of material to withstand sharp changes in temperature. If a material is rapidly cooled, its surface reaches the temperature of cooling environment and tends to contract (thermal contraction). Since the interior regions of the material are still hot, thermal contraction of the skin surface is impossible. This leads to formation of tensile stress (**thermal stress**) in the skin. Such thermal stresses may cause cracks and consequent failure. **Thermal Shock Resistance** of a material may be estimated in accordance to the formula:

$$Rs = (\lambda * \sigma_F)/(\alpha * E)$$

Where Rs is thermal shock resistance, λ- thermal conductivity, σ_F – flexural strength, $\alpha$is the coefficient of thermal expansion (CTE) and E is the elastic modulus.

Sensitivity of soils and clays to thermal shock may be also determined by the Hasselmann Method experimentally. The experiment is almost the same to the one used to calculate the TRS (traversal stress) which has been already described above, only this time, the sample is heated up progressively till a specific temperature and then three or four point bending stress-compression is applied to it up to its upper limit of the elastic modulus (exactly before breaking) then the sample is cooled down fast (normally by dropping it into room temperature water). Then, the sample is put to dry in an oven (100 ºC) and the experiment is repeated each time heating the sample up to higher temperature until after the cooling down the sample is collapses (breaks).

E. Experimental Study of the Atterberg's Limits (plastic and liquid limits/water absorption):

The Swedish soil scientist Albert Atterberg originally defined seven "limits of consistency" to classify fine-grained soils, but in current engineering practice only three of the limits, the liquid, the plastic and shrinkage limits. The **Atterberg's limits** are based on the moisture content of the soil.

The **plastic limit** is the moisture content that defines where the soil changes from a semi-solid to a plastic (flexible) state. The **liquid limit**, on the other hand, is the moisture content that defines where the soil changes from a plastic to a viscous fluid state. Finally the **shrinkage limit** is the moisture content that defines where the soil volume will not reduce further if the moisture content is reduced.

A wide variety of soil engineering properties have been correlated to the liquid and plastic limits, and these **Atterberg's limits** are also used to classify a fine-grained soil according to the Unified Soil Classification system or AASHTO system. Atterberg's limits will be measured experientially by the following way:

<u>Experimental Procedure:</u>

Liquid Limit

(1) We will take roughly 3/4 of the soil and place it into the porcelain dish (Liquid Limit Device, Porcelain-Evaporating Dish). The soil will previously passed though a No. 40 sieve, air-dried and then pulverized. Thoroughly we will mix the soil with a small amount of distilled water until it appears as a smooth uniform paste. We will cover the dish with cellophane to prevent moisture from escaping.

(2) We will weigh four of the empty moisture cans with their lids, and record the respective weights and can numbers on the data sheet

.

(3) We will adjust the liquid limit apparatus by checking the height of drop of the cup. The point on the cup that comes in contact with the base should rise to a height of 10 mm. The block on the end of the grooving tool is 10 mm high and should be used as a gage.

(4) We will place a portion of the previously mixed soil into the cup of the liquid limit apparatus at the point where the cup rests on the base, then we will squeeze the soil down to eliminate air pockets and spread it into the cup to a depth of about 10 mm at its deepest point until obtaining a horizontal surface.

(5) We will clean a straight groove down the centre of the cup. The tool should remain perpendicular to the surface of the cup as groove is being made without sliding the soil to the surface of the cup.

(6) We will turn the crank of the apparatus at a rate of approximately two drops per second let the drops fall down to the sample. We will count the number of drops, N they won't be higher than 50.

(7) We will weight the humid sample, then put it in the oven up to 100 ºC during 16h and weight it again.

(8) Then we will remix the entire soil specimen with a small amount of distilled water and repeat the process tying different number of drops.

Plastic Limit

(1) We will weigh the remaining empty moisture cans with their lids, and record the respective weights and can numbers on the data sheet. Then, take the remaining 1/4 of the original soil sample and add distilled water until the soil is at a consistency where it can be rolled without sticking to the hands.

(2) We will form the soil into an ellipsoidal mass until it reaches 3.2 mm of diameter.

(3) When the diameter of the thread reaches the correct diameter we will separate the thread into several pieces.

(4) The portions of the crumbled thread together and place into covered moisture can when they humid (counting the drops again) they will be weighted immediately, then they will be weighted again after being 16 hours in an oven up to 100ºC.

(5) We will repeat the procedure two more times for statistical reasons and analytical precision reasons.

Calculations:

Liquid Limit

To calculate the liquid limit we will calculate first the water content of each of the liquid limit moisture cans after they have been in the oven for at least 16 hours. Then plot the number of drops, N, (on the log scale) versus the water content (w) and draw the line through the plotted points to finally determine the liquid limit (**LL**) as the water content at 25 drops.

Plastic Limit

To calculate the plastic limit we will calculate the water content of each of the plastic limit moisture cans after they have been in the oven for at least 16 hours, then compute the average of the water contents to determine the plastic limit, PL. Finally, we will calculate the plasticity index by the equation: **PI=LL-PL.**

F. Experimental Study of Linear shrinkage:

Approximately 300 g of the material will be mixed in a bowl and thoroughly with deionised water until the mass becomes a thick homogeneous paste, adding sufficient water to bring it to a consistency equal to or slightly wetter than the Liquid Limit.

The final paste will be moulded inside of a clean shrinkage mould and the longitude (L) of the humid specimen (briquette) taken out from the mould will be measured. The specimen will be let to dry at room temperature for about 24 hours until a distinct change in colour will be noticed. Consecutively, it will be transferred into an oven to dry completely at between 105 °C and 110 °C and its longitude will be measured again (Ls). The linear shrinkage will be calculated then according to the following equation:

Were: L = Length of the mould (mm) and Ls = Longitudinal shrinkage of the specimen (mm)

G. Analytical study of the organic mean of the paintings:

The *in situ* observation of the mural paintings indicates that there might be some kind of organic medium used for their fabrications. We propose an organic residue study in order to see if this is the case and in order to be able to identify which was exactly the organic binding media that were used. For the organic analysis the following analytical methodology will be used:

Total lipid extraction

500 mg of grounded sample are extracted twice with 3 ml of $CHCl_3$.MeOH (2:1 v/v) in ultrasound bath for 40 min. at 70°C. 5 µl of a standard solution of C28 (3mg/ml) are added to the powder before the solvent extraction. The surnatant is recovered after centrifugation and reduced to a volume of 100µl using a gentle stream of nitrogen. Part of the sample (50µl) is dried, derivatized adding 50µl of N,O-bis(trimethylsilyl)trifluoroacetamide (BSTFA) and heating at 70°C for 1h. Then, 1µl of the resulting mixture is used for the analyses. The remaining 50µl are used for further analyses.

Hydrolysis

500 mg of sample is extracted twice with 3 ml of 0.5 M NaOH in MeOH /H_2O (9:1 v/v) in ultrasound bath at 70°C for 90 min. After cooling the surnatant is recovered after centrifugation and acidized with 20 drops of 1 M HCl. 3 ml $CHCl_3$ are added twice to the surnatant and mixed with the vortex. They are then separated and dried using a gentle stream of nitrogen. The extraction is repeated and 3 ml of ethyl acetate are added twice to the surnatant and mixed with the vortex. They are then separated and dried using a gentle stream of nitrogen. All the samples are derivatized adding 25µl of N,O-bis(trimethylsilyl)trifluoroacetamide (BSTFA) and heating at 70°C for 1h. 1µl of the resulting mixture is used for the analyses.

Analyses

The GC-MS analyses will be performed by using a gas chromatographer CP3800 (Varian, Walnut Crick, CA, USA) equipped with a 30 m x 0.25 mm (i.d.) x 0.25 µm film thickness fused silica capillary column (Rtx-5MS, Restek corporation, Bellefonte, PA, USA), and a mass spectrometer Saturn 2000 (Varian, Walnut Crick, CA, USA) operated in the electron ionization mode (70 eV). The mass range will be scanned in the range of *m/z* 40-650. The GC oven temperature is held isothermally at 50°C for 1 min, and then it will be raised at 5°C/min up to 300°C and held isothermally for 10 min.

Some Remarks

It is obvious from the above described methodology that, the study of the wall paintings will be much simpler, as they lay directly upon thin calcareous cement (*intonaco*) that has been straight applied upon the raw mud brick structures, without any mortar background. The complete identification of the pigments and the *intonaco* can be done directly upon 1gr of powdered sample by XRD (already described before) as pigments and *intonaco* correspond to specific minerals that can be perfectly identified by this technique. SEM-EDS (already explained above) can be complementary used to confirm the pigments composition by chemical microanalysis or identify the crystallised salts on the wall paintings surface. Additionally, and only for the wall paintings organic residue analysis, is programmed in order to identify the character of an organic binding medium if there is any.

Proposal of the experimental study to find the suitable conservation and rehabilitation treatment

Paksha Stucture:

Regarding to the high archaeological and historical value, not only of the building but also of the technology used for its construction, that is typical only at the Middle and Far East and absent mainly in the west Mediterranean world, we consider that, any conservation and rehabilitation process has to respect fully its material, artistic and cultural integrity by intervening materially and aesthetically altering only at minimum possible extend the original aspect and the originally used raw materials.

Therefore, the use of *silicates*, like TEOS (terra silicates), ethyl-silicates and *silane* conservation product that are very in fashion in the restoration of historical buildings nowadays (proposed at 1993 at Lisbon's ICCROM Congress), are not recommended here. Mainly because there are almost not reversible, so they can not be easily removed and less from a porous material like these *pakhsa* structures and second, because such treatment had provoked serious damages in treated porous material, lately, such as wall painting in South Italy. For the same reasons any treatment with other *synthetic resin* has to be excluded (epoxy, acrylic and vinilic compound are not suggestible).

In fact, we consider that the rehabilitation process for the building structure should reproduce and complete the structure using the original soil base material that has been applied for its construction and, in this expectance, the proposed preliminary study of the raw material is absolutely necessary.

Nevertheless, the already described viewable weathering processes, at the second section of this report, suggest that the reproduction of the mud bricks might involve the mixture of the soil with other natural substances that might improve the new structure's mechanical and thermal properties and even its water conductivity. The use of such natural substances have been ethnographically documented for the fabrication of mud brick walls or raw soil mortars, as they were frequently applied in traditional rustic architecture, during the recent history, not only in the oriental world, but also in west and central Europe (see relevant bibliography at the end of this report). It can be even stressed out that in the modern occidental world the original technology of these ancient central and far oriental *pakhsa* constructions is very relevant nowadays, as in the new bio and eco-architecture raw soil mortars (mainly in Sweden and Germany) are used mainly for the internal and less for external wall constructions. Thus, new scientific studies are developed in traditional architecture (Italy, Germany, etc.) that studying additional treatments in order to improve the physical properties by using only natural additive substances like: *casein, linseed oil or phycus resigns* (see related bibliography at the end of this report)or simply by adding *plant straw*.

Therefore in order to check if the physical properties of the mud-brick reconstructions could be improved with the addition of these materials, we propose the repetition of the study of the mechanical and thermal properties as well of the Atterberg's Limit and the Linear Shrinkage following exactly the same experimental methodology that has been described in the above section, adding also a simple test to check permeability and salt precipitation, upon specimens (briquettes) prepared with the original soil, adding specific quantities of the above mentioned natural products:

Briquette 1: original soil + 6% of casein
Briquette 2: original soi + 6% phycus resin
Briquette 3: original soil + 8% of linseed oil
Briquette 4: original soil + 6% of phycus resin and 8% of linseed oil.
Briquette 5: original soil+6% of casein + 8% linseed oil.
Briquette 7: original soil + plant straw.

Another inorganic natural material that we would like to check to see if it can improve the new mud brick structure is a fine mixture of lime milk: $Ca(OH)_2$ with the addition of 8-10% $Ba(OH)_2$ that would proportion to the bricks impermeably and stop the precipitation water soluble salt in the structure. This inorganic mixture would be added to the original soil to produce and test **Briquette 8**. Finally, we would study the mechanical and thermal comportment of **Briquette 9** corresponding to briquette 8 but with the addition 8% *linseed oil* which hypothetically would improve even more the permeability and the mechanical properties of the wall.

Here, it is important to mention that, natural products such as *casein* (protein) or natural resins (like *phycus resin*) are non aggressive interventions, however, they can produce problems like easy thermal decomposition (natural resins) and they are easily attacked by and altered by microorganism, therefore we consider that the trial of inorganic compounds has to be seriously considered during the experimentations as they can act as water-repellent stabilizers that would protect from certain alteration processes not only the bricks but also the natural substances if they will be finally used.

Finally, the use of plant straw is also highly recommendable as ethnographically it was used with success in past mud brick constructions or soil based mortars to improve the mechanical properties. The experimentation will define the most adequate combination of materials for the new mud brick fabrication.

To finish with this section, though, it has to be stressed out that, other mechanical problems, such as the wind mechanical action, require in the further future a complete architectonical study for the construction of a protective structure that could slow down the wind's mechanical impact. Yet, this specific project, at the moment, does not include such long-term objectives.

Wall Paintings:

For the restoration and rehabilitation of the wall paintings we propose a methodological different approach. The existence of painted areas in the recovered structures attributes a special importance to site of Termez, that is because, there are only very few mud-brick archaeological constructions in the Middle and Far East that conserve such kind of decorations, therefore we consider that try to restore and conserve the mural paintings *in stiu* would not only advisable but it would be the best option. Such kind of methodological approach also would be in accordance with the ***ICOMOS PRINCIPLES FOR THE PRESERVATION AND CONSERVATION /RESTORATION OF WALL*** **PAINTINGS** published at 2003 (http://www.international.icomos.org/charters/wallpaintings_e.htm)

However the special weathering conditions at the site oblige us to confirm if this is possible. Consequently, after the preliminary analytical study, in a second phase, we propose, an *in situ* restoration trial program to examine if the weathering problems can be solved using a specific treatment methodology and if such methodology could have log-term effectiveness in order to be able to conserve the wall-paintings *in situ*.

It is important to stress out that there are different ambients where the wall paintings are conserved, that can be mainly separated into two basic categories from the environmental point of view. On one hand, there are the wall paintings that the recovered during excavation in different “rooms” or construction areas of both *Kara Tepe* and *Tchinguiz Tepe* and now they are in the open air. In these areas the wall paintings would be exposed to mechanical weathering (described above) much more than to the chemical one (secondary salt mineral formation). On the other hand, there are the painted decorations preserved at the closed much more humid environment of the underground cells of *KaraTepe*, where the salt precipitation problems are much more obvious than the mechanical weathering processes (because the effect of capillary precipitation of humidity). This fact can have as a consequence some differences in the restoration process according to the area where the mural paintings have been recovered. Nevertheless, in both cases the general restoration and rehabilitation trial program will include:

- Superficial salt precipitation cleaning, with or without applying first facing (we will decide *in situ* depending in the fact if the state of preservation of the wall paintings permits facing or not).
- In situ consolidation and permeablilization and neutralization of the salt effect.
- Final cleaning.

Only if the *in situ* trial restoration program proves to be insufficient for the long term preservation of the wall paintings we will proceed, in a third phase, to the elaboration of a new conservation project which will include unfortunately the detachment of the paintings leaving only martyrs and detailed visual information *in situ* in order to show how the paintings were originally.

Here it is important to stress out that one of the most important chemical weathering problems mainly observed in the wall paintings of the underground cells of *Kara Tepe* was the salt precipitation that can not be eliminated *in situ* if the environmental conditions (humidity and temperature changes) are not controlled. Consequently, this fact might condition the possibility of an *in situ* treatment.

The cementation of gypsum is generally obvious at the site. However, the preliminary analytical study proposed above will sort out the kind and the extension of the already precipitated secondary salt minerals. If this is the case, treatments based on mineral substances, essentially those based on calcium and barium hydroxide can be suitable for the consolidation of mural paintings. Nonetheless, there are some limitations on the use of calcium and barium hydroxide on wall paintings:

a) when there are high concentrations of nitrates
b) when there is an organic binding medium
c) when an adhesive function is required (such as exfoliation or macroflaking that require an adhe sive)

The fist two conditions have to be confirmed by the analytical study proposed as a first step. The last one, unfortunately, has been already clearly seen as a viewable weathering problem at the sites. However, one of the experimental trial adhesives will be fine mixture of $Ca(OH)_2$ + $Ba(OH)_2$ and the second will be this fine mixture plus an organic adhesive. The use of *nanolime* also would be advisable, the only problem is that this product still is not available in the market but it is under preindustrial development.

Regarding now the organic products, the special archaeological, cultural, aesthetical and even material value of these mural paintings requires non aggressive reversible treatments that will respect the original character of the artefacts as much as it is possible. Thus, the traditional and largely used restoration processes for the conservation of the European Cultural Heritage with *synthetic polymers,* such as Paraloid B72, Mowilith 30 and Primal AC 33, and that have produced devastating and completely unexpected degradation processes are absolutely excluded from the proposed restoration and rehabilitation program. The normal problems that these interventions have been provoked are the detachment and flaking of surfaces and a strong acceleration of the chemical reactions involved in the paintings degradation, which is an enough important reason to not use any of the above mentioned polymers for consolidation. The same experience has been produced lately in wall painting restoration (mainly in Italy) using inadequate *silicates* or *silanes* or using these precise products in a wrong way, thus we would like to avoid the application of such adhesives.

Instead of using the above synthetic materials to add into the inorganic mixture of $Ca(OH)_2$ + $Ba(OH)_2$ for further consolidation treatment we suggest to use natural organic substitutes, because even though we know the possible problems that the natural adhesives can produce, we consider that long term *in situ* damages that they might cost are less important than the ones that any synthetic based or silicate based treatment can provoke.

As we have already mentioned in the previous part the way that the wall paintings are applied are indicating the use of some kind of organic binding medium. The organic residues analysis described above will confirm the presence or absence of such mean and by it also we will be able to identify the specific organic mean originally used in the mural paintings. If this is the case we suggest to use the same organic substance mixed with the fine mixture of $Ca(OH)_2$ + $Ba(OH)_2$.

If the analytical study gives negative results for the existence of any organic media we will try the same organic materials that are mentioned in the previous part for *pakhsa structure* rehabilitation added to the mixture of $Ca(OH)_2$ + $Ba(OH)_2$ in a combination of different proportions. As we have already mentioned above, the inorganic compound in this case can act as water-repellent stabilizer that would protect from certain alteration processes not only the wall paintings but also the natural substances if they will be finally used.

The results of this trial program will finally define which kind of consolidation process should be followed and which kind of materials should to be used.

For cleaning also different solvents will be tied after consolidation in very small areas: including neutral soaps (vulipex), sepiolite, cellulose pulp of beech wood, mixed with deionized water and a disinfectant (Thymol, a phenol derivative) also the mixture of ammonium sodium bicarbonate Desogen and carboxymethylcellulose will be tried among other solutions.

Our only serious concern mainly affecting the *in situ* conservation the mural paintings of the underground cells of *Kara Tepe*, as the only final overcome of soluble salt precipitation can be done by controlling the relative humidity and temperature at the ambients. Specifically, the climate has to be maintained at about 20 °C and 80% RH, which, if we want to maintain them *in situ* might suppose the acclimatization of these areas or, if it is impossible, finally, the detachment of the paintings, their reconstruction and preservation at a museum controlled environment might be necessary.

To resum, we want to stress out that this report just involves the preliminary definition of the products and processes to follow during the trials. However, this product can be modified during the proceeding of the trial restoration program depending on the immediate results.

RELEVANT BIBLIOGRAPHY

A. Arnold, and A. Kueng, Crystallization and Habits of Salt Efflorescences on Walls, Part I: Methods of Investigation and Habits.” *5th International Congress on the Deterioration and Conservation of Stone, Lausanne 25-27 September, 1985. at* G. Felix and V. Furlan, eds. Lausanne. 255-267. 1985

Appropriate plasters, renders and finishes for cob and random stone walls in Devon, Devon; Earth Building Association, Exeter, 1993.

Earth Building and the Cob revival : a Reader, Cob Cottage Company, Cottage Grove,1996.

The cob buildings of Devon I: history, building methods and conservation, Historical Buildings Trust Devon, Exeter, 1992.

P., Baglioni and R., Giorgi, *Soft and Hard nanomaterials for restoration and conservation of cultural heritage*, Soft Matter, available online at: www.rsc.org

T. Bee, *The cob builders handbook. You can hand-sculpt your own home*, Groundwork, Murphy, 1997.

M.-A. Brier, *La maison de terre en Normandie*, “Energie Verte”, n.16, 1997.

D., Chelazzi and R., Giorgi, Dei, L., Baglioni, P., *Nanotecnologie per la conservazione del patrimonio culturale*, La Chimica e l’Industria, 87 (10), 78-82. 2005.

Del Monte, M., and C. Sabbioni, A Study of the Patina Called ‘Scialbatura’ on Imperial Roman Marbles., *Studies in Conservation* 32:114-121. 1987

De la Manche, *Les secrets de la terre,* Conseil d’Architecture, d’Urbanisme et de l’Environnement de la Manche, Saint-Lo, 1997.

J.Y. Chauvet, *Le centre de découverte du Marais Breton- Vendéen*, “M.P.F.”, n.88, 1988.

C. Delabie, *Wellerbau in Frankreich* in *Modern bauen mit lehm,* Overall Verlag, Berlin, 1998.

C. Delabie*, Maisons en terre des marais de Cotentin,* Biomasse Normandie, Caen, 1992.

I. S. Evans, Salt Crystallization and Rock Weathering: A Review.” *Revue de géomorphologie dynamique* 19:153-177. Paris: Edition de la Société d’edition d’enseignement. 1970

E. Egeland, *Cob and tatch,* Devon Books, Exeter, 1988..

S. Goodhew, R. Griffiths, D. Short, L. Watson, *Some preliminary studies of the termal properties of Devon cob walls,* in *Terra 2000. 8th International Conference of the study and conservation of earthen architecture*, James & James, London, 2000.

R. Harrison, *Earth. The conservation and repair of Bowhill, Exeter: working with cob. English Heritage research translations vol.3*, James & James, London, 1999.

J.-F. Josselin, *Rehabiliter la terre,* “Tiez Breiz-Maisons et paysages de Bretagne, Bulletin Régional”, n.5, 1985.

L. Keefe, *The cob buildings of Devon 2: Repair and Maintenance,* Historical Buildings Trust Devon, Exeter, 1993.

L.Greenspan, Humidity Fixed Points of Binary Saturated Aqueous Solutions, *Journal of Research of the National Bureau of Standards, Section A: Physics and Chemistry* 81A:89-96. Washington, D.C.: National Bureau of Standards. 1977

S.Lewin, “The Mechanism of Masonry Decay through Crystallization.” In *Conservation of Historic*

Buildings and Monuments. Washington, D.C.: NationalAcademy Press. 120-124. 1982

L. Keefe, L. Watson, R. Griffiths, *Possible causes of structural failure in traditional cob buildings,* in *Terra 2000. 8th International Conference of the study and conservation of earthen architecture*, James & James, London, 2000.

F. Lahure, *Qu'est-ce que la bauge ?*, "Energie Verte", n.16, 1987.

F. Lahure, *Pisé ou Bauge ?*, "M.P.F.", n.111, 1994.

M. Lhuillery, *La bauge en Bauce*, "M.P.F.", n.3, 1979.

Mc Cann, *Clay and cob buildings,* Shire Publications, Princes Risborough, 1995.

R. W. Nother, *Continuity of tradition-new earth building. Reception building, NordenPark and Ride, CorfeCastle, Dorset. A case study*, in *Terra 2000. 8th International Conference of the study and conservation of earthen architecture*, James & James, London, 2000.

G. Pearson, *As cheap to rebuild in chalk: the rebuilding of a fallen cob wall following traditional methods,* "Chartered quantity surveyor", n.6, 1984.

Remer, *Cob: the amazing alternative,* "South African Country Life", n.4, 1996

M. Rouault, *Géographie de l'habitat rural traditionnel du Bassin de Rennes et redécouverte des maisons de terre*, "Tiez Breiz-Maysons et Paysages de Bretagne, Bulletin Regional", n.4, 1984.

G.R. Sharpe, *The fascination of cob*, "Architect and Surveyor", n.9, 1988.

M.G. Smith, *The cobber's companion: how to build your own earthen home,* Cob Cottage Company, Cottage Grove, 1999.

L. Watson, J. Fidler (a cura di), *Out of Earth,* Media Services University of Plymout,1994.

L. Watson, R. Harries (a cura di), *Out of Earth II* , Media services University of Plymout, 1995.

L. Watson, *Wellerbau in Devon/England,* in *Modern bauen mit lehm,* Overall Verlag, Berlin, 1998.

C. Williams-Ellis, J & E. Eastwick-Field, *Building in Cob, Pisé and Stabilised Earth*, Country Life Limited, London, 1919.

C. Ziegert, *Wellerbauten in Deutschland,* in *Modern bauen mit lehm,* Overall Verlag, Berlin, 1998.

C. Ziegert, *Analysis of material, construction and damage in historical cob buildings in central Germany*, in *Terra 2000. 8th International Conference of the study and conservation of earthen architecture*, James & James, London, 2000.